

Aus der Medizinischen Klinik mit Schwerpunkt Nephrologie  
der Medizinischen Fakultät der Charité–Universitätsmedizin Berlin

DISSERTATION

**Role of Cytochrome P450 (CYP)-dependent Eicosanoids in  
Experimental Acute Kidney Injury (AKI)**

zur Erlangung des akademischen Grades  
Doctor medicinae (Dr. med.)

vorgelegt der Medizinischen Fakultät  
Charité – Universitätsmedizin Berlin

von

Ye Zhu

aus Hebei, China

Datum der Promotion: 11.12.2015

To my beloved family  
献给我挚爱的家人

# CONTENTS

LIST OF FIGURES .....	IV
LIST OF TABLES .....	V
ABBREVIATIONS .....	VI
ABSTRACT .....	1
ZUSAMMENFASSUNG .....	2
1. INTRODUCTION.....	3
1.1 Acute kidney injury (AKI) .....	3
1.1.1 Acute kidney injury — epidemiology and clinical impact.....	3
1.1.2 Pathogenesis of renal ischemia/reperfusion injury.....	4
1.2 Biosynthesis of CYP/sEH-dependent eicosanoids .....	5
1.2.1 CYP enzymes .....	5
1.2.2 sEH enzyme.....	6
1.2.3 Role of CYP and sEH enzymes in biosynthesis of CYP-dependent eicosanoids ..	7
1.3 Biological functions of CYP-dependent eicosanoids.....	9
1.3.1 Physiological role of CYP-dependent eicosanoids in the kidney .....	9
1.3.1.1 Physiological role of 20-HETE and EETs in the control of renal hemodynamics.....	9
1.3.1.2 Physiological role of 20-HETE and EETs in the regulation of renal tubular function.....	10
1.3.2 Pathophysiological roles of 20-HETE and EETs in I/R-induced injury .....	11
2. AIMS AND HYPOTHESIS .....	15
3. MATERIALS AND METHODS.....	16
3.1 Animals.....	16
3.2 Groups of examined animals.....	16
3.2.1 Groups of examined rats .....	16
3.2.2 Groups of examined mice .....	17
3.3 Animal models of renal I/R injury.....	17
3.3.1 Rat renal I/R injury model.....	17
3.3.2 Mice renal I/R injury model .....	18
3.4 Renal function .....	19
3.5 Histology .....	19
3.5.1 Embedding and sectioning .....	19
3.5.2 Hematoxylin and eosin (HE) staining .....	19
3.5.3 Periodic acid-schiff (PAS) staining .....	19
3.5.4 Acute tubular necrosis (ATN) score .....	20
3.5.5 TUNEL staining .....	20
3.5.6 Immunohistochemical staining in rats.....	20
3.5.7 Immunofluorescence staining with renal cryo-sections in mice .....	21
3.5.8 Immunofluorescence staining with renal paraffin sections in mice .....	21
3.6 DNA isolation and genotypic analysis .....	22
3.7 Gene-expression analysis .....	23
3.7.1 Total RNA extraction and cDNA synthesis .....	23

3.7.2 Quantitative real time PCR (qRT-PCR) .....	23
3.8 Enzyme linked immunosorbent assay (ELISA) in mice .....	25
3.9 Western blot analysis .....	25
3.10 Eicosanoid determination in mice and rats .....	26
3.10.1 Tissue endogenous CYP-eicosanoid profile estimation in mice .....	26
3.10.2 Plasma endogenous CYP-eicosanoid profile estimation in mice.....	27
3.10.3 Tissue endogenous CYP-eicosanoid profile estimation in rats .....	27
3.11 Determination of sEH enzyme activities in mice .....	28
3.11.1 Preparation and protein quantification of cytosolic fraction .....	28
3.11.2 sEH activity assessment .....	28
3.12 Evaluation of testosterone and dihydrotestosterone (DHT) in mice .....	29
3.13 Statistics.....	29
4. RESULTS .....	31
4.1 Utility of a synthetic EET analog for the prevention of renal I/R-injury in a rat model of AKI.....	32
4.1.1 Confirmation of EET analog levels in the kidney .....	32
4.1.2 Ischemia induced the accumulation of free 20-HETE .....	32
4.1.3 EET analog alleviates I/R-induced deterioration of kidney damage 48 h after reperfusion.....	34
4.2 Effect of sEH gene deletion on I/R-induced AKI in mice.....	35
4.2.1 Confirmation and initial characterization of sEH-KO mice.....	35
4.2.1.1 Genotyping .....	35
4.2.1.2 The basal mRNA and protein level of sEH in mice .....	36
4.2.1.3 sEH activity .....	37
4.2.1.4 Baseline renal characterization of sEH-KO mice .....	38
4.2.2 sEH gene disruption aggravated I/R-induced kidney damage .....	38
4.2.2.1 sEH gene disruption aggravated I/R-induced decline of renal function ...	38
4.2.2.2 Expression of AKI biomarkers 48 h after I/R injury .....	39
4.2.2.3 sEH-KO aggravated I/R-induced histomorphologic tubular damage .....	40
4.2.2.4 sEH gene knockout aggravated I/R-induced apoptosis.....	41
4.2.2.5 sEH gene knockout aggravated I/R-induced inflammation .....	42
4.2.3 Kidney-specific 20-HETE overproduction in sEH-KO mice.....	43
4.2.3.1 Plasma oxylipin profiles .....	43
4.2.3.2 Renal oxylipin profiles .....	47
4.2.3.3 Liver oxylipin profiles.....	50
4.2.4 sEH gene disruption caused a strong upregulation of Cyp4a12a expression in the kidney.....	53
4.2.4.1 Renal mRNA level of Cyp4a12a was upregulated in sEH-KO mice .....	53
4.2.4.2 Renal protein expression of Cyp4a12a was upregulated in sEH-KO mice .....	54
4.2.4.3 Intrarenal localization of Cyp4a12a protein expression.....	54
4.2.5 Potential mechanism of 20-HETE overproduction in the kidney .....	56
4.2.5.1 The serum and renal testosterone level in native group .....	56
4.2.5.2 Enzymes in the androgen-related metabolism .....	56

5. DISCUSSION .....	58
5.1 Establishment of I/R-induced AKI animal models .....	58
5.2 The synthetic EET analog alleviates I/R-induced kidney damage.....	59
5.3 sEH deficiency aggravates I/R-induced kidney damage.....	60
5.4 sEH deletion results in an increase of AKI related biomarkers.....	62
5.5 sEH-deficiency causes renal vascular-specific 20-HETE overproduction.....	63
5.6 The imbalance of 20-HETE and EETs contributes to the pathophysiology of AKI .....	64
5.7 The potential mechanism of 20-HETE overproduction .....	66
5.8 Novel therapeutic options for the prevention of ischemic AKI?.....	68
6. BIBLIOGRAPHY .....	70
AFFIDAVIT .....	79
CURRICULUM VITAE.....	80
PUBLICATION.....	81
ACKNOWLEDGEMENT .....	83

## LIST OF FIGURES

Figure 1: Causes of reduction in generalized or regional renal blood flow .....	3
Figure 2: Alterations of the microvasculature and tubule cell structures in the clinical phases of ischemic AKI.....	4
Figure 3: Structure of CYP enzyme and CYP-dependent AA-derived eicosanoids .....	6
Figure 4: Structure of mammalian sEH enzyme and EET-substrate conversion to DHET products by sEH.....	7
Figure 5: Simplified overview of the synthesis and functions of CYP-dependent eicosanoids .....	9
Figure 6: Role of CYP-dependent AA metabolites in the control of vascular tone.....	10
Figure 7: Role of CYP-dependent AA metabolites in the regulation of renal tubular function ...	11
Figure 8: Pharmacological and genetic interventions to test the roles of increased endogenous EETs in ischemia AKI.....	15
Figure 9: Role of EET analog administration in rats in I/R-induced AKI.....	31
Figure 10: Role of sEH gene deletion in mice in I/R-induced AKI.....	31
Figure 11: Ischemia induced the release of 20-HETE but not of EETs in the rat kidney .....	33
Figure 12: EET analog greatly alleviates I/R-induced kidney damage 48 h after reperfusion .....	35
Figure 13: PCR analysis of genomic DNA from mouse-tail biopsy.....	36
Figure 14: Confirmation of abolished sEH-expression in sEH-KO mice.....	36
Figure 15 : sEH activity determination .....	38
Figure 16: sEH gene disruption aggravated functional impairment 48 h after I/R injury .....	39
Figure 17: Expression of AKI biomarkers 48 h after I/R injury .....	40
Figure 18: sEH-KO mice showed aggravated I/R-induced histomorphologic tubular damage....	41
Figure 19: sEH gene knockout aggravated I/R-induced apoptosis .....	42
Figure 20: sEH gene knockout aggravated I/R-induced inflammation.....	43
Figure 21: Plasma oxylipin profiles .....	45
Figure 22: Renal oxylipin profiles .....	48
Figure 23: Liver oxylipin profiles .....	51
Figure 24: sEH gene disruption caused a strong upregulation of 20-HETE-producing gene Cyp4a12a in the kidney.....	53
Figure 25: Renal protein expression of Cyp4a12a was upregulated in sEH-KO mice.....	54
Figure 26: Intrarenal localization of Cyp4a12a protein expression .....	55
Figure 27: Serum and renal testosterone level in native group .....	56
Figure 28: Enzymes in androgen-related metabolism.....	57
Figure 29: Prospects--novel therapeutic options for the prevention of ischemic AKI by targeting renal CYP-dependent eicosanoids pathway .....	68

## LIST OF TABLES

Table 1: Groups of examined rats .....	16
Table 2: Groups of examined mice .....	17
Table 3: Genotyping primer sequences .....	22
Table 4: Components and conditions of genotyping PCR .....	22
Table 5: Components and conditions of reverse transcription .....	23
Table 6: Primer Sequences .....	24
Table 7: Components and conditions of qRT-PCR.....	25
Table 8: Tris-glycin-gel system.....	26
Table 9: Antibodies for western blot.....	26
Table 10: Baseline renal characterization of sEH-KO mice .....	38
Table 11: Correlations between kidney function and biomarkers of AKI.....	40
Table 12: Comparison of plasma oxylipin profile between WT and sEH-KO mice .....	46
Table 13: Comparison of renal oxylipin profile between WT and sEH-KO mice .....	49
Table 14: Comparison of liver oxylipin profile between WT and sEH-KO mice .....	52

## ABBREVIATIONS

AA	Arachidonic acid
AKI	Acute kidney injury
Ang II	Angiotensin II
ATN	Acute tubular necrosis
AUDA	2-(3-adamantan-1-ylureido)-dodecanoic acid
BK	Calcium-activated potassium
bp	Base pair
BSA	Bovine serum albumin
cDNA	Complementary DNA
cm	Centimeter
COX	Cyclooxygenase
CYP	Cytochrome P450
CPR	Cytochrome P450 reductase
d	Day
DDMS	N-methylsulfonyl-12,12-dibromododec-11-enamide
DNA	Deoxyribonucleic acid
DHA	Docosahexaenoic acid
DHET	Dihydroxyeicosatrienoic acid
DHT	Dihydrotestosterone
DiHOME	Dihydroxyoctadecenoic acid
dL	Deciliter
DOCA	Deoxycorticosterone acetate
EDP	Epoxydocosapentaenoic acid
EET	Epoxyeicosatrienoic acid
EEQ	Epoxyeicosatetraenoic acid
ELISA	Enzyme linked immunosorbent assay
EPA	Eicosapentaenoic acid
EpOME	Epoxyoctadecenoic acid
FAD	Flavin adenine dinucleotide
FMN	Flavin mononucleotide
FoV	Fields of view
DiHDPA	Dihydroxydocosapentaenoic acid
DiHETE	Dihydroxyeicosatetraenoic acid
g	Gram
GAPDH	Glyceraldehyde 3-phosphate dehydrogenase
GFR	glomerular filtration
Gusb	$\beta$ glucuronidase
h	Hour

HDHA	Hydroxydocosahexaenoic acid
HE	Hematoxylin and eosin
6,15-20-HEDE	20-hydroxyeicosa-6(Z),15(Z)-dienoic acid
HET0016	N-hydroxy-N'-(4-butyl-2-methylphenyl)-formamidine
20-HETE	20-hydroxeicosatetraenoic acid
HEPE	Hydroxyeicosapentaenoic acid
IgG	Immunoglobulin class G
I/R	Ischemia/Reperfusion
kD	Kilodalton
KIM-1	Kidney injury molecule-1
kg	Kilogram
KO	Knockout
LC-MS/MS	Liquid chromatography tandem mass spectrometry
M	Molar
mA	Milliampere
min	Minute
mg	Milligram
mL	Milliliter
mm	Millimeter
mM	Millimolar
mRNA	Messenger RNA
NADPH	Nicotinamide adenine dinucleotide phosphate
ng	Nanogram
nM	Nanomolar
NGAL	Neutrophil gelatinase associated lipocalin
NO	Nitric oxide
ODYA	17-octadecanoic acid
PAS	Periodic Acid-Schiff
PBS	Phosphate-buffered saline
PCR	Polymerase chain reactions
PLA2	Phospholipases A2
PTH	Parathyroid hormone
PUFA	Polyunsaturated fatty acid
qPCR	Quantitative real time PCR
rRNA	Ribosomal RNA
RP-HPLC	Reversed-phase high performance liquid chromatography
s	Second
sEH	Soluble epoxide hydrolase
SDS-Page	Sodium dodecyl sulfate-polyacrylamide gel electrophoresis
Srd5 $\alpha$ 1	5 $\alpha$ -reductase 1

TALH	Thick ascending limb of Henle's loop
tRNA	Transfer RNA
μg	Microgram
μL	Microliter
μm	Micrometer
UniNx	Unilateral nephrectomy
V	Voltage
WT	Wild type
× g	Times gravity

## ABSTRACT

**Background and hypothesis:** Ischemic acute kidney injury (AKI) greatly contributes to patients' morbidity and mortality in various clinical settings. Searching for novel therapeutic strategies, the present work has been focused on the potential role of cytochrome P450 (CYP)-dependent eicosanoids in the development of AKI. These eicosanoids include 20-hydroxyeicosatetraenoic acid (20-HETE) and epoxyeicosatrienoic acids (EETs) that play opposite roles in the regulation of vascular tone, inflammation, and apoptosis. The specific hypothesis was that pharmacological or genetic interventions enhancing EET actions may prevent the initiation of AKI.

**Experimental strategy and methods:** First, the capacity of a synthetic EET analog to provide protection against renal ischemia/reperfusion (I/R)-injury was evaluated in rats. In a second approach, the effect of reducing endogenous EET degradation was analyzed by comparing renal I/R-injury in wild type (WT) and soluble epoxide hydrolase-knockout (sEH-KO) mice. Kidney damage was evaluated by functional and histomorphological parameters in male animals that underwent renal ischemia (45 min in rats, 22 min in mice) followed by two days of reperfusion. CYP-eicosanoids were analyzed by liquid chromatography tandem mass spectrometry.

**Results:** In rats, ischemia induced a massive release of 20-HETE in the kidney, whereas free EETs were not accumulated. Administration of the EET analog before ischemia compensated for the lack of endogenous EET release and significantly alleviated I/R-induced reduction of kidney function, tubular apoptosis, and inflammatory cell infiltration. In contrast to the initial expectations, renal function declined more severely in sEH-KO compared to WT mice as indicated by higher serum creatinine and urea levels. The sEH-KO mice also featured higher tubular lesion scores, increased tubular apoptosis and inflammation. Plasma and renal EET levels were higher in sEH-KO than WT mice. However, renal, but not plasma and hepatic, 20-HETE levels were significantly increased in sEH-KO compared to WT mice. In line with this finding, renal expression of Cyp4a12a, the murine 20-HETE-generating enzyme, was up-regulated both at the mRNA and protein levels, and Cyp4a12a immunostaining was more intense in the renal vessels of sEH-KO than WT mice. These results indicate that the potential beneficial effects of reducing EET degradation were obliterated by a thus far unknown mechanism leading to kidney-specific upregulation of 20-HETE formation in sEH-KO mice.

**Conclusions:** The data obtained both in rats and mice suggest that imbalances in the formation of 20-HETE and EETs play a pivotal role in setting the stage for the cascade of events leading to renal I/R-injury. Pharmacological interventions with synthetic EET analogs could offer promising new options for AKI prevention.

## ZUSAMMENFASSUNG

**Hintergrund und Hypothese:** Ischämie-bedingtes akutes Nierenversagen (ANV) kann als schwerwiegende Komplikation in verschiedenen klinischen Situationen auftreten und führt zu erhöhter Morbidität und Mortalität der Patienten. Zur Entwicklung neuer therapeutischer Ansätze wird in der vorliegenden Arbeit die Rolle von Cytochrom P450 (CYP)-abhängigen Eicosanoiden bei der Entstehung des ANV untersucht. Zu diesen Eicosanoiden gehören 20-Hydroxyeicosatetraensäure (20-HETE) und Epoxyeicosatriensäuren (EETs), welche als Gegenspieler bei der Regulation des Gefäßtonus, Inflammation und Apoptose fungieren. Mittels pharmakologischer und genetischer Interventionen wurde die Hypothese untersucht, ob durch Verstärkung der EET-Wirkung die Auswirkungen des akuten Nierenversagens abgemildert werden können.

**Experimentelles Design und Methoden:** Zunächst wurde die Wirkung eines synthetischen EET-Analogons auf den renalen Ischämie/Reperfusion (I/R)-Schaden bei der Ratte untersucht. In einer zweiten Versuchsreihe wurden Wildtyp (WT)- und Knockout (KO)-Mäuse für das Enzym lösliche Epoxidhydrolase (sEH) (sEH-KO-Mäuse) eingesetzt, um die Effekte eines verminderten EET-Abbaus auf den Schweregrad des I/R-induzierten Nierenschadens zu analysieren. Das Ausmaß des Nierenschadens wurde anhand funktioneller und histomorphologischer Parameter bewertet, nach dem die Tiere einer renalen Ischämie (45 Minuten in Ratten, 22 Minuten in Mäusen) gefolgt von einer zweitägigen Beobachtungsphase nach Reperfusion unterworfen wurden. Die CYP-Eicosanoide wurden mittels Flüssigchromatographie Tandem-Massenspektrometrie bestimmt.

**Ergebnisse:** In der Rattenniere kam es während der Ischämie zu einer gesteigerten Freisetzung von 20-HETE, während eine vermehrte EET-Bildung ausblieb. Die Gabe eines EET-Analogons vor Ischämie führte zu einer signifikanten Verminderung des I/R-induzierten renalen Funktionsverlusts, der tubulären Apoptose sowie der Infiltration von Entzündungszellen. Im Gegensatz zur Ausgangshypothese, zeigten sEH-KO Tiere einen größeren Nierenfunktionsverlust als WT-Tiere. Auch das Ausmaß des tubulären Schadens, sowie der tubulären Apoptose und der inflammatorischen Gewebsreaktion war in den sEH-KO Tieren signifikant stärker als in den Wildtypmäusen. Auf metabolischer Ebene führte der sEH-KO wie erwartet zur Erhöhung der endogenen EET-Spiegel in allen untersuchten Geweben (Niere, Leber und Plasma). Zugleich wiesen die sEH-KO Tiere jedoch auch einen erhöhten 20-HETE-Gehalt im Nierengewebe aber nicht in Plasma und Leber auf. Die erhöhten renalen 20-HETE-Spiegel korrelierten mit einer verstärkten mRNA und Protein Expression von Cyp4a12a, der murinen 20-HETE-Synthase, sowie einer erhöhten immunhistochemischen Cyp4a12a-Expression in Nierengefäßen bei sEH-KO Mäusen. Diese Ergebnisse deuten darauf hin, dass der potenziell schützende Effekt des verminderten EET-Abbaus durch eine Nieren-spezifische Steigerung der 20-HETE-Bildung in sEH-KO Mäusen aufgehoben wurde.

**Zusammenfassung:** Die Ergebnisse aus beiden Tiermodellen zeigen, dass eine Imbalanz zwischen 20-HETE und EETs das Ausmaß des I/R-induzierten Nierenversagens entscheidend beeinflusst. Pharmakologische Interventionen mit synthetischen EET-Analoga könnten ein vielversprechender neuer Ansatz zur ANV-Prävention sein.

# 1. INTRODUCTION

## 1.1 Acute kidney injury (AKI)

### 1.1.1 Acute kidney injury — epidemiology and clinical impact

Acute kidney injury (AKI), characterized by an abrupt deterioration in kidney function over a period of hours to days, is a common clinical problem and a major contributor to patient morbidity and mortality [1]. Recent studies reported that AKI appeared in 20% of hospitalized patients, and exceed 45% in patients admitted to intensive care units [2]. The annual incidence of AKI in the general population is even higher than that of stroke based on US data, which was estimated to be 550 per 100,000 individuals [3]. Moreover, the severity of AKI is highly correlated with short-term and long-term mortality in patients who survive hospitalization with AKI. It is estimated that about 2 million people worldwide die of AKI every year [2]. Patients who have uncomplicated AKI present a mortality rate of around 10% and even over 50% if they suffer complications with multi-organ failure [2]. Moreover, lack of precise diagnosis and effective therapy greatly influence the epidemiology and outcome of AKI, which poses a personal and public health burden. Therefore, searching for a specific preventive strategy of AKI is becoming an important and urgent research topic.

Based on etiology, AKI can be divided into three categories: prerenal, intrinsic renal, and postrenal. Among them, intrinsic renal AKI is quite challenging for evaluation because of the wide variety of injuries that can occur to the kidney [4]. As a major cause of intrinsic renal AKI, ischemia/reperfusion (I/R) injury is a complex process and can be caused by many pathophysiological states and medications [3]. Figure 1 gives an overview about major clinical conditions that may cause generalized or localized ischemia within the kidney leading to AKI [3].

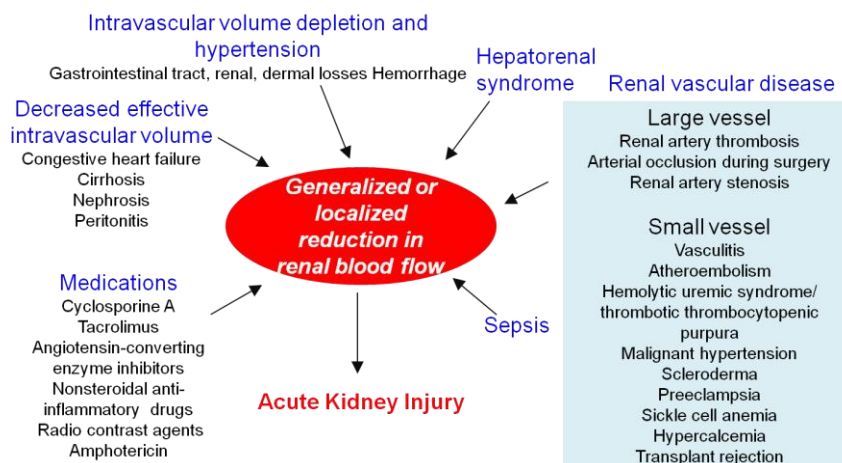


**Figure 1: Causes of reduction in generalized or regional renal blood flow**

## 1.1.2 Pathogenesis of renal ischemia/reperfusion injury

Renal I/R injury results from a mismatch of general or local tissue oxygen supply/demand and accumulation of waste products of metabolism [3]. The pathological condition of I/R develops as an effector phase of ischemic injury causing profound tissue hypoxia and microvascular dysfunction, followed by restoration of perfusion that exacerbates the activation of innate and adaptive immune responses and tubular cell death.

Clinically, ischemic AKI can be divided into four phases: initiation, extension, maintenance, and recovery. Recent studies illustrate a direct relationship between the clinical phases and the cellular phases of ischemic AKI (Figure 2) [5, 6]. The initiation phase occurs when renal blood flow dramatically decreases. Subsequent ATP depletion potentiates the injury and dysfunction of endothelial and tubular epithelial cells [5, 6]. If the injury is alleviated at this stage, the kidney potentially can recover. With persisting ischemia there will be less probability of organ recovery which leads to the extension phase. This is characterized by inflammation, apoptosis and oxidant injury leading to further tubule damage. Furthermore, also injured tubular cells exhibit a maladaptive response by generating cytokines and chemokines that further amplify the injury [5]. The overall deleterious effects of these events aggravate microvascular dysfunction and damage cellular proteins, deoxyribonucleic acid (DNA), and the plasma membrane [7]. Repair and regeneration processes occur simultaneously with cellular apoptosis, autophagy, and necrosis, while the fate of an organ depends on whether cell death or regeneration prevails [8] (Figure 2).

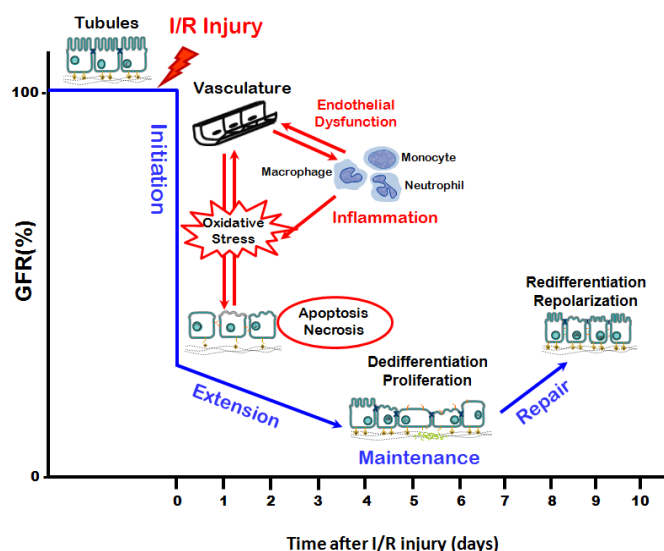


**Figure 2: Alterations of the microvasculature and tubule cell structures in the clinical phases of ischemic AKI**

Cellular phases are directly correlated to the clinical phases of ischemic AKI, which temporally have an impact on renal function represented by a decrease in glomerular filtration (GFR). Modified from [5, 6].

Therefore, the net result of the perturbations is damage to all bio-molecules in cells and tissues. The mechanisms contributing to the pathogenesis of renal I/R-injury are multi-factorial, complex, and highly intertwined [7]. There is a great need to establish pharmacological intervention to provide protection against renal endothelial and tubular injury based on a better understanding of the molecular mechanisms that underlie AKI. Recent preclinical studies suggest that arachidonic acid (AA) metabolites generated by cytochrome P450 (CYP) enzymes play an important role in the development of I/R-injury in the heart and brain [9-12], there is also first experimental evidence for a contribution of CYP-eicosanoids to the initiation of AKI [13]. Thus, targeting the formation and action of CYP-dependent eicosanoids will probably have beneficial effects on the prevention of ischemic AKI in clinical settings.

## **1.2 Biosynthesis of CYP/sEH-dependent eicosanoids**

### **1.2.1 CYP enzymes**

CYP enzymes comprise a superfamily of heme-thiolate proteins in all domains of life. Repeated gene duplications and divergent evolution has given rise to one of the largest multi-gene families. Until now, more than 21,000 distinct CYP enzymes are known when counting all the isoforms thus far detected in organisms from bacteria to man. The human genome harbors 57 and the mouse genome 112 functional CYP genes [14]. To distinguish among these isoforms, the nomenclature is based on the similarities of their amino acid sequences. The root symbol “CYP” is for human, while “Cyp” is for mouse and drosophila sequences. An enzyme belonging to a family with the amino acid sequence possessing more than 40% homology, is identified by a number (e.g. Cyp2 or Cyp4). Each family can be further separated into subfamilies with a match of the sequences of more than 55%. This is denoted by a letter following the family designation (e.g. Cyp2J or Cyp4A). The individual members of a subfamily are subsequently indicated by Arabic numerals (e.g., Cyp2J2 or Cyp4a12) [15].

Most mammalian CYP isoforms are membrane-bound proteins, which are tethered to the endoplasmic reticulum membrane through a hydrophobic transmembrane helix at N-terminus of the protein [16]. The remainder of the CYP molecule forms a large cytosolic domain that encloses the heme prosthetic group. Some hydrophobic regions of the cytosolic domain locate directly on the membrane surface. This may cause a direct access to the substrate-binding channel for those compounds distributed in the phospholipid bilayer [17]. The most common reaction catalyzed by CYP enzymes is monooxygenation. This reaction, previously known as mixed-function oxidation, requires molecular oxygen and nicotinamide adenine dinucleotide

phosphate (NADPH) which provides electrons to activate the oxygen. CYP proteins perform this reaction by cooperating with NADPH-cytochrome P450 reductase (CPR) which contains flavin adenine dinucleotide (FAD) and flavin mononucleotide (FMN) as prosthetic groups. This CYP-component binds and introduces the oxygen atom into the substrate and releases the products from the active site [17]. Figure 3 shows the reaction of CYP-dependent AA metabolism as an example.

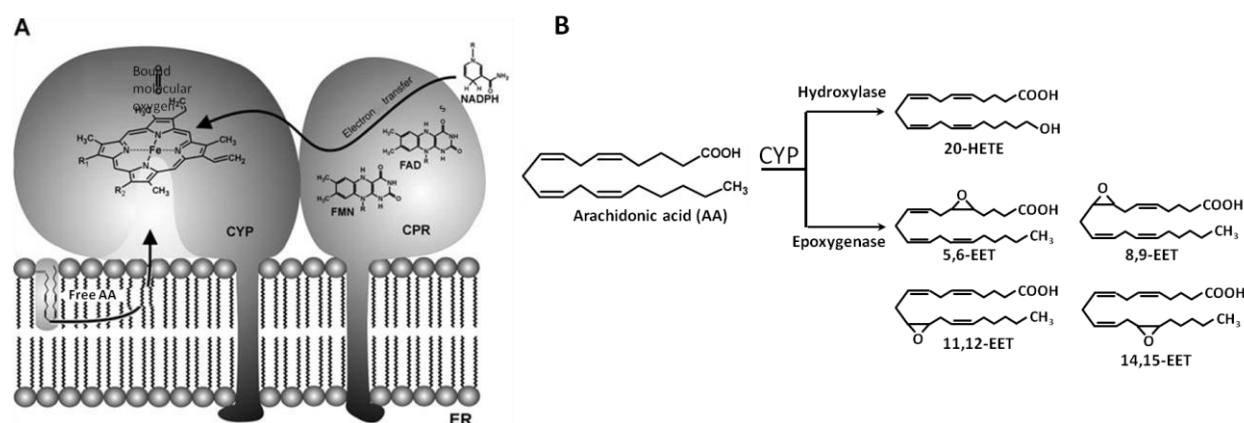


**Figure 3: Structure of CYP enzyme and CYP-dependent AA-derived eicosanoids**

A: Microsomal CYP system consists of a CYP-protein and CPR. The CPR transfers electrons from NADPH via FAD and FMN to heme of CYP protein. The CYP-component binds free AA, activates molecular oxygen at the heme iron and inserts an oxygen atom into the substrate [17]. B: CYP-dependent AA metabolic pathway, and structures of AA-derived eicosanoids.

### 1.2.2 sEH enzyme

sEH enzyme also plays an important role in the metabolism of CYP-dependent eicosanoids. sEH, encoded by the *Ephx2* gene, was first identified through its epoxide hydrolase activity, and is highly expressed in liver and kidney [18]. Human sEH is a 62kDa enzyme composed of two domains [19]. In mammals sEH is a homodimer consisting of two identical 62kDa monomers which are arranged in an antiparallel fashion in the intracellular environment. In this homodimer, each monomer is built in two domains (N- and C-terminal domain) which are separated by a proline-rich linker and have distinct activities [20]. The 25kDa N-terminal domain, exhibiting a  $Mg^{2+}$ -dependent phosphatase activity, has the typical topology for the haloacid dehalogenase superfamily and hydrolyzes lysophosphatidic acids [21]. For the 35kDa C-terminal domain, which is similar to that of haloalkane dehalogenase, contains the epoxide hydrolase activity and is involved in the metabolism of epoxides [22]. The activity of sEH has been found in all vertebrates examined so far, and the phosphatase and epoxide hydrolase domains may be inhibited independently. The few known inhibitors developed for this N-terminal phosphatase

activity are not efficient, and data on their possible endogenous substrates and biological roles are limited [23-25]. In contrast, most of the known biological roles of sEH have been attributed to its more well-defined C-terminal epoxide hydrolase activity [26]. According to this activity, sEH hydrolyzes several endogenous substrates such as CYP-dependent AA-derived epoxides (EETs) (Figure 4).

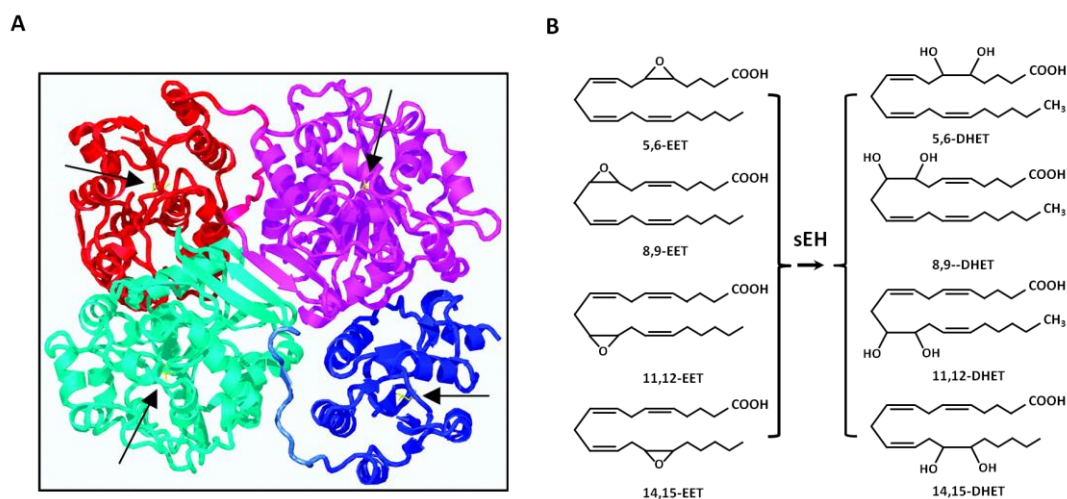


**Figure 4: Structure of mammalian sEH enzyme and EET-substrate conversion to DHET products by sEH**

A: The N- and C-terminal domains of one subunit are shown in blue and cyan respectively, whereas in the other subunit they are red and magenta. The side chains of the catalytic nucleophiles of all four active sites are shown in yellow and indicated by black arrows [20]. B: Substrates and products of sEH enzyme in CYP-dependent AA metabolic pathway. DHET, dihydroxyeicosatrienoic acids.

### 1.2.3 Role of CYP and sEH enzymes in biosynthesis of CYP-dependent eicosanoids

Notably CYPs are involved in a diversity of reactions including catalysis of the oxidative metabolism of a wide variety of exogenous chemicals including drugs, carcinogens, toxins, and endogenous compounds such as steroids, fatty acids, and prostaglandins [27]. CYP-determined AA metabolism, the third metabolic pathway of AA, has been recognized recently.

AA (20:4  $\omega$ -6), one of polyunsaturated fatty acids (PUFAs), is present in membrane glycerophospholipids at stereospecific numbering (sn)-2 position. AA-metabolizing CYP enzymes are expressed throughout the vascular and tubular system of the kidney [28]. CYP-eicosanoid synthesis occurs under normoxic conditions and is dependent on extracellular signal-induced activation of phospholipases A2 (PLA2), which releases free AA from membrane phospholipids [26, 29]. As shown in Figure 5, free AA can then be further metabolized by CYP enzymes to several biologically active eicosanoids by two distinct enzymatic reactions. Members

of the CYP4A and CYP4F subfamilies function as  $\omega/(\omega-1)$ -hydroxylases that convert AA predominantly to 20-hydroxyeicosatetraenoic acid (20-HETE), while a set of regio- and stereoisomeric epoxyeicosatrienoic acids (EETs) is produced through the action of CYP 2J and 2C enzymes [28]. However, once produced, 20-HETE and EETs are partially re-esterified into phospholipids, generating a membrane pool of preformed CYP-eicosanoids that is also accessible to PLA2 [30, 31]. The ability of 20-HETE and EETs to shuttle between an esterified and a free form may have a high physiological relevance [17]. These features link the biosynthesis, storage, and the release of CYP-eicosanoids to various signaling pathways triggered by vasoactive hormones and growth factors [28, 32]. Moreover, the same features may also be involved in pathological conditions such as ischemia, which stimulates phospholipases activation and thus leads to an excessive production and release of CYP-eicosanoids in the affected tissues [32, 33].

EETs can be rapidly further hydrolyzed by sEH to the corresponding diols termed dihydroxyeicosatrienoic acids (DHETs) (Figure 5). Compared to EETs, DHETs have increased water solubility that easily to removal and excretion from the site of action. This reaction results in the loss of some biological activities of EETs [17, 34], and then partially affects the balance and functions of 20-HETE and EETs [19].

The intracellular balance between EETs and 20-HETE influences the biological response to these eicosanoids [35]. Under physiological conditions, 20-HETE and EETs, as the primary products of AA, are involved in the regulation of renal vascular and tubular function. When formed in excess under pathological conditions, these molecules can contribute to the onset and progress of many acute and chronic diseases [36, 37]. In pathophysiological processes, 20-HETE presents vasoconstrictor, pro-inflammatory and pro-apoptotic properties. EETs show a profile of biological activities that partially oppose those of 20-HETE, which makes these metabolites promising candidates for mediating organ protection. Thus, specific fields are emerging for investigating biological functions of CYP-dependent eicosanoids under normal or pathological conditions. The role of CYP-dependent AA metabolites in renal physiology and pathophysiology will be described in details in the following sections.

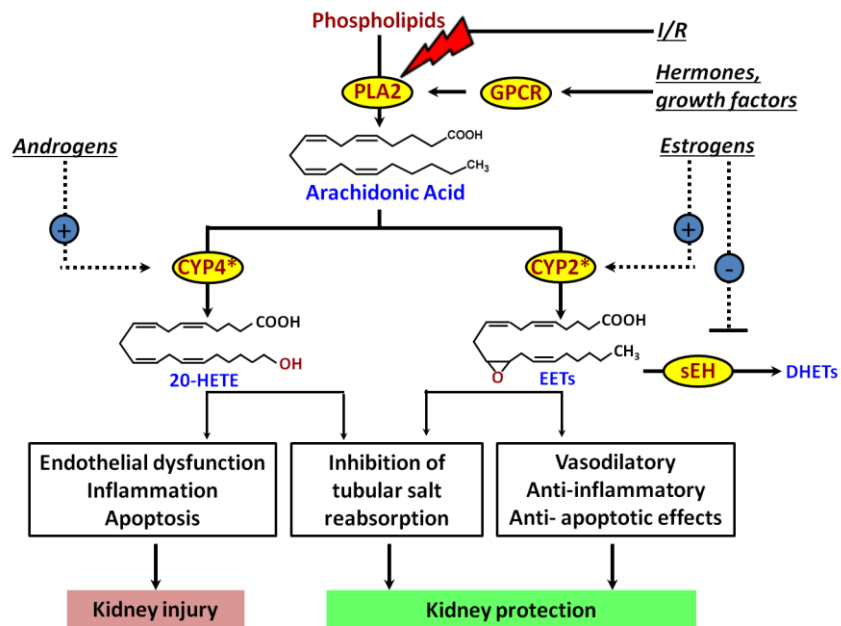


**Figure 5: Simplified overview of the synthesis and functions of CYP-dependent eicosanoids**

20-HETE and EETs, the primary metabolites of AA, play important roles in renal physiology and pathophysiology. The balance of their signals can be shifted through the action of sEH, which metabolizes EETs to diol species.

## 1.3 Biological functions of CYP-dependent eicosanoids

### 1.3.1 Physiological role of CYP-dependent eicosanoids in the kidney

#### 1.3.1.1 Physiological role of 20-HETE and EETs in the control of renal hemodynamics

Under physiological conditions, 20-HETE and EETs play opposite roles in the regulation of renal hemodynamics (Figure 6).

EETs are produced in vascular endothelial cells and activate calcium-activated potassium (BK) channels in the underlying vascular smooth muscle cells, eventually leading to vasorelaxation [38, 39]. This property enables EETs to mediate vasodilator responses, and EETs have been considered as the major endothelium-derived hyperpolarizing factor in renal arterioles [39].

In contrast to the formation of EETs, 20-HETE, which is produced by renal vascular smooth muscle cells, acts as a potent vasoconstrictor of small arteries and arterioles (<100  $\mu\text{m}$ ) such as renal interlobular and afferent arterioles [28]. The response to 20-HETE is associated with depolarization of vascular smooth muscle cells and results in a sustained rise of intracellular calcium by inhibiting the BK channel [40]. Moreover, vascular formation of 20-HETE also contributes to autoregulation of renal blood flow and tubuloglomerular feedback mechanisms

[41]. The biosynthesis of 20-HETE is inhibited by nitric oxide (NO) that binds to the heme prosthetic group of the CYP enzymes. This mechanism substantially contributes to NO-mediated vasodilation in renal microcirculation [42].

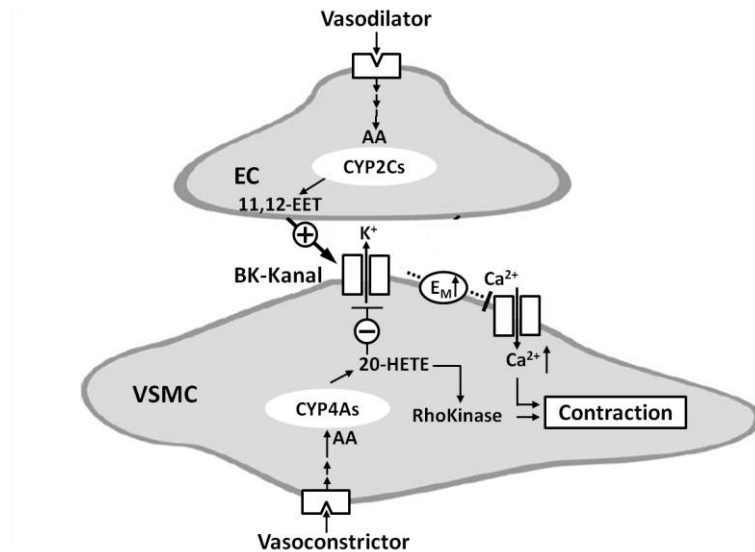


**Figure 6: Role of CYP-dependent AA metabolites in the control of vascular tone**

EETs are produced in endothelial cells by CYP2C, and are potent vasodilators that hyperpolarize renal vascular smooth muscle cells by increasing the activity of BK channels. 20-HETE is produced by CYP4A enzymes in vascular smooth muscle cells, and triggers vasoconstriction via inhibition of BK channels and activation of Rho kinase [17].

### 1.3.1.2 Physiological role of 20-HETE and EETs in the regulation of renal tubular function

Apart from the regulation of renal vascular response, the role of CYP-dependent AA metabolites in the control of sodium excretion has emerged as a dynamic new field [43]. 20-HETE and EETs are formed in different segments of the nephron and mediate tubular function with the net effect of inhibiting sodium reabsorption [41, 44] (Figure 7).

20-HETE promotes salt excretion by inhibiting Na<sup>+</sup>-K<sup>+</sup>-ATPase in proximal tubules and the Na<sup>+</sup>-K<sup>+</sup>-2Cl<sup>-</sup> co-transporter in the thick ascending limb of Henle's loop (TALH). Blockade of 20-HETE formation upon antagonist treatment decreases the salt excretion via both mechanisms [45].

Moreover, EETs also inhibit sodium transport by inhibiting the translocation of the Na<sup>+</sup>-H<sup>+</sup> exchanger to the apical membrane of proximal tubule cells. In cortical collection duct and TALH, EETs serve as inhibitors of epithelial Na<sup>+</sup> channel, which mediates the reduction of transepithelial voltage and inhibition of sodium transport [45].

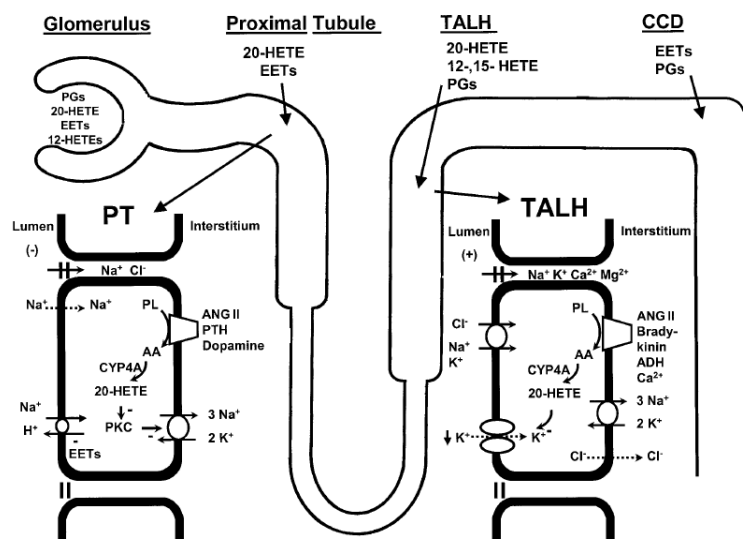


**Figure 7: Role of CYP-dependent AA metabolites in the regulation of renal tubular function**

20-HETE and EETs are produced in various parts of the nephron and modulate the activity of ion channels involved in salt reabsorption [17, 28, 45].

Overall, in the kidney, these eicosanoids (20-HETE and EETs) have concordant effects on sodium reabsorption but contradictory effects on vascular reactivity. The proportional distribution of 20-HETE and EETs could potentially influence fluid homeostasis and vascular tone, and become a key determinant for controlling blood pressure [46]. Moreover, 20-HETE and EETs play a wide range of regulatory and opposing roles in the pathophysiology of certain diseases, for instance, hypertension, polycystic kidney disease, and diabetic nephropathy [28, 47]. The findings on the roles of 20-HETE and EETs in I/R-induced injury will be described in the following chapter.

### 1.3.2 Pathophysiological roles of 20-HETE and EETs in I/R-induced injury

The extent, severity, and reversibility of I/R-induced damage depend on organ-specific susceptibility. The three most susceptible organs are the brain, heart, and kidney [7]. An important role of CYP-eicosanoids in I/R-injury has been first demonstrated in the heart and brain.

Some studies showed that the level of 20-HETE was significantly increased in transient middle cerebral artery occlusion or thromboembolic animal model of stroke. The increased 20-HETE contributed to brain injury after ischemic stroke by mitigating the recruitment of collateral flow to the ischemic penumbra and activating a number of the intracellular signaling pathways. Blockade of the synthesis or vasoconstrictor actions of 20-HETE improved the neurologic

outcomes by preventing the fall in cerebral blood flow and reversing delayed vasospasm which led to the infarct volume reduction of the brain after ischemia [48]. Similar results were found in myocardial infarction models in dogs and rats. Pretreatment with a nonselective CYP inhibitor, miconazole, and two specific CYP  $\omega$ -hydroxylase inhibitors, 17-octadecanoic acid (ODYA) and N-methylsulfonyl-12,12-dibromododec-11-enamide (DDMS), markedly decreased the coronary venous plasma concentrations of 20-HETE and reduced the activity of CYP  $\omega$ -hydroxylase isoforms including CYP4A1, CYP4A2, and CYP4F in heart tissue. These compounds also produced a marked reduction in myocardial infarct size. Conversely, exogenous 20-HETE administration prior to coronary artery occlusion produced a significant increase in infarct size [9]. However, there are few reports that have addressed the role of 20-HETE on renal I/R-injury. In vitro experiments showed that 20-HETE overproduction can significantly exacerbate the cytotoxic and pro-apoptotic effects of chemical hypoxia on cultured renal tubular epithelial cells [13], suggesting that 20-HETE may play a similar detrimental role in renal I/R-injury as identified before in the heart and brain. Moreover, Hoff et al. [32] concluded that ischemia-induced 20-HETE generation and action are primarily responsible for initiating the pathophysiological cascade leading to I/R-induced kidney injury. This conclusion is also in line with a recent clinical study on renal transplantation showing that the extent of 20-HETE released within the first 5 min of allograft reperfusion is a negative predictor of post-transplant allograft function [49]. In contrast, protective effects of 20-HETE were observed in another rat model of AKI. In this model, systemic long-term inhibition of 20-HETE formation aggravated and antagonizing 20-HETE action in the reperfusion phase ameliorated renal I/R injury [50]. Taken together, the studies clearly indicated an important role of 20-HETE in ischemic injury.

To evaluate the role of EETs in certain diseases, current studies used pharmacological, gene knockout or transgenic approaches to either increase EET formation or reduce EET degradation. Among those approaches, reduction of sEH activity is the common way used to stabilize or increase the endogenous levels of EETs. Thus, pharmacological inhibition and gene deletion of sEH have been investigated in several physiological states of disease such as I/R-injury [24, 51, 52].

The first study to demonstrate the importance of sEH in I/R-induced organ injury was performed in isolated hearts of sEH-KO mice. When isolated hearts in a Langendorff apparatus were subjected to ischemia and followed by reflow, hearts from sEH-null mice displayed enhanced recovery of contractile function compared to WT controls [53]. It has also been reported that inhibition of sEH (either with targeted gene knockout or with a specific inhibitor) reduced infarct

size in murine, canine, and rat hearts [54, 55]. In a myocardial I/R mouse model with 40 min of left coronary artery occlusion and 2 h of reperfusion in vivo, sEH-KO mice displayed a significantly smaller infarct area and reduced myocardial injury [56]. The use of sEH inhibitors also prevented progressive cardiac remodeling and ventricular arrhythmias associated with I/R-injury [57].

Afterwards, a number of studies were performed to investigate the role and mechanism of sEH in I/R-induced brain injury. Genetic deletion as well as pharmacological sEH inhibition resulted in less tissue damage and enhanced recovery in animal models of cerebral I/R-injury and acute brain trauma, but mechanisms seem to differ. One study demonstrated that the use of a sEH inhibitor did not influence the regional collateral blood flow rates at the end of ischemia, which suggested that sEH inhibition was protective against ischemic injury by non-vascular mechanisms [58]. However, in an experimental ischemia stroke model of middle cerebral artery occlusion, sEH-KO mice had a smaller infarct size but an increased collateral blood flow compared to WT mice. Surprisingly, there was no difference in hydrolase activity and free 14,15-EET levels in brain tissues between these two models. These results indicate that the protective effect against ischemic stroke in sEH-KO mice might be caused by reduced hydration of circulating EETs through a vascular mechanism [59]. Moreover, in an ischemic stroke model with 90 min focal cerebral ischemia followed by reperfusion, the sEH inhibitor exerted its neuroprotective effects by affecting multiple components of neurovascular areas, including neurons, astrocytes, and microvascular flow [60]. When using optical micro-angiography to study endogenous revascularization in living mice with induced brain injury, sEH-KO mice exhibited accelerated revascularization and enhanced restoration of blood volume at lesion sites over a one-month period after the injury [61]. These data indicated that repair of the tissue was due to revascularization after the injury, rather than a decrease in the damage or immediate repair after injury [19].

Other than these studies on I/R-induced heart and brain injury, there is little knowledge about the role of sEH in AKI. Intraperitoneal administration of the sEH inhibitor, 2-(3-adamantan-1-ylureido)-dodecanoic acid (AUDA), in C57BL/6 mice which suffered from I/R injury, attenuated the deterioration of kidney function, tubular necrosis, and intrarenal infiltration of inflammatory cells. The results of this study suggest that treatment with sEH inhibitors could reduce the severity of AKI [62]. Determining the role of sEH in I/R-induced organ injury is still under investigation. In general, the success in elevating tissue EET levels by inhibiting the activity of sEH will largely depend on endogenous EET production and thus on the expression and activity

of CYP epoxygenases under the given pathological conditions. Compared to the extensive studies on inhibiting sEH enzymes, the development of metabolically robust EET analogs suitable for in vivo application is only at the beginning [63-65]. Such compounds would offer a direct way to compensate for EET deficiency in I/R-injury and other cardiovascular disease states.

## 2. AIMS AND HYPOTHESIS

As outlined above, 20-HETE and EETs play opposite roles in the regulation of vascular tone, inflammation, and apoptosis. Accordingly, it was hypothesized that imbalances in the formation of these two classes of CYP-eicosanoids might contribute to the development of ischemic AKI. Previous studies of the host laboratories revealed that inhibiting the formation and action of 20-HETE protects against renal I/R-injury in rat [32]. Extending these studies, the present work was primarily aimed at investigating the role of EETs in the pathophysiology of ischemic AKI (Figure 8).

We hypothesized that EETs have the potential of ameliorating ischemic AKI by suppressing I/R-induced processes leading to sustained vasoconstriction, inflammation, and tubular epithelial cell apoptosis. To test this hypothesis, pharmacological interventions were performed in a rat model of AKI using a synthetic EET analog. The compound was designed to share the biological activities of the naturally occurring 11,12- and 14,15-EETs [65] and thus provided the opportunity of directly testing their putative beneficial effects.

In a second series of experiments, the effect of reducing sEH-mediated EET degradation should be analyzed by comparing the extent of renal I/R-injury in sEH-KO and WT mice. Here, the specific hypothesis was that sEH gene deletion results in increased levels of endogenous EETs that in turn provide protection against renal I/R-injury. However, this part of the work yielded results that apparently contradicted the initial hypothesis. Therefore, the work program with sEH-KO mice was extended in order to identify the factor(s) potentially obliterating the beneficial effects expected from reducing EET degradation.

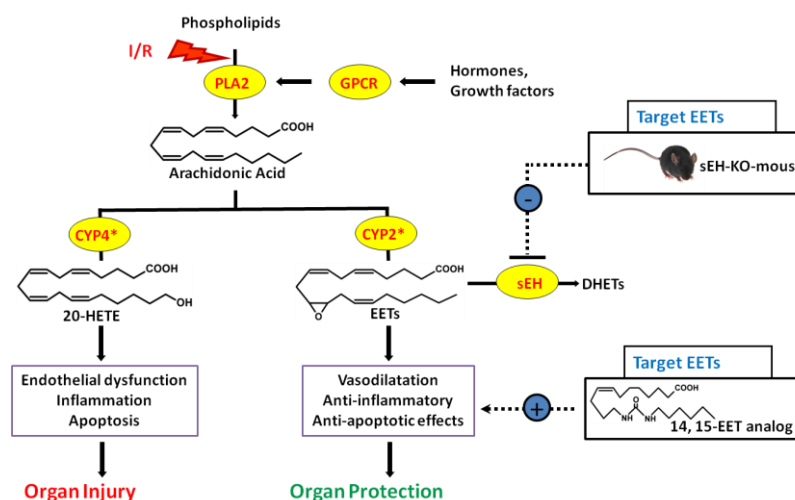


**Figure 8: Pharmacological and genetic interventions to test the roles of increased endogenous EETs in ischemia AKI**

### 3. MATERIALS AND METHODS

#### 3.1 Animals

The animal experiments designed for this thesis were performed on rats and mice. Inbred male Lewis rats were purchased from Harlan-Winkelmann (Borchen, Germany). The sEH-KO mice were originally established by Boehringer Ingelheim Pharmaceuticals, Inc [66] and then further backcrossed for nine generations onto C57BL/6ByJ before being used in our studies [67]. The sEH-KO mice and WT littermates were kindly provided by Dr. Wolf-Hagen Schunck (Max-Delbrück Center for Molecular Medicine, Berlin). All animals were kept under specific pathogen free environment with a standard 12:12 hour (h) light-dark cycle and had ad libitum access to water and standard chow (Ssniff, Soest, Germany) throughout the entire experiment. All procedures were performed in accordance with the animal welfare guidelines of the Charité Medical University Berlin and the protocol was approved by local authorities (Landesamt für Gesundheit und Soziales, LaGeSo, G121-11, G 330-11, Berlin, Germany).

#### 3.2 Groups of examined animals

##### 3.2.1 Groups of examined rats

Rats were randomly divided into nine groups (Table 1). First of all, all rats underwent right unilateral nephrectomy, and the right kidneys were used as native group. Second, rats were categorized into two groups, either vehicle or EET analog group, according to the applied pharmacological intervention after right unilateral nephrectomy. Finally, rats with each pharmacological treatment were divided into four groups according to the different types of surgery (UniNx or I/R) and the three time points of reperfusion (0 h, 2 h and 48 h) which were chosen for the examination of the ischemic kidney. UniNx (sham) animals solely underwent right unilateral nephrectomy. Additionally I/R of the left kidneys were performed in I/R group, and the left kidneys were harvested directly after ischemia (0 h reperfusion group), 2 h post-reperfusion (2 h reperfusion group) or 48 h post-reperfusion (I/R + 48 h reperfusion group).

**Table 1: Groups of examined rats**

<b>Treatment</b>	<b>Native</b>	<b>Vehicle</b>				<b>EET analog</b>			
<b>I/R</b>	None	UniNx	0 h	2 h	48 h	UniNx	0 h	2 h	48 h
<b>Number</b>	64	8	8	8	8	8	8	8	8
<b>In total</b>	<b>64</b>								

### 3.2.2 Groups of examined mice

Mice of both genotypes (WT and sEH-KO) were randomly categorized into three groups (Table 1). The native group received no treatment, whereas sham mice underwent right unilateral nephrectomy (UniNx) but without clamping of left renal pedicle. Animals of the experimental I/R group were uni-nephrectomized (right kidney) at first, and afterwards I/R of the contralateral kidney (left kidney) was additionally performed as described in chapter 3.3.2 (Table 2).

**Table 2: Groups of examined mice**

Group	Native	UniNx	I+48h R (I/R)
WT	18	8	9
sEH-KO	18	8	9
In total	70		

### 3.3 Animal models of renal I/R injury

#### 3.3.1 Rat renal I/R injury model

Male rats at 7-9 weeks of age and a body weight of 210-260 gram (g) were used for the rat experiments. All rats underwent midline laparotomy and right nephrectomy under isoflurane ("Forene", Abbott GmbH & Co., KG Wiesbaden) induced anesthesia (4.5 % for induction, 2.5 % for maintenance). Body temperature was kept at a constant core body temperature (36.5-37.5°C). Right kidneys served as control (native group) for determination of CYP-eicosanoids. EET analog (60 microgram ( $\mu\text{g}$ )) or its vehicle (1% DMSO in saline) was infused into the remaining left kidney by single intra-aortic injection (100 microliter ( $\mu\text{L}$ )) between two short-time aortic clamps (FST, Essen, Germany) placed above and below the level of the left renal artery. The left kidney was further exposed to 45 minute (min) of warm ischemia by clamping the renal pedicle 5 min after drug administration. Renal-reflow was initiated by releasing the clamp and confirmed by visual inspection. After occlusion, 1 milliliter (mL) of pre-warmed (37°C) saline was placed in the abdominal cavity to prevent dehydration and the wound was closed in two layers by using a 6/0 Mersilene suture (Ethicon, Germany). Left kidneys were harvested immediately after ischemia (0 h reperfusion group) or 2 h post-reperfusion (2 h reperfusion group). Additional rats were allowed to recover (48 h reperfusion group) and animals with uninephrectomy but without I/R served as controls (UniNx group). To mitigate pain and distress, a single injection of diluted buprenorphine (0.1 milligram (mg) per kilogram (kg) per day (d), Gruenthal GmbH, Germany) was administered subcutaneously 5 min prior to reperfusion, and further analgesic management (2.5 mg per 100 mL, tramadol, Bayer, Germany) was applied to the drinking water. Rats were housed in metabolic cages for urine collection over a period of 24 h beginning one day after

surgery. Blood samples were collected by puncture of the V. cava and the remaining left kidneys were harvested 48 h post-reperfusion. The kidneys were washed with ice-cold normal saline (0.9% NaCl), then they were cut into pieces and frozen in liquid nitrogen or formalin-fixed. The surgery in rat was performed by Dr. Mandy Fechner.

### **3.3.2 Mice renal I/R injury model**

Male mice at the age of 10-13 weeks, weighting 25-30 g were used for the experiments. Animals were anesthetized by inhalation of isoflurane (4.5 % for induction, 2.5 % for maintenance) under oxygen flow of 364 mL/min and placed on a heating plate with thermostatic monitor system (TCAT-2, Physitemp Instruments Inc, Clifton, NJ, USA). Body temperature was kept constant in the range of 36.5-37.5°C. Eyes of mice were protected by eye ointment (Bayer, Germany). After removing the coat at the abdomen, the mouse was placed on a horizontal supine position with its limbs fixed by tape. Under aseptic conditions, a 1.5-centimeter (cm)-long midline abdominal incision was made and the incision was extended with wound-hooks. The intestine was carefully pushed aside to achieve access to the right kidney. The pedicle of the right kidney was dissected and then ligated with two fibers of 6-0 silk and carefully harvested. The kidney weight of the right kidney was examined after removal of its capsule. Then the intestine was stored on the other side of the abdomen to allow preparation of the left kidney. Ischemia was induced by applying a non-traumatic vascular clamp (FST, Essen, Germany) to the left renal pedicle for 22 min. Renal-reflow was initiated by releasing the clamp and confirmed by visual inspection. After occlusion, 1 mL of pre-warmed (37°C) saline was placed in the abdominal cavity to prevent dehydration and the wound was closed in two layers by using a 6/0 Mersilene suture. To mitigate pain and distress, a single injection of diluted buprenorphine (0.1 mg per kg per d) was administered subcutaneously 5 min prior reperfusion, and further analgesic management (tramadol 2.5 mg per 100 mL) was applied to the drinking water for 2 d. After suturing, mice were allowed to regain consciousness on a surgical heating pad and then returned to their cages with free access to food and water. One day after the surgery, all animals were set into metabolic cages for urine collection over a period of 24 h. Uni-nephrectomy sham groups underwent identical procedures without clamping of renal pedicle. Mice were sacrificed by exsanguination under deep general anesthesia after 48 hours post-I/R. Blood, urine, and tissue samples were collected 48 h post-I/R. Renal tissues were washed with ice-cold normal saline (0.9% NaCl), cut sagittally into two halves, and then immediately either fixed in 4% paraformaldehyde for paraffin embedding, or snap frozen in liquid nitrogen and stored at -80°C for subsequent mRNA or protein extraction.

### **3.4 Renal function**

Renal functions were evaluated both in rats and mice which suffered ischemia and 48 h reperfusion. Blood was coagulated and centrifuged at 3,500 times gravity ( $\times g$ ) for 10 min to collect serum. The urine was centrifuged at 2,000 $\times g$  for 15 min. Creatinine and urea in serum and urine were determined in the central laboratory (Charité Campus Virchow-Klinikum, Berlin, Germany).

### **3.5 Histology**

#### **3.5.1 Embedding and sectioning**

Formalin-fixed renal specimens were immersed in paraffin using a standard protocol for tissue embedding. The tissues were dehydrated through an ascending series of graded alcohol baths (70, 80, 96, 99 and 100 %) to displace the water, placed in xylol, heated and infiltrated with liquid paraffin (56 °C). Paraffin-blocks were cut into 2-micrometer ( $\mu m$ )-thick sections with a sliding microtome (Leitz 1512, Germany), transferred to microscope slides and dried in an oven at 55-60 °C. For cryo-sections, kidneys were embedded in Tissue-Tek O.C.T. (Sakura, Japan) and cut into 6  $\mu m$  sections. After fixing in pre-cold acetone (- 20 °C) for 20 min, the slides were stored at - 80 °C for further staining.

#### **3.5.2 Hematoxylin and eosin (H&E) staining**

HE staining is routinely used for examination of tissues under light microscope. In brief, paraffin-embedded renal tissue sections were deparaffinized and rehydrated through Roti-clear (3 $\times$ 10 min), 100% ethanol (2 $\times$ 10 min), 95%, 70%, and 50% ethanol and distilled water (each 1 $\times$ 5 min). Then the paraffin sections were stained in a Hematoxylin-Mayer solution for 15 min, subsequently washed under running tap water. The final eosin staining was counterstained with a 0.5 % Eosin Y-solution for 5 min. After re-rinsing with tap water, the slides were dehydrated in an ascending ethanol series (70, 80, 96, 100 and 100%), dipped shortly in Roti-Clear, and coverslipped immediately with xylene-based mounting medium. Cytoplasmic compartments appear in pink and nuclei of cells in blue color.

#### **3.5.3 Periodic acid-schiff (PAS) staining**

PAS staining method is commonly used to highlight molecules with high carbohydrate content in tissues, especially glycogen rich residues. Aldehydes within the polysaccharide structures react with the Schiff reagent to form a purple-magenta chromogen. As suitable counterstaining with contrast rich nuclei haematoxylin was used. For staining, paraffin sections were deparaffinized as

described in point 3.5.2 and then immersed in 0.5% periodic acid solution for 5 min. Subsequently, the chromogenic complex formation was exposed in Schiff's reagent for 15 min and followed by Mayer's hematoxylin for 1min. Stained sections were then dehydrated and coverslipped using a synthetic mounting medium.

### **3.5.4 Acute tubular necrosis (ATN) score**

Morphologic criteria were examined for assessment of tubular lesions in HE- and PAS- stained renal paraffin-embedded sections. To assess tubulointerstitial injuries, ten randomly selected fields of view (FoV) (400×) of each renal section were analyzed and counted using ATN score. In rats, ATN score was graded from 0 to 3 corresponding to none, mild, moderate, or severe necrosis as described previously [68]. However, the severity of renal morphologic criteria in mice was higher than that in rats, therefore to better grade the ATN score in mice, a five-point semiquantitative scale was used for mice. Quantitative analysis was performed under the microscope (Zeiss, Jena, Germany) by calculating the percentage of tubules that displayed tubular cast formation, cell swelling, dilatation and tubular degeneration (loss of brush border, detachment of tubular epithelial cells). The ATN score was graded from 0 to 4 according to the severity of tubular damage (0, no damage; 1, 0-25% damaged tubules; 2, 25-50% damaged tubules; 3, 50-75% damaged tubules; 4, >75% damaged tubules) [69].

### **3.5.5 TUNEL staining**

TUNEL staining was used to investigate tubular epithelial cell apoptosis. DNA fragmentation associated with apoptosis was visualized by In Situ Cell Death Detection Kit, TMR red (Roche Diagnostics GmbH, Mannheim, Germany) according to the manufacturer's instructions. Each section was randomly chosen and evaluated for 10 FoV at 400× magnification under a fluorescence microscope (Zeiss Axio Imager A1, Jena, Germany). Positive staining was quantified using a digital imaging system (Zeiss AxioCam HR with Axiovision 4.4 software) and expressed as the percentage of TUNEL-positive area in FoV.

### **3.5.6 Immunohistochemical staining in rats**

I/R-dependent macrophage infiltration in rat kidneys was assessed by ED1 immunohistochemical staining. Paraffin-embedded renal tissue sections were briefly deparaffinized and rehydrated as described in point 3.5.2. To block endogenous peroxidase, sections were immersed in 0.3% H<sub>2</sub>O<sub>2</sub> for 20 min. Then incubation with CAS solution (Zymed, San Francisco, CA, USA) was carried out for 30 min to block unspecific antibody binding and

followed by incubation with ED-1 primary antibodies (1:50 diluted in phosphate-buffered saline (PBS), Serotec, Oxford, UK) for 1 h at room temperature. After rinsing twice with PBS, the sections were incubated with the horseradish peroxidase-labeled secondary antibody and followed by alkaline phosphatase antialkaline phosphatase complex (Dako, Denmark) for 30 min at room temperature. Visualization was performed using diaminobenzidine (Vector Labs, Burlingame, CA, USA) or amino ethyl carbazole color detection. Negative control was performed by incubation with corresponding isotype controls instead of primary antibody (blank). The number of ED1+ monocyte/macrophages and CD8+ lymphocyte-positive cells was scored in 10 randomly chosen FoV at 400× magnification in cortex and outer medulla. The quantification of positive signals was evaluated as the percentage of macrophage-positive area in FoV.

### **3.5.7 Immunofluorescence staining with renal cryo-sections in mice**

I/R-induced inflammation in mice was analyzed by the detection of monocyte/macrophage infiltration visualized through immunofluorescence labeling. In mice, acetone-fixed frozen renal sections were defrosted and pre-washed with PBS for 15 min at room temperature. Nonspecific binding sites were blocked with 10% bovine serum albumin (BSA) diluted in PBS (blocking solution) for 1 h at room temperature. The immunofluorescence staining was performed using an indirect cocktail method. The mixture of primary antibodies rat-anti-mouse macrophage F4/80 (1:100, Serotec, Oxford, UK) and rat-anti-mouse monocyte CD11b (1:250, clone 1/70, Pharmingen, Oxford, UK) was incubated overnight at 4°C. Slides were washed three times with PBS for 5min, and then incubated with a secondary antibody goat-anti-rat IgG Alexa green 588 (1:1000, Invitrogen, Darmstadt, Germany) for 1 h at room temperature. After washing, nuclear staining was developed with DAPI for 5min and then slides were mounted in an anti-fade mounting medium. Control sections were subjected to secondary antibody only (blank). Images of monocyte/macrophage infiltration were evaluated in 10 randomly chosen FoV at 400× magnification under a fluorescence microscope (Zeiss, Jena, Germany). The quantification of positive signals was evaluated as the percentage of macrophage-positive area in FoV.

### **3.5.8 Immunofluorescence staining with renal paraffin sections in mice**

The location of Cyp4a12a in mouse renal sections was analyzed using an affinity purified antibody (1:200, provided by Dr. Schunck) raised in rabbits against a Cyp4a12a-specific peptide [70] without or after pre-saturation with the corresponding synthetic peptide. A goat anti-rabbit IgG Alex Red 568 conjugate (1:1000, Vector Labs, Burlingame, CA, USA) served as secondary

antibody. Paraffin-embedded renal sections were deparaffinized and rehydrated briefly, then permeabilized with citrate acid buffer (0.1 molar (M), PH 6.0) in a pressure cooker for 3 min. To block unspecific antibody binding, sections were incubated with 10% BSA diluted in PBS (blocking solution). The incubation steps for primary antibody and secondary antibody were as described in point 3.5.7. After washing, DAPI staining for 5 min at room temperature was used to visualize nuclei. Sections were mounted in anti-fading mounting medium. The intrarenal localization of Cyp4a12a was observed under a fluorescence microscope at a 200× magnification.

### 3.6 DNA isolation and genotypic analysis

Tail biopsies ( $\leq 3$  millimeter (mm)) were obtained for genotypic confirmation. For extracting genomic DNA from the tissue, biopsies were incubated at 55 °C overnight in a 100  $\mu$ L mixture volume of proteinase K (1 mg/mL) and lysis buffer (Tris/HCl (pH 8.5) 100 millimolar (mM), EDTA 5 mM, NaCl 200 mM, SDS 0.2%). The inactivation of the proteinase K was carried out by heating at 95 °C for 5 min. To degrade the RNA, 750  $\mu$ L of a mixture of TE buffer (Tris/HCl (pH 8.0) 10mM, EDTA 1 mM) and RNase A (20  $\mu$ g/mL) was added into the reaction. Samples were amplified with sEH specific primers for polymerase chain reactions (PCR)-based genotyping. The PCR products were separated on 2% agarose gel by using TAE buffer at 100 voltage (V) for 30 min and visualized under UV light after staining with GelRed<sup>TM</sup> (Biotium, Hayward, CA, USA). The primer sequences and PCR protocol are shown in Table 3 and Table 4 respectively.

**Table 3: Genotyping primer sequences**

(BioTez, Berlin-Buch GmbH, Germany)

<b>sEH genotyping</b>	SEPOH 5'	5'-CCACCTACCTTGTGCTTGCC-3'
	SEPOH 3'	5'-GGGAAGAGGGGAAGGATTGT-3'
	LTR2	5'-AAATGGCGTTACTTAAGCTAGCTTGC-3'

**Table 4: Components and conditions of genotyping PCR**

Components			Conditions		
Component	1×	Concentration	Temperature [°C]	Time	Cycle
ddH <sub>2</sub> O	6	-	95	3 min.	40
Mix buffer	10	2×	95	30 s.	
Primer Mix	3	10nM	55	30 s.	
DNA-Probe	1	250ng	72	45 s.	
			72	5 min.	

## 3.7 Gene-expression analysis

### 3.7.1 Total RNA extraction and cDNA synthesis

Total RNA (a mixture of ribosomal RNA (rRNA), transfer RNA (tRNA) and messenger RNA (mRNA)) was extracted with the Qiazol RNeasy Micro kit including DNase digestion (Qiagen, Hilden, Germany) according to the manufacturer's instructions. The concentration of isolated RNA was measured spectrophotometrically by using a NanoDrop 100 (ND1000, Thermo Fisher Scientific Rockford, USA) against a blank (nuclease-free water). The quality of the isolated RNA was verified by running a non-denaturing agarose gel electrophoresis. The total RNA was loaded on 1% agarose gel (stained with ethidium bromide) by using TBE buffer at 100 V for 90 min and visualized under UV light. Two intensive bands representing 28S and 18S rRNA could be observed against a light smear. The intensities of these rRNA bands on denaturing agarose gel were used to calculate a ratio that served as an indication of RNA integrity. A 28S/18S ration of two is considered to be good quality RNA. Afterwards, 1000 nanogram (ng) of total RNA was used for complementary DNA (cDNA) synthesis with a High-Capacity cDNA Reverse Transcription kit (Applied Biosystems, Foster City, CA, USA) according to the manufacturer's instructions. The reverse transcription conditions are shown in Table 5.

**Table 5: Components and conditions of reverse transcription**

Components			Conditions	
Component	1×	Concentration	Temperature	Time
10× RT Buffer	2.0	1×	25	10
25× dNTP Mix (100 mM)	0.8	1×	37	120
10× RT Random Primers	2.0	2×	85	5
MultiScribe™	1.0	1×	4	∞
Nuclease-free H <sub>2</sub> O	4.2	-		
Total-RNA Probe	10	1000 ng		

### 3.7.2 Quantitative real time PCR (qRT-PCR)

The investigation of gene expression at the mRNA level was carried out by TaqMan method. The relative amount of gene transcript was calculated by using the standard curve method. Briefly, all the nucleic acid samples were pooled into a tube. A blank (non-template control) and a standard series (the dilutions of the pool containing different amounts of RNA with 1.25 ng, 2.5 ng, 5 ng, 10 ng and 20 ng respectively) were used for relative standard curve analysis. Specific oligonucleotide primers for mouse Ephx2, Cyp4a10, Cyp4a12a, Cyp4a12b, Cyp4a14, kidney injury molecule-1 (KIM-1), neutrophil gelatinase associated lipocalin (NGAL), cyclooxygenase 1 (COX1), 5 $\alpha$ -reductase 1 (Srd5 $\alpha$ 1), Srd5 $\alpha$ 2, and  $\beta$  glucuronidase (Gusb) were

used for quantitative real time PCR on a ABI 7500 Fast Real Time PCR system (Applied Biosystems, Foster City, CA, USA). Each amplification reaction was performed in duplicate. The number of PCR cycles (Ct) was determined by using ABI PRISM® Sequence Detection System software to identify the point on the amplification plot at which the intensity value exceeds the threshold. The fractional cycle at which the intersection occurred and showed statistically significant increase in the fluorescence is defined as the Ct value. The Ct value of each experimental sample was first calculated with the relative standard curve. Final results were normalized on glyceraldehyde 3-phosphate dehydrogenase (GAPDH) or 18s. The primer sequences shown in Table 6 were synthesized by BioTez, Berlin-Buch GmbH, Germany. Other primers and probes (COX1, Srd5α1, Srd5α2, Cyp19a1 and Gusb) were purchased from Applied Biosystems, Foster City, CA, USA. Table 6 shows the primer sequences and Table 7 shows the components and the qRT-PCR protocol.

**Table 6: Primer Sequences**

Gene	Description	Primer Sequence ( 5'→ 3' )
<b>KIM-1</b>	forward	CTGGAGTAATCACACTGAAGCAATC
	reverse	GATGCCAACATAGAAGCCCTTAGT
	probe	Fam- CTCCAGGGAAGCCGCAGAAAAACC-Tamra
<b>NGAL</b>	forward	TGATCCCTGCCCCATCTCT
	reverse	GGAAGTATCGCTCCGGAA
	probe	Fam-TCACTGTCCCCCTGCAGCCAGA-Tamra
<b>Cyp4a12a</b>	forward	GCC TTA TAC GGA AAT CAT GGC A
	reverse	TGG AAT CCT GGC CAA CAA TC
	probe	6-Fam-ACT CTG TTC GTG TAA TGC TGG ATA AAT GGG AA-CCT TAT ACG GAA ATC ATG GCA GA
<b>Cyp4a12b</b>	forward	CCT TAT ACG GAA ATC ATG GCA GA
	reverse	TGG AAT CCT GGC CAA CAA TC
	probe	6-Fam TCT GTT CAT GTC ATG CTG GAT AAA TGG GAA-Tamra
<b>Cyp4a10</b>	forward	TCT CTG CTC TAA GCC CAA CC
	reverse	CGA GCA CAG AGG CCA CTT G
	probe	6-Fam TTT GCA GAC AGC CTC TCT GGC TTC CT-Tamra
<b>Cyp4a14</b>	forward	GAC CCT CCA GCA TTT CCC A
	reverse	TCC TTG TCC TTC AGA TGG TGC
	probe	6-Fam CAT GCC TTC CCA CTG GCT TTG GG-Tamra
<b>Ephx2</b>	forward	CCA TAA GTC AAA TAT TCA GCC AAG CT
	reverse	ATG CTT CAG GCA GCC ATT G
	probe	TGG CAG CAA GAA GCA TCA ACC GC
<b>GAPDH</b>	forward	AAGCTGGTCATCAATGGGAAAC
	reverse	ACCCCATTTGATGTTAGCGG
	probe	CATCACCATCTTCCAGGAGCGCGGAT
<b>18s</b>	forward	ACATCCAAGGAAGGCAGCAG
	reverse	TTTTCGTCACTACCTCCCCG
	probe	Fam-CGCGCAAATTACCCACTCCCGAC-Tamra

**Table 7: Components and conditions of qRT-PCR**

Components			Conditions		
Component	1×	Concentration	Temperature	Time	Cycle
20× TaqMan® Gene Expression	1	1×	95	3	40
2× TaqMan® Gene Expression	10	2×	95	30 s.	
RNase-free water	5	-	55	30 s.	
Primer sense	1	150 nM	72	45 s.	
Primer antisense	1	150 nM	72	5	
Dye-labeled TaqMan Probe	1	250 nM			
cDNA Probe	1	±10 ng/μl			

### 3.8 Enzyme linked immunosorbent assay (ELISA) in mice

The concentration of urinary calprotectin was quantified by using an ELISA kit (PhiCal® Calprotectin, Immundiagnostik AG, Bensheim, Germany) according to the manufacturer's protocols. The colorimetric reaction was determined with an ELISA reader (Microplate photometer, Multiscan Ascent 354, Thermo Scientific) at 450 nm. The tests were carried out in duplicate and the results were expressed as nanogram/deciliter (ng/dL). In order to take the current concentration status of the urine into account, creatinine was assessed in the urine and used for urinary calprotectin/creatinine ratio calculation. Each determination was performed in triplicate. The calprotectin-assay was performed in the lab of Dr. Timm H. Westhoff.

### 3.9 Western blot analysis

Snap-frozen tissues were immersed into ice-cold RIPA lysis buffer containing protease and phosphatase inhibitors. The homogenization was carried out immediately by using mechanical tissue disruptor (FastPrep-24, M.P. Biomedicals, California, USA) twice for 20 seconds at 6000 vibrations per min. Subsequently, the samples were incubated with 6.5 μL of 10% SDS solution on ice for 30 min, and then centrifuged at 14,000×g, 4 °C for 15 min to eliminate the tissue debris. Protein concentrations were determined by using the BioRad DC™ (BioRad, Denmark) protein assay in triplicates and calculated with a standard curve (a range of 0 to 2 μg/μL BSA diluted in the same lysis buffer). Lysates (50 μg of protein per lane) were prepared according to a standard protocol (Laemmli, 1970) and denatured with a reducing condition at 95 °C for 5 min. Samples were loaded respectively into the wells of pre-cast 10% sodium dodecyl sulfate-polyacrylamide gel electrophoresis (SDS-PAGE) gels (Table 8). A Protein Marker VI (5 μl, AppliChem, Darmstadt, Germany) was applied to verify the size of the proteins. Recombinant Cyp4a12a protein was loaded as positive control. For better focusing of the protein bands,

electrophoresis was started with a voltage of 80 V for 30 min and further separation was achieved at 120 V for 1.5 h.

**Table 8: Tris-glycin-gel system**

10% Separation gel		5% Stacking gel	
Component	Volume (10ml)	Component	Volume (3.5ml)
H <sub>2</sub> O	4.0 ml	H <sub>2</sub> O	2.1 ml
30% Acrylamide Mix	3.3 ml	30% Acrylamide Mix	500 µl
Tris 1,5M pH 8,8	2,5 ml	Tris 1,0MpH 6,8	380 µl
10% SDS	100 µl	10% SDS	30 µl
10% -APS	100 µl	10% -APS	30 µl
TEMED	10 µl	TEMED	5 µl

Subsequently the proteins were transferred to methanol-activated PVDF membranes (GE Healthcare, Amersham, UK) with a semi-dry transfer chamber (SD-10, Kisker Biotech GmbH, Steinfurt, Germany) at 0.45 milliamper (mA) for 1.5 h. Afterwards, membranes were blocked with 5% (weight/volume) BSA in Tris-buffered saline containing 0.1% Tween-20. Primary antibodies (Table 9) were allowed to bind overnight at 4 °C. Thereafter, the membranes were washed three times and then incubated with a secondary antibody for 1 h at room temperature. Chemiluminescent detection and image analysis were performed with ECL substrate (SuperSignal West Pico/Dura, Thermo Scientific, Rockford, IL, USA) and G:BOX Chemi XL 1.4 imaging system (Syngene, Cambridge, UK).

**Table 9: Antibodies for western blot**

Antibody	Manufacturer	kDa	Dilution
<b>Primary antibody</b>			
Anti-sEH, rabbit, polyclonal	Dr. Schunck	55	1:1000
Anti-aromatase, rabbit, polyclonal	Cayman	60	1:1000
Anti-Cyp4a12a, rabbit, polyclonal	Abcam	58	1:1000
Anti-GAPDH, mouse, monoclonal	Hyttest	38	1:20000
<b>Secondary antibody</b>			
Peroxidase-conjugated AffiniPure Donkey Anti-Mouse IgG	Dianova		1:25000
Peroxidase-conjugated AffiniPure Donkey Anti-Rabbit IgG	Dianova		1:15000

### 3.10 Eicosanoid determination in mice and rats

#### 3.10.1 Tissue endogenous CYP-eicosanoid profile estimation in mice

Native kidneys and livers of mice were transferred individually into the mortar and the corresponding stamp mash (Cryo Pulverizer, BioSpec. Products Inc., USA) and minced into powder (2-3 hammer blows to the punch). Aliquots (30 µg of protein per lane) of homogenized tissue were mixed with 1000 µL of methanol:water 50:50 including 0.005% BHT, and 10 µL of

internal standard containing 10 ng of 20-HETE-d6, 10 ng of 14,15-EET-d8, and 10 ng of 14,15-DHET-d11 in acetonitrile. The samples were hydrolyzed after adding 300  $\mu$ L NaOH (10 M) for 30 min at 60°C. Then the solution was neutralized by adding 290  $\mu$ L of 58% acetic acid and 2 mL of SPE buffer (Sodium acetate 0.1M, Methanol 5%, pH 6.0 adjusted with acetic acid), vortexed for 15 s and centrifuged at 2000 $\times$ g at 4°C for 15 min. The pellet was washed with 1000  $\mu$ L of methanol:water 50:50, vortexed, and then 2000  $\mu$ L of SPE buffer was added. After vortexing and centrifugation again, the pH value of the collected supernatant was adjusted to 5.9-6.1 by using small volumes of 58% acetic acid. Subsequent solid-phase extraction was performed using Bond Elut Certify II columns (200 mg, Varian Inc., CA, USA), which were preconditioned with 3 mL of methanol and 6 mL of SPE buffer before applying the hydrolyzed samples. The columns were washed with 3 mL of methanol:water 50:50 and dried for 5-10 min. The CYP-metabolites and internal standards were eluted with elution buffer containing hexane:ethyl acetate:acetic acid 75:25:1 and evaporated under a continuous stream of nitrogen. Residues were then dissolved in 100  $\mu$ L of methanol:water 50:50 and transferred into glass vials. The analysis of the samples was carried out by liquid chromatography tandem mass spectrometry (LC-MS/MS, Lipidomix GmbH, Berlin, Germany) as described previously [71]. Results are given in ng metabolites per g organic wet weight.

### **3.10.2 Plasma endogenous CYP-eicosanoid profile estimation in mice**

WT and sEH-KO mice of the native group were pre-treated with heparin through intraperitoneal injection. Whole blood was collected by cardiac puncture and centrifuged for 15 min at 2,000 $\times$ g for plasma-extraction. 200  $\mu$ L of plasma sample was transferred into a centrifuge tube, filled with 750  $\mu$ L of methanol, 300  $\mu$ L of 10 M NaOH and 10  $\mu$ L of the internal standard (10 ng 20-HETE-d6, 10 ng 14,15-DHET-d11, and 10 ng 14,15-EET-d8). This mixture was saponified for 30 min at 60°C, neutralized with 290  $\mu$ L 58% sodium acetic acid, then vortexed with 2 mL of SPE buffer and centrifuged for 15 min at 2000 $\times$ g 4°C twice. The pH of the supernatant was adjusted to 5.9-6.1 by adding small volumes of 10% acetic acid. The solid-phase extraction of plasma samples was performed as described in section 3.10.1. Results are shown as ng metabolites per mL plasma.

### **3.10.3 Tissue endogenous CYP-eicosanoid profile estimation in rats**

The left kidneys of rats were subjected to 45 min of warm ischemia and removed either immediately (0 h reperfusion) or after a subsequent 2 h reperfusion phase. The EET analog was quantified simultaneously, extending the multiple reactions monitoring protocol to include the

transition of its parent ion to the diagnostic fragment ion (339.3→238) at collision energy of 8 V. To differentiate between esterified and free metabolites, the samples were extracted with or without prior alkaline hydrolysis. Unlike the preparation of the total metabolites, for the free metabolites the solvent used in the initial extraction step (methanol:water 50:50) contained 2 mM Zn<sub>2</sub>SO<sub>4</sub> to block the sEH activity in the renal samples. This is necessary to protect free EETs and the corresponding internal standard from hydrolysis during the extraction procedure. Solid phase extraction and quantification of 20-HETE and EETs was performed as described in section 3.10.1. The amounts of 20-HETE, 5,6-, 8,9-, 11,12- and 14,15-EET and the corresponding regioisomeric DHETs in the renal samples were calculated from respective calibration curves. Results were presented as ng 20-HETE, EETs (sum of the four regioisomeric EETs) or DHETs (sum of the four regioisomeric DHETs) per g kidney wet weight. This experiment in rats was performed by Maximilian Blum.

### **3.11 Determination of sEH enzyme activities in mice**

#### **3.11.1 Preparation and protein quantification of cytosolic fraction**

Renal or liver cytosolic fractions were prepared using freshly dissected organs of 10-12 week-old male WT and sEH-KO mice from native groups. The renal capsule and fatty tissue were removed. Kidneys or livers were minced and homogenized in 5 vol. of ice-cold 50 millimolar (mM) Tris/HCl buffer (pH 7.4) containing 0.25 M sucrose, 150 mM potassium chloride, 2 mM EDTA, 2 mM dithiothreitol, 1 micromolar (μM) FAD, FMN, and 0.25 mM PMSF in a motor-driven Teflon/glass Potter-Elvehjem homogenizer (Potter S, Braun, Germany). Supernatant (cytosolic fractions) was aliquoted after differential centrifugation procedure (10 min, 1000×g; 20 min, 10000×g; 90 min, 100000×g). The protein content of given samples, either renal or liver cytosolic supernatants, was estimated by using the standard Lowry method in duplicate. The quantification of the amount of protein was based on an absorbance measurement at 750 nm against a blank. The samples were pre-diluted 1:10 with 0.1 M NaOH to the total volume of 200 μL and incubated with 1 mL of Lowry assay buffer for 10 min. After adding 0.1 mL of Folin reagent, the samples were incubated for 30 min with subsequent photometric measurement. The entire process was carried out at room temperature. The absorbance of the Lowry reaction was determined for BSA protein (100 μg/mL), which was used as a calibration standard to determine the protein concentrations of unknown samples.

#### **3.11.2 sEH activity assessment**

sEH activities were determined in renal and hepatic cytosolic fractions (10000×g supernatants) obtained as described above (3.11.1). The assay was performed at 37 °C for 20 min in a final volume of 100 µL potassium phosphate buffer (0.1 M, pH 7.2) containing 50 µM 14,15-EET (Cayman Chemicals, Ann Arbor, USA) as substrate. The reactions were started by adding cytosolic fraction (3.5 µg of protein) and terminated by adding 300 µL acetate. After vortexing and centrifuging at 13000×g for 1 min, the supernatants were collected and evaporated under a continuous stream of nitrogen. Residues were dissolved in 50 µL of ethanol and transferred into glass vials. The remaining substrate and its product (14,15-DHET) were extracted and analyzed by reversed-phase high performance liquid chromatography (RP-HPLC) [70].

### **3.12 Evaluation of testosterone and dihydrotestosterone (DHT) in mice**

Approximately 50 mg of each snap-frozen kidney tissue from native groups was used for the organic extraction of testosterone and DHT [72]. Samples were homogenized with 1 mL of methanol by using mechanical tissue disruptor twice for 20 s at 6000 vibrations per min. An internal standard, 1 µL of testosterone stearate (1ng/µL) was added to correct for losses during experimental processing. After adding 2 mL of chloroform and 1 mL of water, the suspension was mixed thoroughly and clarified by centrifugation at 1600×g for 10min. The bottom organic layer was removed with a Pasteur pipette into a new tube. The aqueous layer with the tissue residue was extracted again with 2 mL of chloroform. Afterwards, the organic extracts were combined, evaporated under a continuous stream of nitrogen to remove all traces of alcohol. The residues were dissolved in 100 µL of acetonitrile and transferred into glass vials. In addition, 100 µL of serum was used for serum testosterone and DHT measurement. Further analysis was performed by using an LC-MS/MS device at Lipidomix GmbH, Berlin, Germany.

### **3.13 Statistics**

Statistical analysis was performed by using GraphPad Prism 5 software (GraphPad Inc., La Jolla, USA). Prior to carrying out any test on continuous data, the normalcy of data was tested by one-sample Kolmogorov-Smirnov test. Two-tailed t-test was used for comparing the difference between the mean of two different groups if data were normally distributed. If data were not found to be normally distributed, the Mann-Whitney U-test was used to test the level of significance between two values. Following normal distribution confirmation and Bartlett's test to confirm equality of variances, the significance of variability among multi groups was evaluated by one-way ANOVA with a Bonferroni multiple comparison post-test. The Kruskal-Wallis test with Dunns multiple comparison post-test was used instead of one-way ANOVA

analysis when the data were not normally distributed. Linear relations between serum renal function parameters and bio-markers of AKI were performed by Pearson correlation analysis. All results were expressed as mean  $\pm$  standard error of mean (SEM). P<0.05 (\*), <0.01 (\*\*), and <0.001 (\*\*\*) were considered as statistically significant.

## 4. RESULTS

Major questions to be addressed in this work were EETs dependent functionalities and mechanisms in I/R-induced AKI. The ischemic AKI model was established using uninephrectomy and contralateral I/R, which partially mimics the situation after renal transplantation. In the present study, EET analog administration in rats and sEH gene deletion in mice were used to establish higher systemic levels of the CYP-dependent eicosanoids (EETs) prior to experimental AKI. Kidney damage and changes in CYP-dependent eicosanoids under baseline or the condition of I/R-induced AKI were evaluated at different time points during the study. The details of this study which was performed in EET analog pre-treated rats or sEH-KO mice in experimental ischemic AKI are showed in Figure 9 and Figure 10.

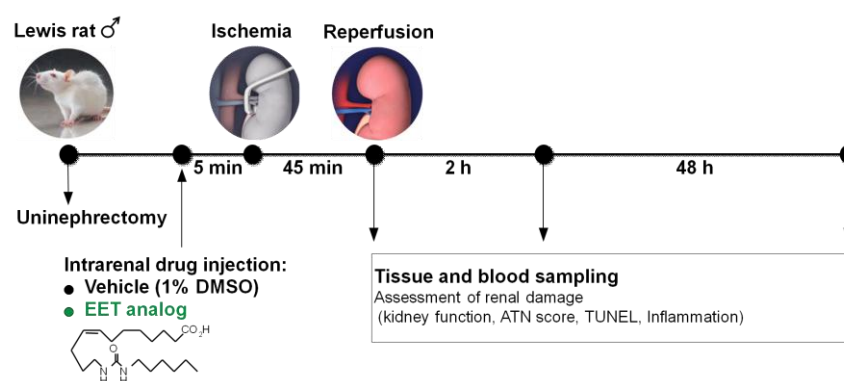


**Figure 9: Role of EET analog administration in rats in I/R-induced AKI**

Figure 9 shows relevant treatments, interventions and examinations of the rat experiment. The CYP-eicosanoids were detected in native group, 0 h reperfusion group, and 2 h reperfusion group, whereas the characterization of the pathological phenotype (kidney function, ATN score, TUNEL and inflammation evaluation) was performed in rats of UniNx group and 48 h reperfusion group.

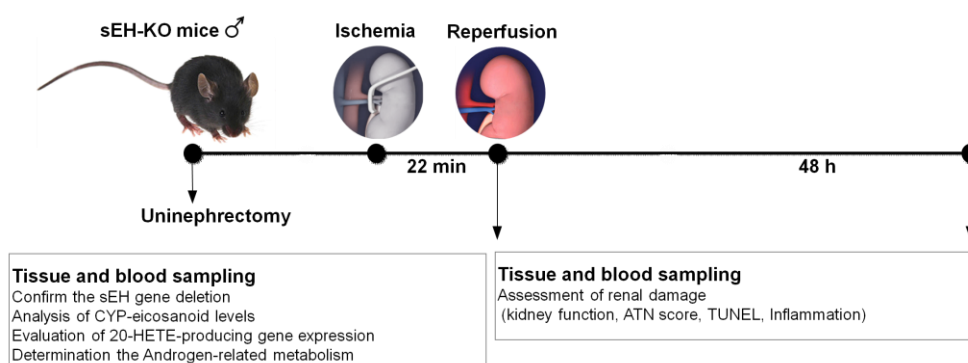


**Figure 10: Role of sEH gene deletion in mice in I/R-induced AKI**

Figure 10 shows relevant treatments, interventions and examinations of the mouse experiment. CYP-eicosanoids and androgen-related metabolism were analyzed in native animals (no surgery), whereas the detailed characterization of the pathological phenotype was performed in mice which were challenged by surgery (UniNx group: mice underwent right uninephrectomy but without I/R. I/R group: mice with right uninephrectomy and left 48 h reperfusion after ischemia).

## **4.1 Utility of a synthetic EET analog for the prevention of renal I/R-injury in a rat model of AKI**

### **4.1.1 Confirmation of EET analog levels in the kidney**

Following the experimental design summarized in Figure 8, the rats were uni-nephrectomized and the remaining left kidney was pretreated by infusing either vehicle (1% DMSO in saline) or the synthetic EET analog (60  $\mu$ g) 5 min before inducing ischemia. The kidneys were then harvested either immediately at the end of the 45 min period of warm ischemia (0 h reperfusion group) or after a subsequent 2 h reperfusion phase. LC-MS/MS results showed that the EET analog was present in the pretreated kidneys after ischemia in a concentration of about 1500 ng per gram wet weight. Subsequent reperfusion resulted in a rapid washout lowering the intrarenal concentration of the EET analog to less than 5 ng/g after 2 h.

### **4.1.2 Ischemia induced the accumulation of free 20-HETE**

To evaluate the amounts of AA-derived metabolites under I/R stimulation, we measured the renal total and free CYP-eicosanoids in native group and early phase of I/R (0 h reperfusion and 2 h reperfusion) with or without pre-treated EET analog in rats.

Ischemia for 45 min (0 h reperfusion) increased free 20-HETE levels 8-fold in the vehicle group and 11-fold in the EET analog pretreated kidneys (Figure 11b). In contrast, free renal EET levels were not significantly higher in either group after ischemia compared with native controls (Figure 11d). Free DHET levels increased almost 23- and 20-fold upon ischemia but were not significantly different compared with vehicle- and EET analog-pretreated kidneys (Figure 11f). As a net effect, the relative abundance of free 20-HETE and free EETs shifted from about 0.13:1 in native kidneys to 0.7:1 (vehicle group) and 1:1 (EET-analog-pretreated kidneys) during 45 min of warm ischemia. The presence of the EET analog had no significant effect on the ischemia-induced changes in the endogenous CYP-eicosanoid profile compared to the vehicle control.

2 h after reperfusion, the renal levels of free 20-HETE and DHETs strongly declined in both experimental groups compared to the ischemic period (Figures 11b and f). The free EET-levels remained largely unchanged in the vehicle group but were significantly increased by a factor of about 1.6-fold in the kidneys pretreated with the EET analog (Figure 11d). Considering the total levels of renal CYP-eicosanoids, we observed significant reperfusion-induced elevations in

esterified 20-HETE that were most pronounced in the vehicle group (Figure 11a). There were no changes in the total EET and DHET levels (Figure 11c and e).

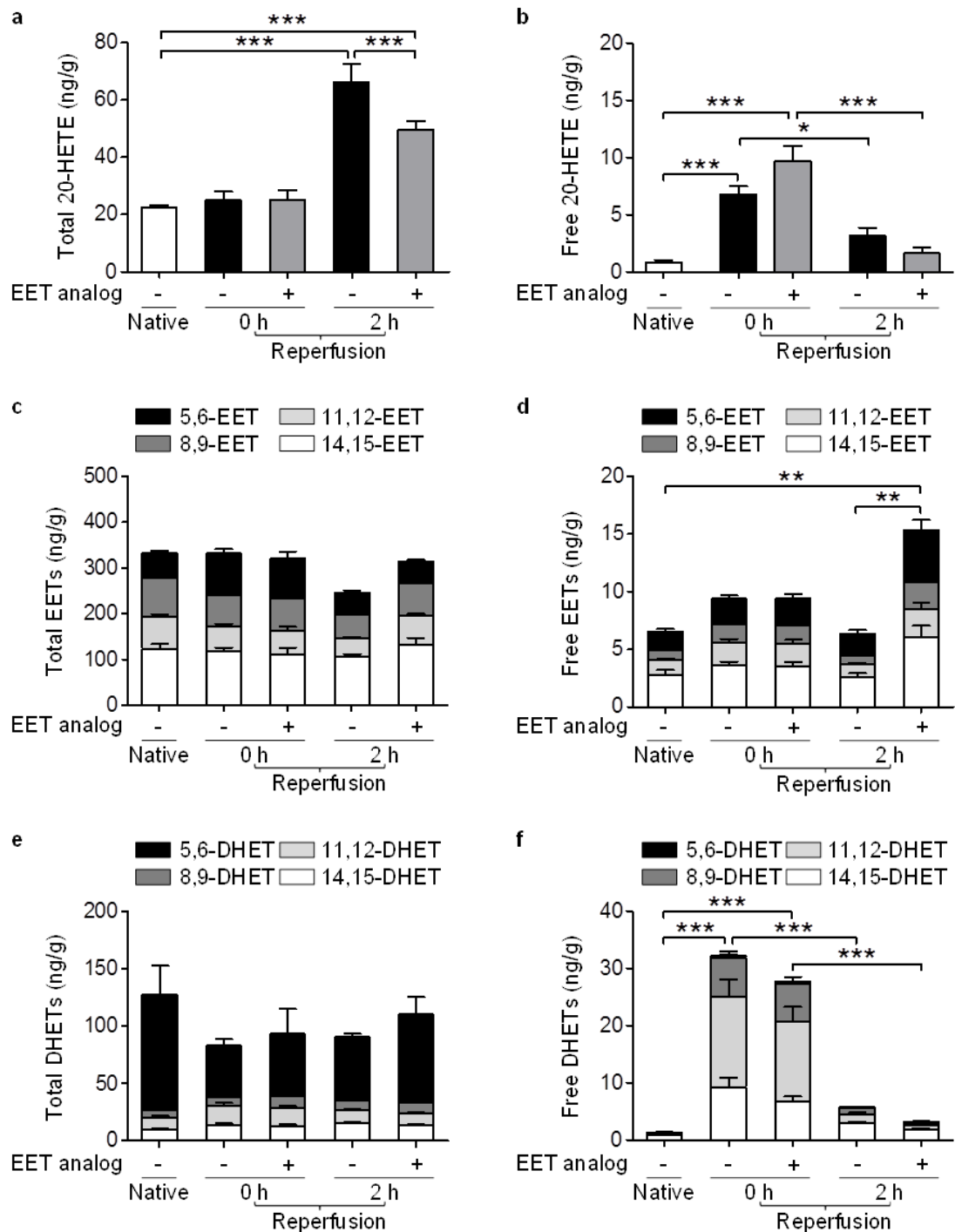


**Figure 11: Ischemia induced the release of 20-HETE but not of EETs in the rat kidney**

Total amounts of 20-HETE (a), EETs (c), and DHETs (e) were determined after alkaline hydrolysis of the kidney samples and represent the sum of membrane-stored (esterified into phospholipids) and free metabolites. Free metabolites (b, d and f) were extracted by treating the kidney samples with methanol without prior hydrolysis. Mean  $\pm$  SEM (n = 5 per group). \*(p<0.05), \*\*(p<0.01), and \*\*\*(p<0.001).

### **4.1.3 EET analog alleviates I/R-induced deterioration of kidney damage 48 h after reperfusion**

The EET analog was administered 5 min prior to induction of ischemia via the renal artery. This single application largely protected against the subsequent development of kidney damage (Figure 12). Animals pretreated with the EET analog featured significantly lower serum creatinine ( $0.61 \pm 0.06$  mg/dL vs. vehicle  $2.41 \pm 0.23$  vs. UniNx  $0.31 \pm 0.01$  mg/dL,  $p < 0.001$ ; Figure 12a) and serum urea levels ( $73.67 \pm 7.65$  mg/dL vs. vehicle  $287.80 \pm 34.81$  vs. UniNx  $37.20 \pm 1.02$  mg/dL,  $p < 0.001$ ; Figure 12b) 48 h after reperfusion. Renal tubular damage was quantified using the ATN score. Severe damage occurred in the vehicle group as indicated by the presence of flattened tubular epithelium, exfoliated tubular epithelial cells, widened tubular lumina, hyaline cast formation, and necrotic tubules. These features were markedly reduced upon pretreatment with the EET analog ( $0.70 \pm 0.11$  vs. vehicle  $2.50 \pm 0.18$  vs. UniNx  $0.08 \pm 0.01$ ,  $p < 0.05$ ; Figure 12c). Pretreatment with the EET analog also had a potent anti-apoptotic effect as quantified by semi-quantitative morphometric evaluation ( $0.26 \pm 0.02$  vs. vehicle  $4.10 \pm 0.24$  vs. UniNx  $0.03 \pm 0.01$  % FoV,  $p < 0.001$ ; Figure 12d) 48 h after reperfusion. Dense infiltration with ED1-positive monocytes/macrophages was observed in the vehicle group 48 h post-ischemia indicating I/R-induced inflammation in the damaged areas of outer medulla. The EET analog significantly repressed inflammatory cell infiltration as shown by morphometric quantification ( $11.5 \pm 2.2$  vs. vehicle  $53.4 \pm 1.5$  vs. UniNx  $3.4 \pm 0.2$  cells per FoV,  $p < 0.001$ ; Figure 12e).

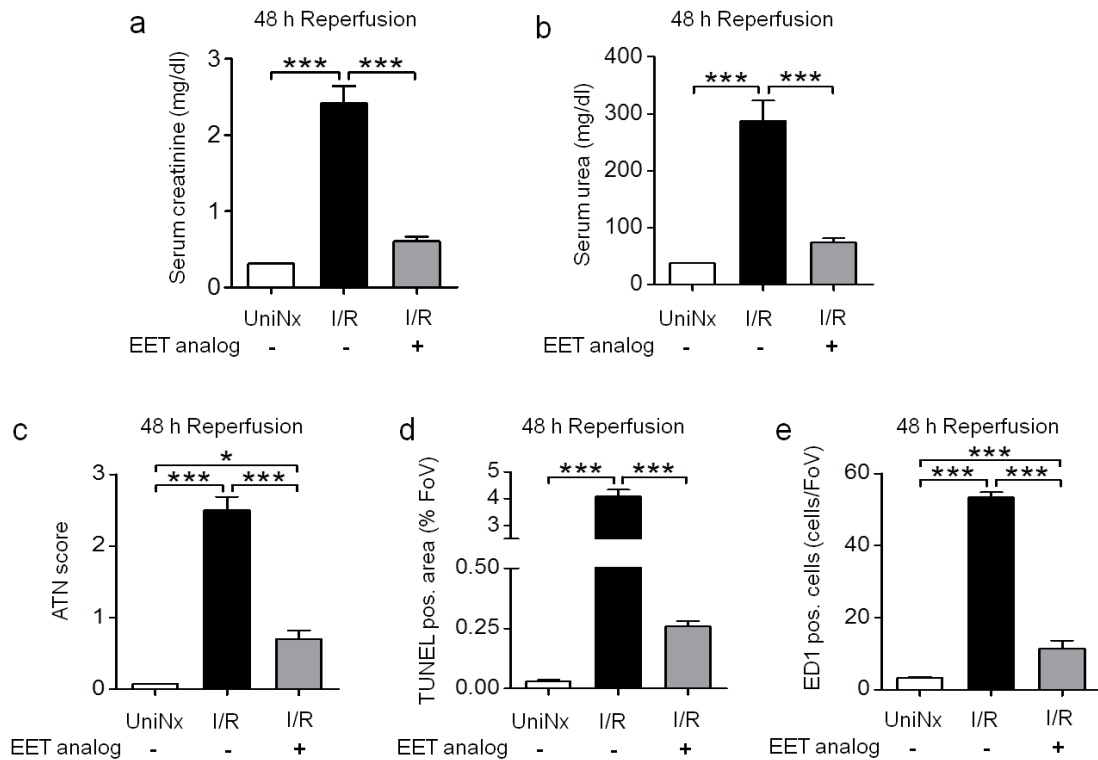


**Figure 12: EET analog greatly alleviates I/R-induced kidney damage 48 h after reperfusion**

Serum creatinine (a) and urea (b) were determined 48 h after reperfusion. Compared to vehicle, EET analog alleviated development of I/R-induced renal function impairment. Quantitative evaluation of ATN score (c), apoptosis (d), and monocyte/macrophage cell infiltration (ED1-positive cells/FoV) (e) show that EET analog treatment significantly attenuates I/R-induced abundant epithelial apoptosis, necrosis and inflammation 48 h after I/R as observed upon vehicle treatment. Mean  $\pm$  SEM (n = 4-6 per group). \*(p<0.05), \*\*(p<0.01).

## 4.2 Effect of sEH gene deletion on I/R-induced AKI in mice

### 4.2.1 Confirmation and initial characterization of sEH-KO mice

#### 4.2.1.1 Genotyping

To confirm the deletion of sEH, genotyping of DNA isolated from tail biopsies (2mm) was performed by PCR analysis. The band with a larger size of 308-base pairs (bp) corresponds to a genomic product of sEH WT allele, whereas the band at 230-bp served as a marker for the mutated sEH-KO allele (Figure 13).

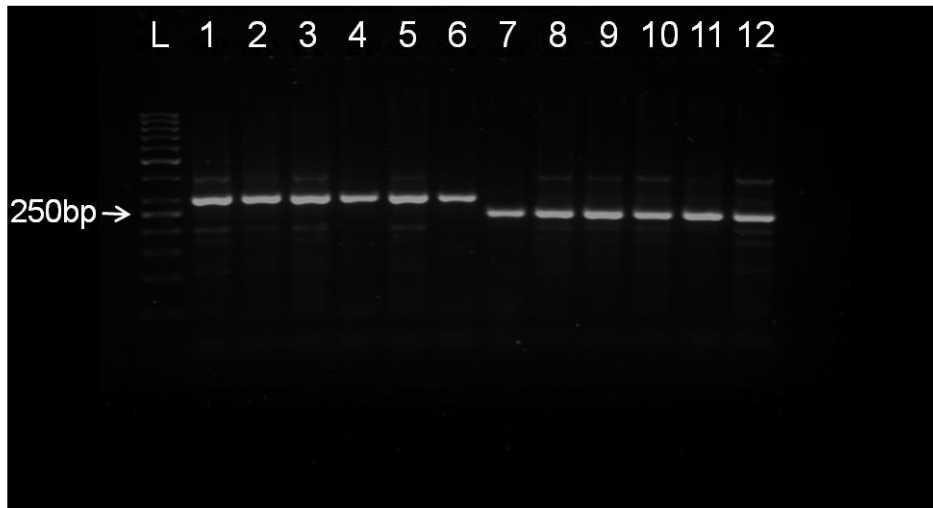


**Figure 13: PCR analysis of genomic DNA from mouse-tail biopsy**

Representative image showing the WT and sEH-KO alleles from genotyping PCR analysis. Lane 1 represents the DNA ladder (50bp). The genotype-specific PCR products had a size of 308bp (homozygous WT, lanes 2-6) and 230 bp (homozygous sEH-KO mice, lanes 7-12).

#### 4.2.1.2 The basal mRNA and protein level of sEH in mice

To further investigate the successful deletion of the sEH gene, mRNA transcripts were measured with qRT-PCR. GAPDH was used as the internal control to account for differences in amplification efficiency and starting amount of mRNA. Gene expression of sEH was calculated by means of a relative standard curve and was only detectable in WT but not in sEH-KO mice (Figure 14a). To confirm that abolished sEH mRNA expression was followed by a corresponding lack of sEH protein, homogenates from the liver and kidney were prepared and analyzed by western blot. Immunoblotting with an sEH-specific antibody indicated that sEH-KO lacked the expression of sEH at protein level both in kidney and liver (Figure 14b).

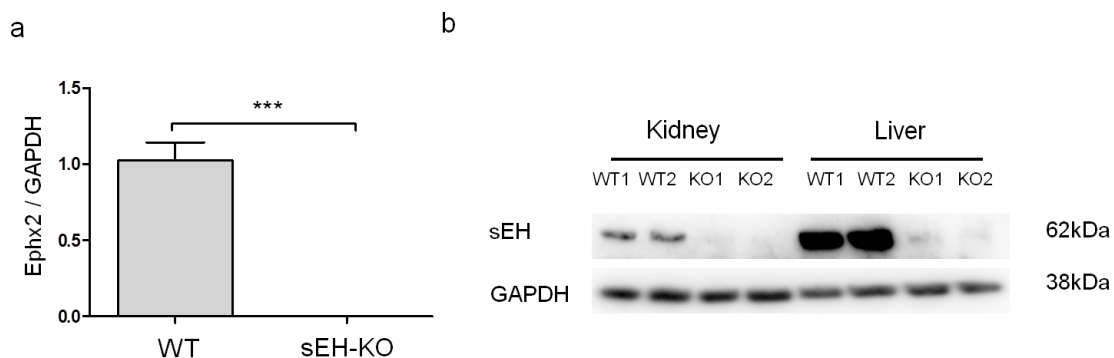
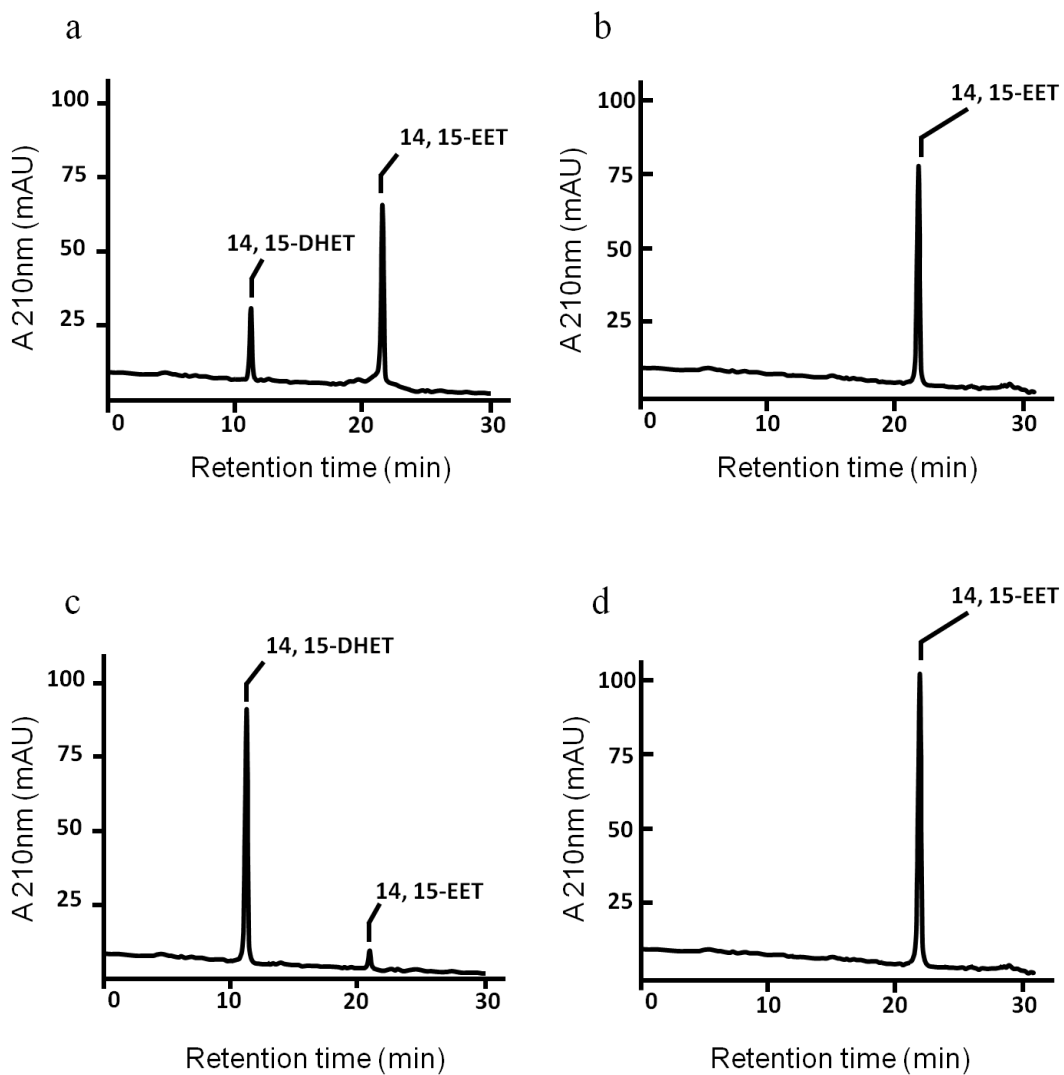


**Figure 14: Confirmation of abolished sEH-expression in sEH-KO mice**

a: qRT-PCR revealed abolished sEH mRNA expression in the kidney of sEH-KO mice. Mean  $\pm$  SEM (n=8 per group). \*\*\* p<0.001 vs WT. b: In accordance with PCR data, polyclonal antibodies raised against recombinant mouse sEH recognized a 62 kDa protein band in the kidney and liver samples of WT but not sEH-KO mice.

### 4.2.1.3 sEH activity

The evaluation of renal and hepatic sEH activities was performed using 14, 15-EET as natural substrate and measuring its conversion to 14, 15-DHET by RP-HPLC. The peaks of 14, 15-DHET and 14, 15-EET emerged at 11 min and 22 min, respectively. Cytosolic fractions prepared from organs of WT mice metabolized 14, 15-EET with hydrolase activities of about 20 (kidney) and 60 nmol/min/mg (liver). In contrast, 14, 15-EET hydrolysis was not catalyzed by any of the corresponding samples derived from homozygous sEH-KO mice (Figure 15). Taken together, these results confirmed that sEH gene disruption resulted in a complete loss of functional sEH expression.



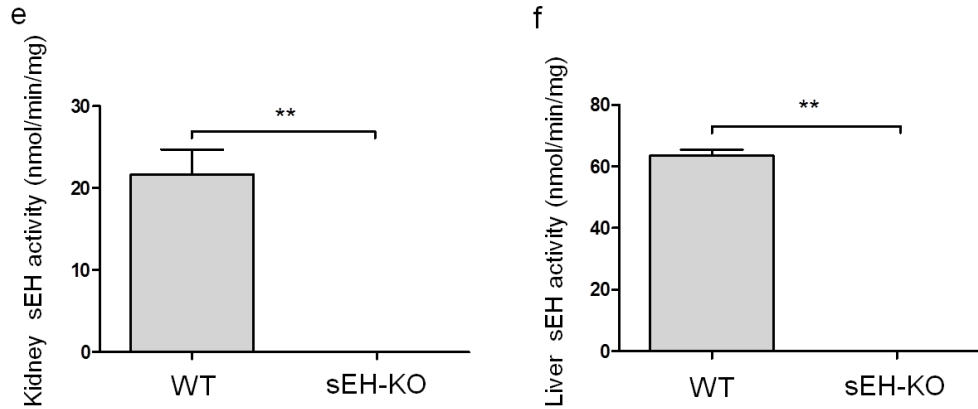


**Figure 15 : sEH activity determination**

Representative HPLC chromatograms showing the metabolism of 14,15-EET to 14,15-DHET by cytosolic fractions prepared from kidney and liver of WT (a and c) and sEH-KO (b and d) mice. sEH activity in renal (e) and liver (f) cytosolic fractions from sEH-KO and WT mice revealed complete loss of activity by gene knock out. Mean $\pm$  SEM (n=6 per group). \*\* p<0.01 vs WT.

#### 4.2.1.4 Baseline renal characterization of sEH-KO mice

Renal phenotype of sEH-KO mice at baseline was characterized by the use of age, kidney weight (right kidney harvested from uninephrectomy), body weight (before surgery), and kidney-to-body weight ratio (n= 5-8 per group). There was no significant difference between sEH-KO and WT mice under basal conditions (Table 10). These data indicated that sEH-KO kidneys were anatomically and functionally normal at baseline.

**Table 10: Baseline renal characterization of sEH-KO mice**

Group	Age (week)	Kidney Weight (mg)	Body Weight (g)	Kidney/Body Weight(mg/g)
WT UniNx	11.88 $\pm$ 0.30	194.80 $\pm$ 9.92	28.14 $\pm$ 0.85	6.90 $\pm$ 0.15
WT I/R	12.38 $\pm$ 0.26	201.80 $\pm$ 4.81	28.69 $\pm$ 0.41	6.91 $\pm$ 0.15
sEH-KO UniNx	11.00 $\pm$ 0.33	184.70 $\pm$ 8.13	26.11 $\pm$ 0.60	7.06 $\pm$ 0.20
sEH-KO I/R	11.50 $\pm$ 0.33	185.70 $\pm$ 4.40	26.21 $\pm$ 0.68	7.06 $\pm$ 0.22

Data was given as Mean $\pm$  SEM (n=8 per group)

## 4.2.2 sEH gene disruption aggravated I/R-induced kidney damage

### 4.2.2.1 sEH gene disruption aggravated I/R-induced decline of renal function

In our ischemic AKI mouse model, animals underwent UniNx and were subjected to 22 min of contralateral renal pedicle clamping followed by 48 h reperfusion (Figure 10). One day after the surgery, all animals were kept in metabolic cages for urine collection over a period of 24 h. Blood and urine were collected 48 h after I/R. Ischemia induced a 3.5 fold increase of serum

creatinine (Figure 16a) and 5.5 fold rise of serum urea (Figure 16b) in WT compared to sham-operated UniNx controls. Surprisingly, the impairment in renal function was significantly aggravated in sEH-KO mice compared to WT animals (creatinine:  $2.54 \pm 0.20$  vs  $1.42 \pm 0.12$  mg/dL,  $p < 0.001$ ; urea:  $562 \pm 30$  vs  $404 \pm 14$  mg/dL,  $p < 0.001$ ; Figure 16).

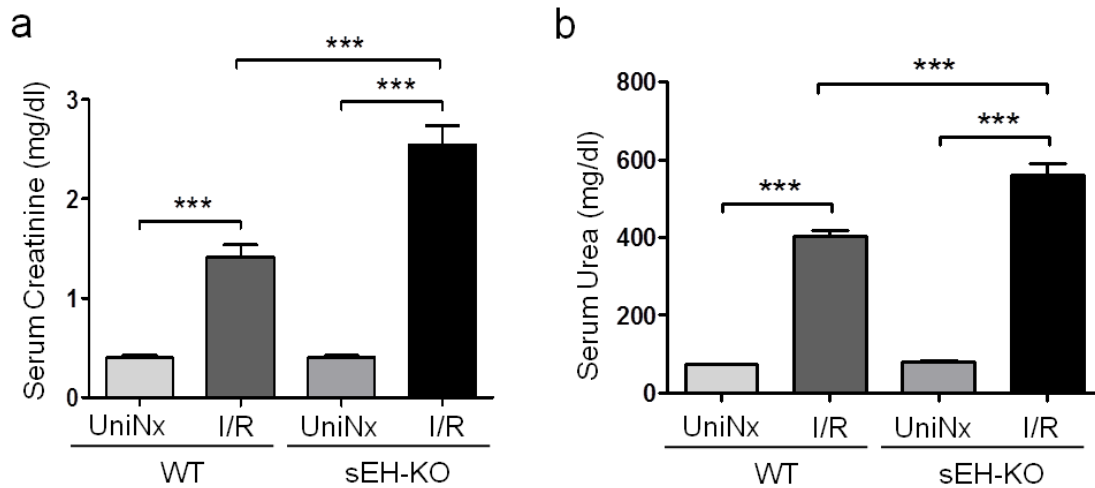


**Figure 16: sEH gene disruption aggravated functional impairment 48 h after I/R injury**

Kidney function as indicated by serum levels of creatinine (a) and urea (b) was measured 48 h after reperfusion. sEH-KO mice presented significantly stronger increases of serum creatinine and urea levels compared to either WT (WT I/R) or uninephrectomized control (sEH-KO UniNx) groups. Mean  $\pm$  SEM (n=5-8 per group). \*\*\*  $p < 0.001$  vs WT.

#### 4.2.2.2 Expression of AKI biomarkers 48 h after I/R injury

To get further insight into the severity of renal I/R injury, renal KIM-1 (Figure 17a), renal NGAL (Figure 17b) and urinary calprotectin concentrations were determined 48 h after reperfusion. The values of individual calprotectin ranged from 32 to 2870 ng/mL. To take the current concentration status of the urine into account, the ratio of calprotectin/creatinine (Figure 17c) was calculated. The three biomarkers were highly increased 48 h after reperfusion both in WT and sEH-KO I/R group. Compared to WT I/R mice, the concentrations of renal KIM-1 and NGAL, and the value of urinary calprotectin / creatinine tended to be 1.5-2 fold higher in sEH-KO I/R group. However, the differences between WT and KO in I/R groups did not reach any significant levels with KIM-1 and NGAL, except the calprotectin/creatinine-ratio (KIM-1:  $4749 \pm 1307$  vs  $7031 \pm 1357$ ,  $P > 0.05$ ; NGAL:  $331.00 \pm 153.9$  vs  $478.60 \pm 99.02$ ,  $P > 0.05$ ; calprotectin/creatinine:  $3201 \pm 1295$  vs  $7677 \pm 2366$  ng/mg;  $P < 0.01$ ; Figure 17).

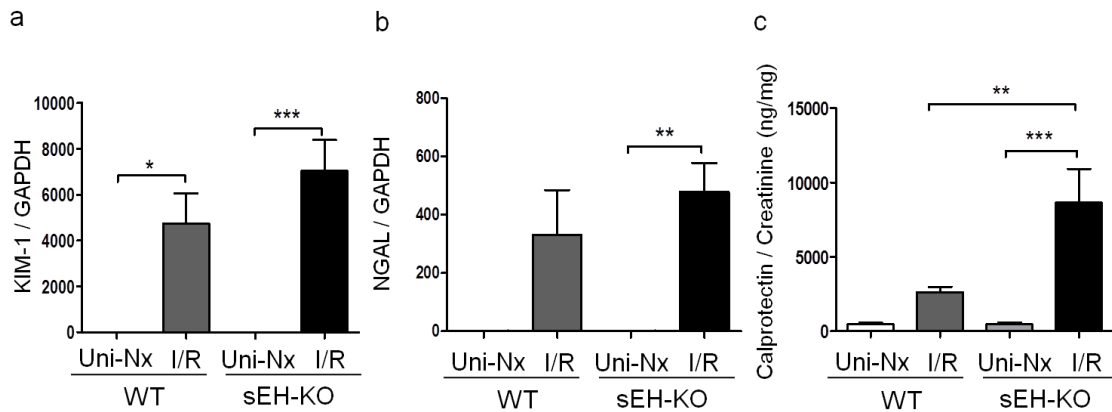


**Figure 17: Expression of AKI biomarkers 48 h after I/R injury**

AKI biomarkers (KIM-1 (a), NGAL (b), and the calculated ratio of urinary calprotectin/creatinine (c) increased in both genotypes 48 h after reperfusion with a trend towards higher values in sEH-KO. Mean  $\pm$  SEM (n=5-8 per group). \*  $p < 0.05$ , \*\*  $p < 0.01$ , \*\*\*  $p < 0.001$  vs WT.

As shown in Table 11, the three biomarkers had significant positive correlation with serum creatinine or serum urea respectively. Urinary calprotectin/creatinine presented the highest positive correlation to kidney function parameters.

**Table 11: Correlations between kidney function and biomarkers of AKI**

Kidney function	KIM-1	NGAL	calprotectin/creatinine
Serum Creatinine	$r = 0.76^{**}$	$r = 0.77^{**}$	$r = 0.85^{**}$
Serum Urea	$r = 0.78^{**}$	$r = 0.78^{**}$	$r = 0.81^{**}$

\*\*  $p < 0.01$

#### 4.2.2.3 sEH-KO aggravated I/R-induced histomorphologic tubular damage

In line with the significantly stronger functional decline compared to WT, sEH-KO mice presented higher tubular lesion scores. I/R-induced progressive renal tubular damage is characterized by widened tubular lumina, hyaline cast formation (loss of brush border, detachment of tubular epithelial cells and nuclear chromatin compaction). Tubular damage was primarily located in the outer medulla and adjacent cortex following the vasculature along the collecting ducts. No tubular damage was detected in sham-operated UniNx controls of the two genotypes. The degree of necrotic renal injury was significantly higher in sEH-KO mice compared to WT mice (quantified by ATN score:  $3.38 \pm 0.08$  vs  $2.43 \pm 0.16$ ;  $p < 0.001$ ; Figure 18).

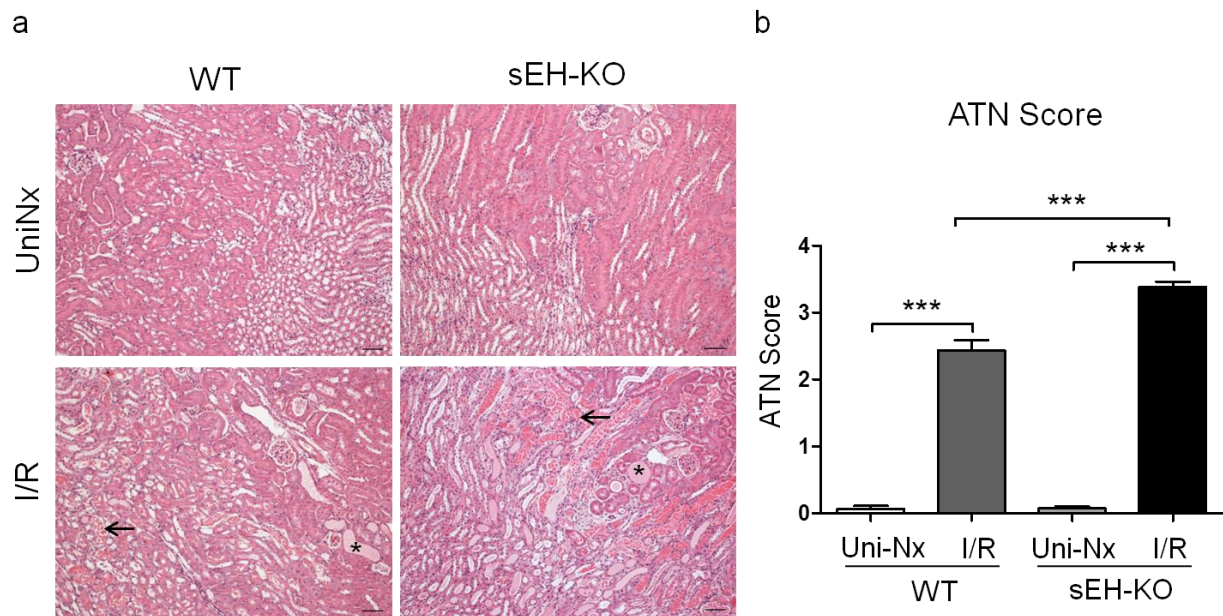


**Figure 18: sEH-KO mice showed aggravated I/R-induced histomorphologic tubular damage**

Representative images of renal sections stained with H&E (a) (magnification 200×, scale bar 50 μm). Arrows indicate necrotic tubules, and asterisks indicate tubular casts. Acute tubular necrosis (ATN) score (b) was determined 48 h after reperfusion. sEH-KO mice displayed significantly aggravated tubular damage compared to either WT (WT I/R) or uninephrectomized control groups (sEH UniNx). Data are given as mean ± SEM (n=5 per group). \*\*\* p<0.001 vs. WT.

#### 4.2.2.4 sEH gene knockout aggravated I/R-induced apoptosis

To assess the extent of I/R-induced apoptosis in the kidney, TUNEL stainings of renal paraffin sections were performed 48 h after reperfusion. Apoptosis was not detectable in UniNx groups of either genotype (WT UniNx or sEH-KO UniNx). sEH-KO mice showed stronger tubular apoptosis compared to the WT mice 48 h after reperfusion ( $0.92 \pm 0.08$  vs  $0.40 \pm 0.02$  % per field of view (FoV), p<0.001; Figure 19). For quantification positive stained area is represented as % per FoV.

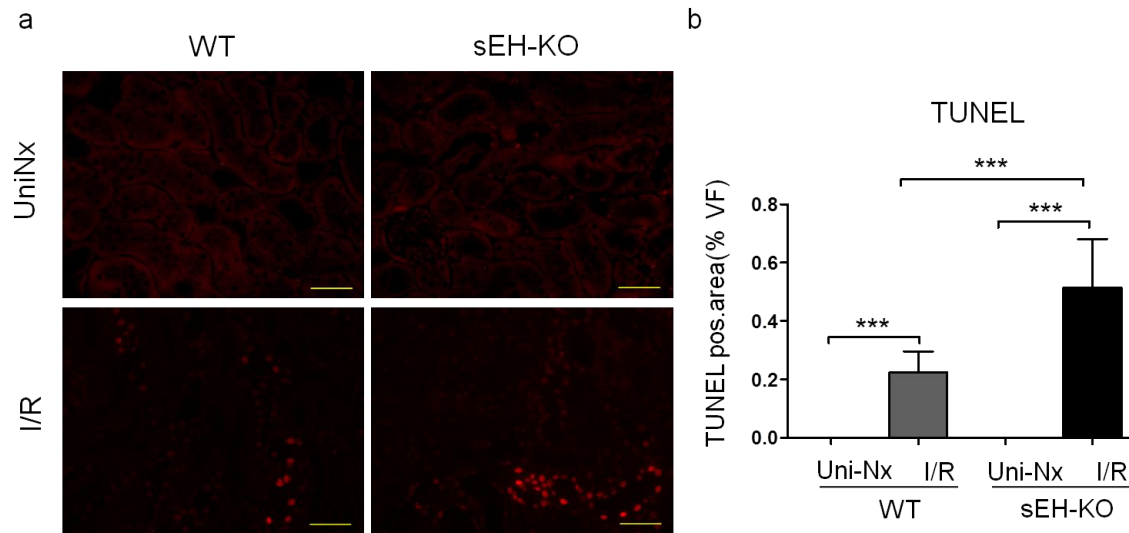


**Figure 19: sEH gene knockout aggravated I/R-induced apoptosis**

Representative images (a) of renal sections stained with TUNEL (magnification 400 $\times$ , Scale bar 100  $\mu$ m). Apoptosis was only detectable in the WT I/R and sEH-KO I/R groups but not in the UniNx controls. Apoptosis positive nuclei were stained in red. Evaluation of apoptosis (b) was performed 48 h after reperfusion. I/R significantly induced apoptosis in the kidneys of both genotypes, however sEH-KO mice displayed significantly stronger apoptosis compared to WT mice. Mean  $\pm$  SEM (n=5 per group). \*\*\* p<0.001 vs WT.

#### 4.2.2.5 sEH gene knockout aggravated I/R-induced inflammation

I/R-induced inflammation was analyzed using specific antibodies against F4/80 and CD11b in renal frozen sections 48 h after reperfusion. Inflammatory cell infiltration was not detectable in the UniNx control groups of either genotype (WT UniNx or sEH-KO UniNx). In contrast, dense infiltration of positive monocytes/macrophages occurred in the damaged zone of the outer medulla and renal cortex upon I/R treatment. Morphometric quantification revealed intensified inflammatory cell infiltration in sEH-KO compared to WT mice ( $0.43 \pm 0.05$  vs  $0.13 \pm 0.00$  % FoV, p<0.05; Figure 20).

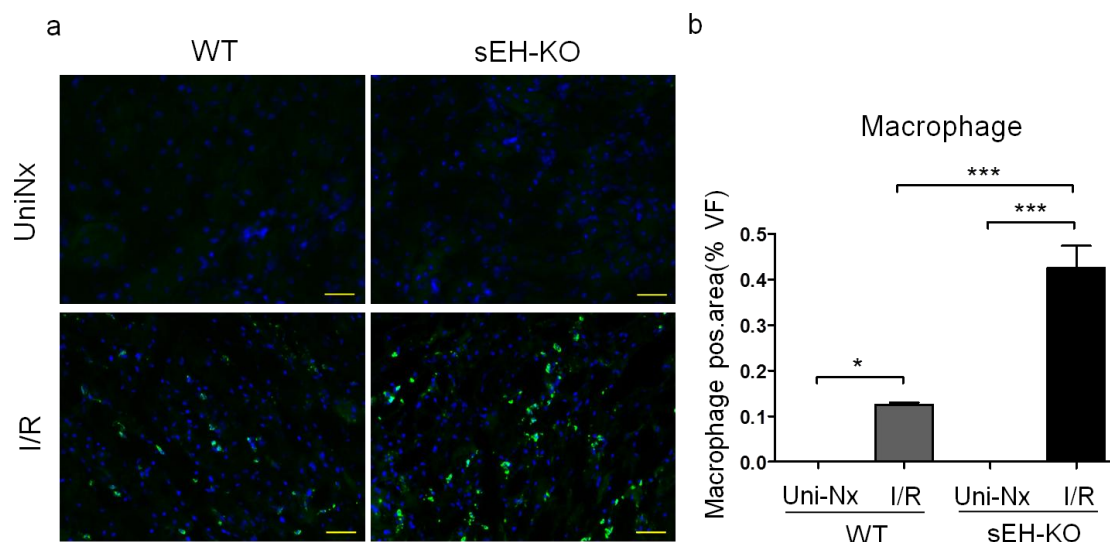


**Figure 20: sEH gene knockout aggravated I/R-induced inflammation**

Representative images (a) of renal sections stained for monocytes/macrophages to evaluate inflammatory cell infiltration that is induced by renal I/R-injury (magnification 400 $\times$ , Scale bar 100  $\mu$ m). Inflammatory cells were stained in green. Nucleus was stained in blue with DAPI. Evaluation of monocytes/macrophages infiltration (b) was performed 48 h after reperfusion. Quantification of inflammatory cell infiltration is shown in the outer medulla by evaluating the intensity ratio of positively stained inflammatory cells to the area of the high power view field. sEH-KO mice displayed significantly more inflammation compared to either WT (WT I/R) or uninephrectomized control groups (sEH-KO UniNx). Mean  $\pm$  SEM (n=5 per group). \* p<0.05, \*\*\* p<0.001 vs WT.

## 4.2.3 Kidney-specific 20-HETE overproduction in sEH-KO mice

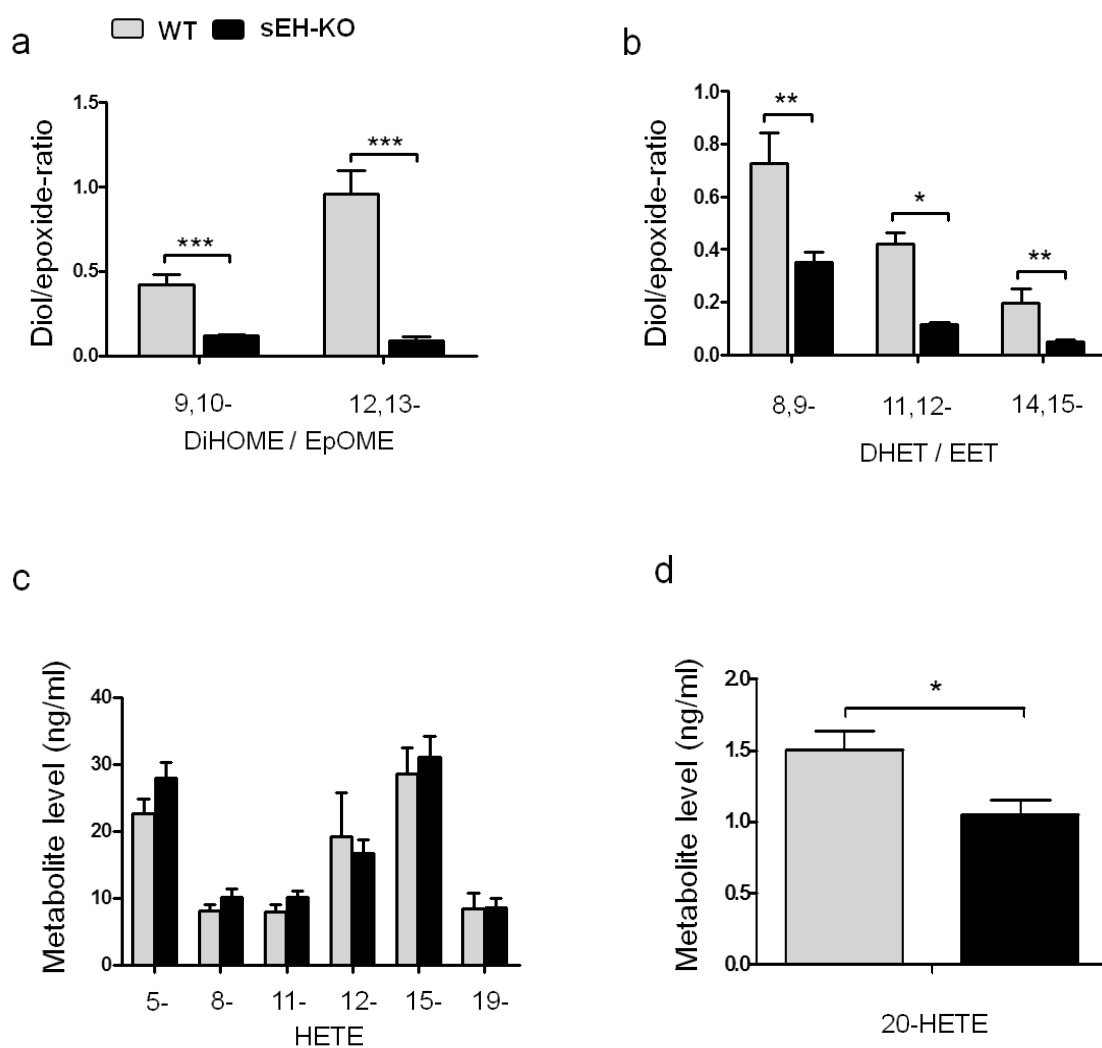
### 4.2.3.1 Plasma oxylipin profiles

To evaluate the amounts of endogenous CYP- and sEH-generated metabolites, plasma from WT and sEH-KO mice of native groups was measured using LC-MS/MS. Besides AA, linoleic acid (LA, 18:2,  $\omega$ -6) and two main  $\omega$ -3 PUFAs, eicosapentaenoic acid (EPA, 20:5  $\omega$ -3) and docosahexaenoic acid (DHA, 22:6  $\omega$ -3), also participated in the metabolism of CYP- and sEH-dependent pathways. The metabolism of these substrates by CYP epoxygenases generates the epoxides including epoxyoctadecenoic acid (EpOME), epoxyeicosatetraenoic acids (EEQs), and epoxydocosapentaenoic acids (EDPs) respectively. These epoxides can be further metabolized by sEH to form their corresponding diols, including dihydroxyoctadecenoic acid (DiHOME), dihydroxyeicosatetraenoic acid (DiHETEs), and dihydroxydocosapentaenoic acid (DiHDPAs). In addition, EPA and DHA can also be converted to  $\omega$ /( $\omega$ -1)- hydroxyeicosapentaenoic acids (19- and 20-HEPE) and  $\omega$ /( $\omega$ -1)- hydroxydocosahexaenoic acids (21- and 22-HDHE) through hydroxylation by CYP enzymes [73, 74]. The results of those oxylipin profiles are summarized in Figure 21 and Table 12. The main results were as follows:

1) All epoxy-metabolites serving as sEH substrates (EpOMEs, EETs, EEQs and EDPs) were increased whereas corresponding products (DiHOMEs, DHETs, DiHETEs and DiHDPAs) were decreased. This is in agreement with the loss of endogenous sEH function in sEH-KO mice. The corresponding sEH product/substrate-ratios are shown in Figure 21a, b, e and f.

2) None of the metabolites produced via other pathways of the AA cascade (5-, 12- or 15-lipoxygenases, AA-oxidation and AA ( $\omega$ -1)-hydroxylation) was different in WT and sEH-KO mice (Figure 21c).

3) The plasma level of 20-HETE was significantly higher in WT than in sEH-KO mice (Figure 21d).



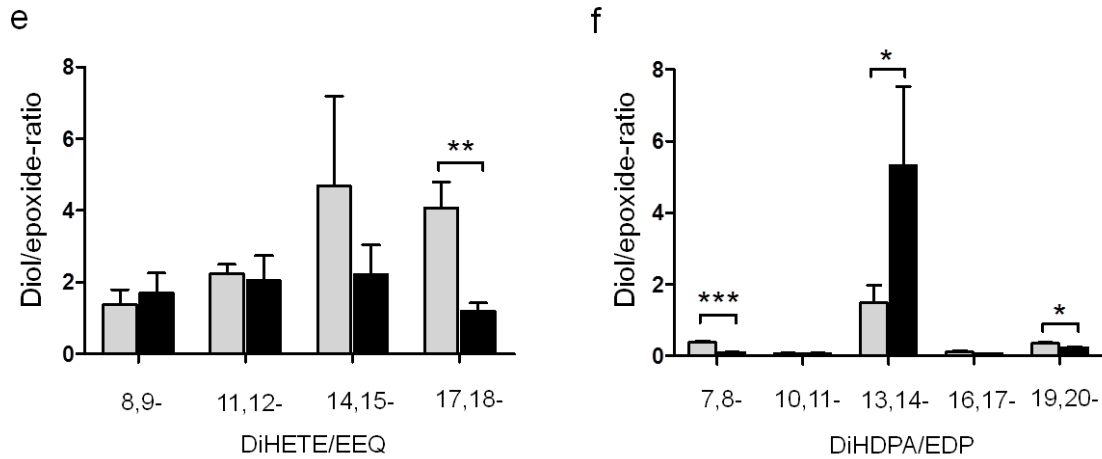


**Figure 21: Plasma oxylipin profiles**

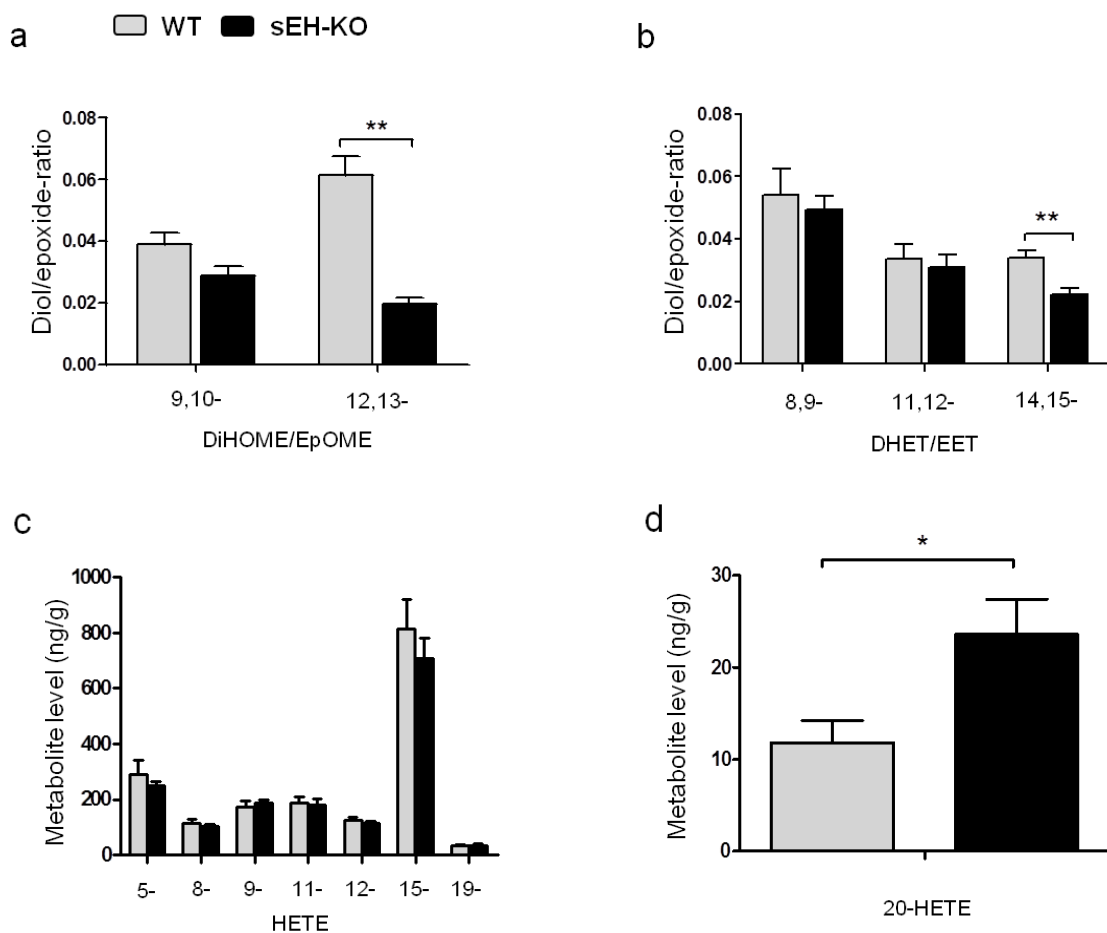
Graphs for plasma concentrations of sEH- and CYP-dependent LA-, AA-, EPA- and DHA-metabolites in WT and sEH-KO mice of native groups. **a:** The conversion of LA-derived epoxides (EpOMEs) to the corresponding vicinal diols (DiHOMEs) was reduced in sEH-KO compared to WT mice as indicated by the decreased DiHOME/EpOME-ratios. **b:** The conversion of AA-derived epoxides (EETs) to the corresponding vicinal diols (DHETs) was reduced in sEH-KO compared to WT mice as indicated by the decreased DHET/EET-ratios. **c:** The plasma levels of AA-derived 5- through 19-HETE were not different in WT and sEH-KO mice. **d:** Plasma 20-HETE levels were significantly lower in sEH-KO compared with WT mice. **e:** The conversion of EPA-derived epoxides (EEQs) to the corresponding vicinal diols (DiHETEs) was reduced in sEH-KO compared to WT mice as indicated by the decreased DiHETE/EEQ-ratios. **f:** The conversion of DHA-derived epoxides (EDPs) to the corresponding vicinal diols (DiHDPA)s was reduced in sEH-KO compared to WT mice as indicated by the decreased DiHDPA/EDP-ratios, except 13,14-DiHDPA/EDP. Mean  $\pm$  SEM (n=6 per group). \* p<0.05, \*\* p<0.01, \*\*\* p<0.001.

**Table 12: Comparison of plasma oxylin profile between WT and sEH-KO mice (ng/mL)**

	WT	sEH-KO
<b>Epoxygenase metabolism</b>		
9,10-EpOME	20.57±4.82	40.30±7.32
12,13-EpOME	31.39±8.12	131.6±16.94***
5,6-EET	0.21±0.13	0.20±0.07
8,9-EET	1.97±0.25	3.43±0.17***
11,12-EET	1.35±0.21	1.73±0.18
14,15-EET	4.00± 0.55	9.39±0.29***
5,6-EEQ	0.00±0.00	0.00±0.00
8,9-EEQ	0.07±0.04	0.24±0.07
11,12-EEQ	0.09±0.02	0.08±0.03
14,15-EEQ	0.10±0.03	0.28±0.09
17,18-EEQ	0.94±0.14	3.73±0.80*
7,8-EDP	2.14±0.32	3.09±2.34
10,11-EDP	1.27±0.14	1.45±0.14
13,14-EDP	0.49±0.10	0.27±0.08
16,17-EDP	2.23±0.28	2.20±0.19
19,20-EDP	4.53±0.22	6.07±0.47*
<b>Soluble epoxide hydrolase metabolism</b>		
9,10-DiHOME	8.99±2.59	4.71±1.01
12,13-DiHOME	31.63±9.60	12.59±4.10
5,6-DHET	3.34±0.34	4.42±0.32*
8,9-DHET	1.35±0.11	1.19±0.09
11,12-DHET	0.54±0.04	0.42±0.04
14,15-DHET	0.68±0.07	0.47±0.07
5,6-DiHETE	0.30±0.02	1.49±0.24**
8,9-DiHETE	0.24±0.07	0.36±0.09
11,12-DiHETE	0.19±0.04	0.23±0.08
14,15-DiHETE	0.47±0.09	0.55±0.09
17,18-DiHETE	3.55±0.56	3.94±0.77
7,8-DiHDPA	0.81±0.09	0.30±0.04***
10,11-DiHDPA	0.09±0.01	0.10±0.01
13,14-DiHDPA	0.62±0.10	0.80±0.09
16,17-DiHDPA	0.24±0.03	0.16±0.02
19,20-DiHDPA	1.59±0.08	1.33±0.10
<b>ω/( ω1)-Hydroxylase metabolism</b>		
19-HETE	8.49±2.24	8.50±1.45
20-HETE	1.50±0.13	1.05±0.11*
19-HEPE	0.17±0.04	0.27±0.03
20-HEPE	0.44±0.04	0.58±0.05
21-HDHA	3.95±0.29	3.08±0.15*
22-HDHA	0.32±0.07	0.30±0.04
<b>Other monohydrolase metabolism</b>		
5-HETE	22.68±2.12	27.93±2.42
8-HETE	8.06±0.95	10.18±1.26
9-HETE	7.25±0.82	9.53±1.05
11-HETE	7.92±1.08	10.07±0.94
12-HETE	19.14±6.70	16.75±1.92
15-HETE	28.64±3.85	31.12±3.03
5-HEPE	1.94±0.38	3.89±0.63*
8-HEPE	0.93±0.14	1.77±0.28*
9-HEPE	0.56±0.06	1.48±0.28*
12-HEPE	2.02±0.37	5.78±0.91**
15-HEPE	1.46±0.40	1.69±0.20
18-HEPE	2.61±0.30	4.79±0.94
4-HDHA	10.67±1.21	10.26±1.02
7-HDHA	7.14±0.66	8.68±0.98
8-HDHA	10.92±1.09	13.19±1.21
10-HDHA	3.64±0.67	4.38±0.52
11-HDHA	4.94±0.53	6.15±0.65
13-HDHA	5.37±0.51	6.59±0.79
14-HDHA	30.49±14.49	19.00±2.32
16-HDHA	6.96±0.79	7.93±0.60
17-HDHA	27.76±7.29	22.50±1.92
20-HDHA	19.39±2.49	20.26±1.59

### 4.2.3.2 Renal oxylipin profiles

To assess the formation of sEH- and CYP-dependent eicosanoids, kidney samples from the native groups were analyzed by LC-MS/MS for the presence of LA-, AA-, EPA- and DHA-derived metabolites in a manner similar to that described above for the corresponding plasma samples. The renal CYP- and sEH- dependent eicosanoid profiles are summarized graphically in Figure 22 and given in detail in Table 13. Resembling the metabolic shift observed in the plasma, the sEH product/substrate-ratios (DiHOME/EpOME, DHET/EET, DiHETE/EEQ, DiHDPA/EDP) were reduced in sEH-KO compared to WT mice (Figure 22a, b, e and f). The concentrations of mid-chain HETEs and 19-HETE did not differ between WT and sEH-KO mice (Figure 22c). Remarkably, however, the renal 20-HETE levels were significantly increased two-fold in sEH-KO mice compared to WT littermates (Figure 22d). In addition to the AA-derived 20-HETE, also the  $\omega$ -hydroxylase products of EPA (20-HEPE) and DHA (22-HDHA) were significantly higher in the kidneys of sEH-KO than WT mice (Table 13).



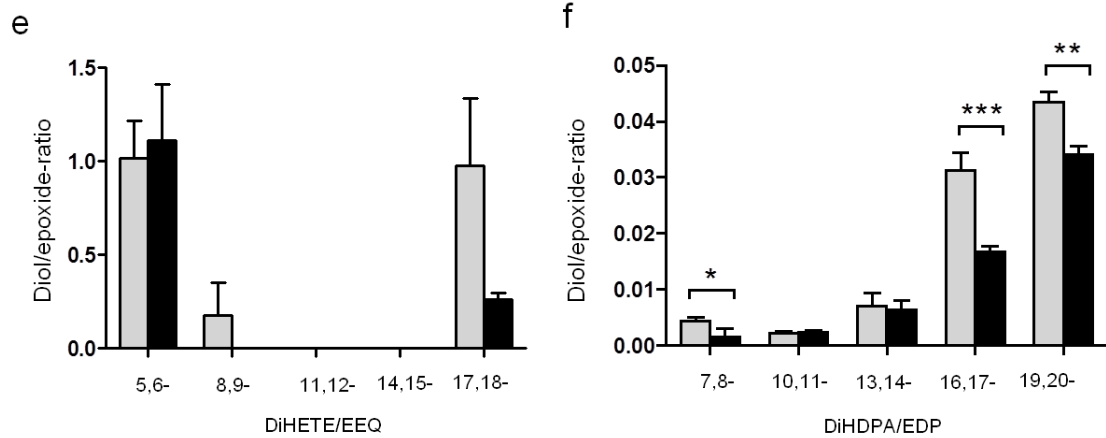


**Figure 22: Renal oxylipin profiles**

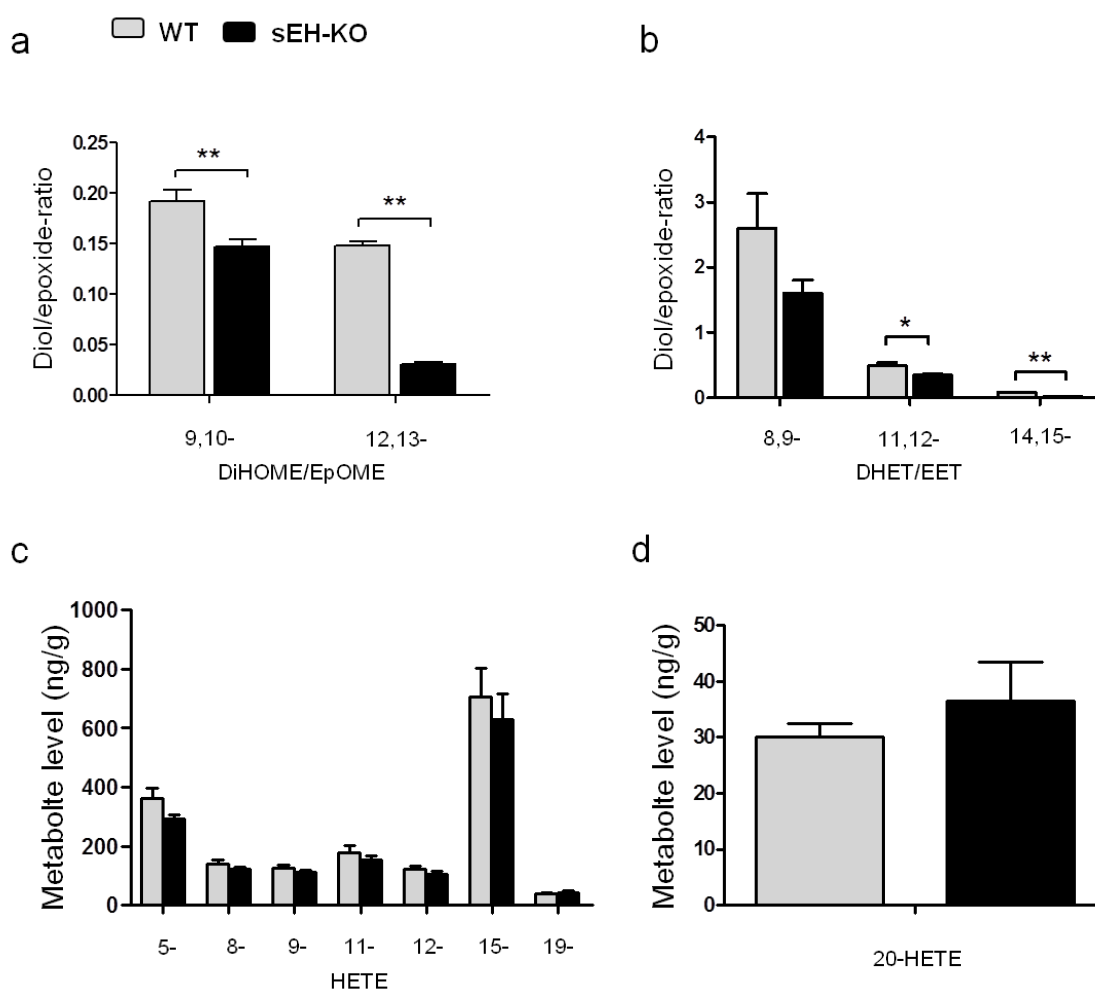
Graphs for concentrations of sEH- and CYP-dependent LA-, AA-, EPA- and DHA-metabolites in renal tissue of WT and sEH-KO mice of native groups. a: The conversion of LA-derived epoxides (EpOMEs) to the corresponding vicinal diols (DiHOMEs) was reduced in sEH-KO compared to WT mice as indicated by the decreased DiHOME/EpOME-ratios. b: The conversion of AA-derived epoxides (EETs) to the corresponding vicinal diols (DHETs) was reduced in sEH-KO compared to WT mice as indicated by the decreased DHET/EET-ratios. c: Plasma 20-HETE levels were significantly higher in sEH-KO compared with WT mice. d: There was no difference in renal levels of AA-derived 5- through 19-HETE between WT and sEH-KO mice. e: The conversion of EPA-derived epoxides (EEQs) to the corresponding vicinal diols (DiHETEs) was reduced in sEH-KO compared to WT mice as indicated by the decreased DiHETE/EEQ-ratios. f: The conversion of DHA-derived epoxides (EDPs) to the corresponding vicinal diols (DiHDPAs) was reduced in sEH-KO compared to WT mice as indicated by the decreased DiHDPAs/EDP-ratios. Mean  $\pm$  SEM (n=5-7 per group). \*  $p < 0.05$ , \*\*  $p < 0.01$ .

**Table 13: Comparison of renal oxylipin profile between WT and sEH-KO mice (ng/g)**

	WT	sEH-KO
<b>Epoxygenase metabolism</b>		
9,10-EpOME	214.2±25.64	300.9±26.37*
12,13-EpOME	247.1±25.14	525.4±58.59**
5,6-EET	141.3±33.19	123.6±11.62
8,9-EET	134.7±14.36	127.6±9.26
11,12-EET	152.3±18.82	154.1±10.81
14,15-EET	345.4± 38.27	361.8±17.25
5,6-EEQ	4.48±0.21	3.50±0.98
8,9-EEQ	2.52±1.03	0.48±0.48
11,12-EEQ	1.64±0.55	3.37±0.29*
14,15-EEQ	3.58±0.92	6.34±1.20
17,18-EEQ	14.23±3.31	43.10±6.29**
7,8-EDP	1184±209.7	1194±71.72
10,11-EDP	927.8±114.4	992.4±75.58
13,14-EDP	442.5±106.5	413.7±115.4
16,17-EDP	342.2±62.22	505.2±15.71
19,20-EDP	843.6±79.13	1078±35.78*
<b>Soluble epoxide hydrolase metabolism</b>		
9,10-DiHOME	8.24±1.05	8.57±1.03
12,13-DiHOME	14.87±1.55	10.08±1.09*
5,6-DHET	44.90±3.30	46.17±5.48
8,9-DHET	7.01±0.73	6.30±0.73
11,12-DHET	4.76±0.38	4.74±0.61
14,15-DHET	11.49±0.87	8.20±1.01*
5,6-DiHETE	4.61±1.02	4.93±0.80
8,9-DiHETE	0.76±0.76	0.81±0.49
11,12-DiHETE	0.00±0.00	0.00±0.00
14,15-DiHETE	0.00±0.00	0.00±0.00
17,18-DiHETE	8.86±1.60	10.02±0.93
7,8-DiHDPA	4.94±0.57	1.52±1.35*
10,11-DiHDPA	2.16±0.30	2.45±0.30
13,14-DiHDPA	2.22±0.32	1.91±0.41
16,17-DiHDPA	9.83±0.48	8.35±0.38*
19,20-DiHDPA	36.53±2.95	37.16±2.48
<b>ω/( ω1)-Hydroxylase metabolism</b>		
19-HETE	32.79±6.58	33.71±6.88
20-HETE	11.83±2.38	23.59±3.85*
19-HEPE	22.42±2.36	22.19±2.11
20-HEPE	26.52±1.33	33.15±2.17*
21-HDHA	320.6±27.61	377.9±16.47
22-HDHA	56.41±4.07	71.26±3.56*
<b>Other monohydrolase metabolism</b>		
5-HETE	289.7±50.61	249.8±17.70
8-HETE	114.7±14.47	102.8±7.21
9-HETE	173.6±22.28	187.3±11.36
11-HETE	187.7±22.09	181.4±22.15
12-HETE	124.3±13.52	116.2±6.97
15-HETE	812.5±106.9	709.1±72.32
5-HEPE	47.54±5.09	55.02±4.57
8-HEPE	4.55±0.86	4.43±0.55
9-HEPE	7.75±2.07	8.11±1.21
12-HEPE	4.07±0.76	2.87±0.72
15-HEPE	6.02±2.17	7.36±1.27
18-HEPE	26.41±5.56	26.24±4.42
4-HDHA	328.6±73.99	277.1±26.83
7-HDHA	144.4±21.89	149.2±8.93
8-HDHA	383.1±52.83	372.8±25.42
10-HDHA	118.7±15.28	108.5±5.68
11-HDHA	141.5±17.63	144.2±8.74
13-HDHA	199.8±22.96	192.4±13.75
14-HDHA	222.3±23.84	222.8±13.53
16-HDHA	424.8±50.92	368.3±32.49
17-HDHA	666.8±93.58	574.0±44.41
20-HDHA	928.3±128.4	839.3±90.76

### 4.2.3.3 Liver oxylipin profiles

Liver baseline levels of CYP- and sEH-dependent LA-, AA-, EPA- and DHA-derived metabolites were also determined using LC-MS/MS. The results are summarized in Figure 23 and given in detail in Table 14. Resembling the metabolic shifts observed in the plasma and kidney samples, the liver samples of sEH-KO mice displayed lower sEH product/substrate-ratios (DiHOME/EpOME, DHET/EET, DiHETE/EEQ and DiHDDPA/EDP) than WT mice (Figure 23a, b, e and f). The levels of mid-chain HETEs and 19-HETE showed no significant differences between WT and sEH-KO mice (Figure 23c). In contrast to the situation in the kidney, the hepatic 20-HETE levels were not significantly increased in EH-KO mice (Figure 23d). The same applied to the other  $\omega$ -hydroxylase products determined (20-HEPE and 22-HDHA; Table 14)



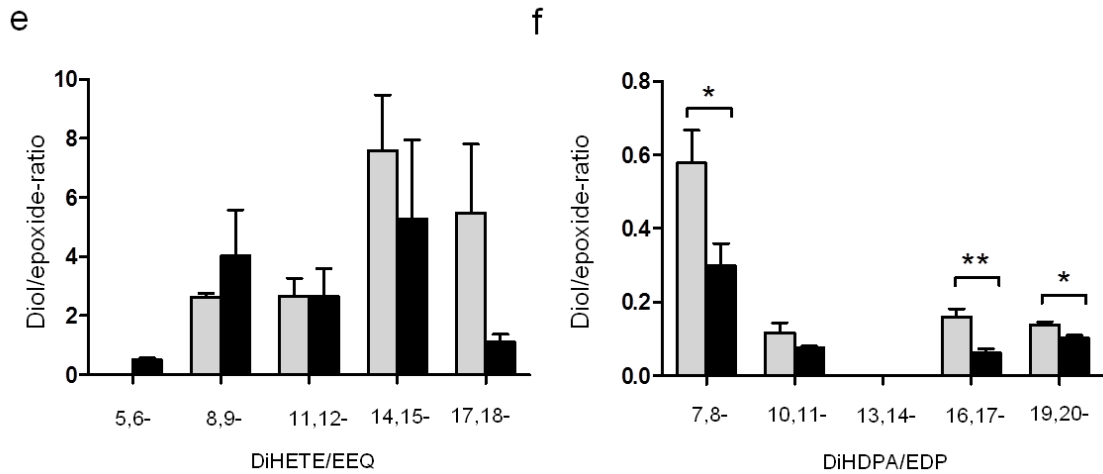


### Figure 23: Liver oxylipin profiles

Graphs for liver concentrations of sEH- and CYP-dependent LA-, AA-, EPA- and DHA-metabolites in WT and sEH-KO mice of native groups. a, b: Metabolic deficiency of sEH resulted in decreased DiHOME/EpOME- (a) as well as DHET/EET-ratios (b). c, d: The hepatic levels of 5- through 19-HETE (c) as well as the hepatic 20-HETE levels (d) were not different in WT and sEH-KO mice. e: No significant differences were detected for the ratios of DiHETEs/EEQs between WT and sEH-KO mice. f: Metabolic deficiency of sEH resulted in decreased 7,8-DiHDPA/7,8-EDP, 16,17-DiHDPA/16,17-EDP, and 19,20-DiHDPA/19,20-EDP-ratios. Mean  $\pm$  SEM (n=5-6 per group). \* p<0.05, \*\* p<0.01.

**Table 14: Comparison of liver oxylipin profile between WT and sEH-KO mice (ng/g)**

	WT	sEH-KO
<b>Epoxygenase metabolism</b>		
9,10-EpOME	144.7±8.38	259.0±26.64**
12,13-EpOME	343.5±19.72	1742±198.4***
5,6-EET	8.19±1.41	17.82±3.24*
8,9-EET	21.81±5.59	28.92±6.78
11,12-EET	41.83±4.77	53.60±6.08
14,15-EET	231.3± 17.82	428.2±24.36***
5,6-EEQ	0.00±0.00	17.97±4.09
8,9-EEQ	0.87±0.54	2.11±0.49
11,12-EEQ	0.71±0.23	1.98±0.47*
14,15-EEQ	1.34±0.26	4.12±1.21
17,18-EEQ	9.89±2.93	38.29±10.64*
7,8-EDP	36.06±7.11	34.56±8.54
10,11-EDP	18.44±3.91	25.26±2.52
13,14-EDP	6.02±1.30	3.21±1.62
16,17-EDP	50.01±6.96	79.96±12.38
19,20-EDP	143.6±11.52	179.8±22.00
<b>Soluble epoxide hydrolase metabolism</b>		
9,10-DiHOME	27.54±1.66	37.65±4.07
12,13-DiHOME	50.53±3.21	52.96±4.66
5,6-DHET	45.99±5.30	56.24±3.16
8,9-DHET	46.20±2.37	40.52±2.66
11,12-DHET	19.79±1.39	18.19±1.47
14,15-DHET	19.68±1.72	8.91±0.75***
5,6-DiHETE	1.80±0.34	8.17±0.62***
8,9-DiHETE	4.11±0.83	6.35±2.17
11,12-DiHETE	2.50±0.52	4.84±0.98
14,15-DiHETE	8.43±1.11	0.04±0.72
17,18-DiHETE	30.64±3.29	30.62±2.61
7,8-DiHDPA	19.06±2.10	8.04±0.36***
10,11-DiHDPA	1.90±0.25	1.93±0.24
13,14-DiHDPA	0.00±0.00	0.00±0.00
16,17-DiHDPA	7.59±0.64	4.69±0.52**
19,20-DiHDPA	19.76±1.70	17.92±1.82
<b>ω/( ω1)-Hydroxylase metabolism</b>		
19-HETE	37.70±6.21	43.96±6.63
20-HETE	30.09±2.42	36.57±6.85
19-HEPE	8.12±1.22	4.81±0.76
20-HEPE	22.08±3.42	15.43±2.00
21-HDHA	575.2±64.3	516.5±61.64
22-HDHA	108.8±23.66	96.78±19.13
<b>Other monohydrolase metabolism</b>		
5-HETE	360.9±35.28	291.0±15.94
8-HETE	141.3±13.15	123.1±6.97
9-HETE	124.9±11.47	114.1±6.20
11-HETE	178.1±25.03	153.8±13.59
12-HETE	121.0±10.76	104.8±9.46
15-HETE	706.3±97.56	630.7±87.48
5-HEPE	113.8±15.85	147.8±11.38
8-HEPE	6.07±0.41	7.48±1.07
9-HEPE	16.93±8.39	9.19±0.00
12-HEPE	6.56±1.10	7.41±0.91
15-HEPE	6.53±1.04	6.91±1.20
18-HEPE	24.91±3.33	26.45±4.83
4-HDHA	152.2±21.41	103.7±10.64*
7-HDHA	99.86±14.60	79.58±7.45
8-HDHA	180.7±22.51	140.5±11.56
10-HDHA	70.84±9.58	58.17±7.97
11-HDHA	81.87±10.16	70.43±6.26
13-HDHA	118.2±13.34	96.68±9.59
14-HDHA	190.1±26.64	163.1±20.40
16-HDHA	227.6±25.70	177.1±22.64
17-HDHA	457.7±47.82	372.1±41.99
20-HDHA	458.7±62.11	387.0±54.10

## 4.2.4 sEH gene disruption caused a strong upregulation of Cyp4a12a expression in the kidney

### 4.2.4.1 Renal mRNA level of Cyp4a12a was upregulated in sEH-KO mice

In mouse kidneys, 20-HETE is produced through the CYP4A subfamily members including Cyp4a10, Cyp4a12 (Cyp4a12a and Cyp4a12b), and Cyp4a14, among which Cyp4a12a is the predominant 20-HETE-producing enzyme [70]. Moreover, 20-HETE can be degraded through a COX-dependent pathway, which also controls the range and diversity of 20-HETE activity and then affect vasomotor activity [75]. Searching for the origin of increased renal 20-HETE levels in sEH-KO mice, native kidneys from sEH-KO and WT mice were analyzed for the expression of 20-HETE-generating and degrading enzymes. As shown in Figure 24a, renal Cyp4a12a expression was about two-fold higher at the mRNA level in sEH-KO than in WT mice. Cyp4a12a mRNA expression levels determined by TaqMan RT-PCR and normalized to GAPDH expression were  $0.71 \pm 0.08$  in WT vs.  $1.22 \pm 0.15$  in sEH-KO mice. In contrast, sEH gene disruption did not affect the renal mRNA expression levels of other members of the Cyp4a subfamily (Cyp4a10, Cyp4a12b, and Cyp4a14) (Figure 24b-d). Also, there was no difference in the mRNA levels of COX-1, an enzyme potentially involved in secondary 20-HETE metabolism between WT and sEH-KO mice (Figure 24e).

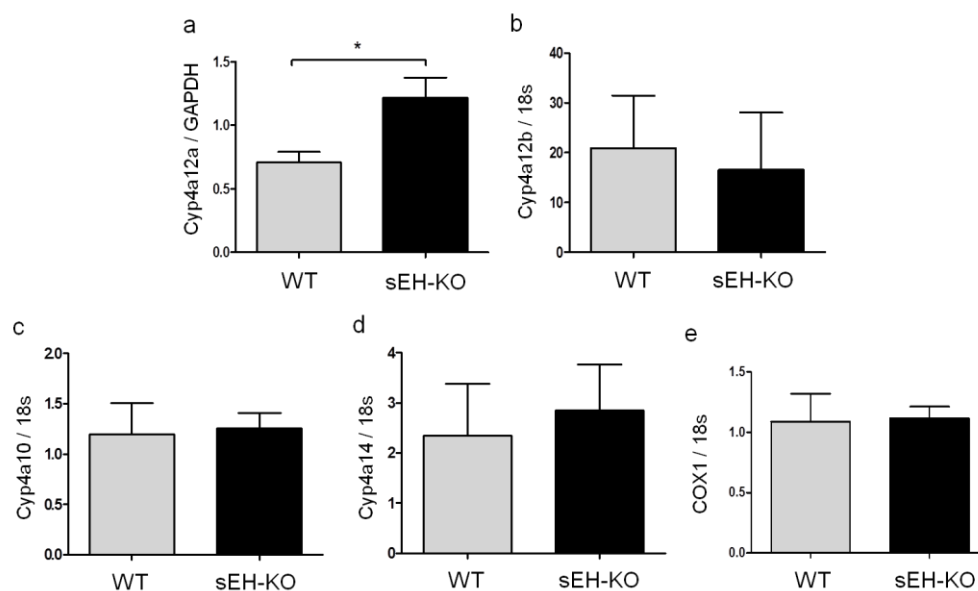


**Figure 24: sEH gene disruption caused a strong upregulation of 20-HETE-producing gene Cyp4a12a in the kidney**

sEH-gene depletion causes a strong mRNA upregulation of 20-HETE-producing enzyme Cyp4a12a in mouse kidneys at baseline compared to WT indicated by qRT-PCR data (a). There were no significant differences between sEH-KO and WT mice for the levels of Cyp4a12b, Cyp4a10, Cyp4a14, and COX1. Mean  $\pm$  SEM (n=5-7 per group). \*  $p < 0.05$  vs WT.

#### 4.2.4.2 Renal protein expression of Cyp4a12a was upregulated in sEH-KO mice

To assess whether the upregulated mRNA expression of Cyp4a12a influences the amount of protein expression, homogenates of native kidney were prepared and analyzed by Western blot. Recombinant CYP4a12a protein was also loaded as a positive control. The peptide-specific Cyp4a12a antibody recognized a single 55 kDa protein band that co-migrated with recombinant Cyp4a12a in SDS-PAGE. Consistent with the mRNA level of Cyp4a12a, quantification of Western blots using GAPDH as loading control showed significantly increased intensities of the Cyp4a12a immunoreactive band in the renal homogenates of sEH-KO compared to WT mice ( $0.33\pm 0.02$  vs  $0.13\pm 0.02$ ,  $P<0.05$ ; Figure 25a and b).

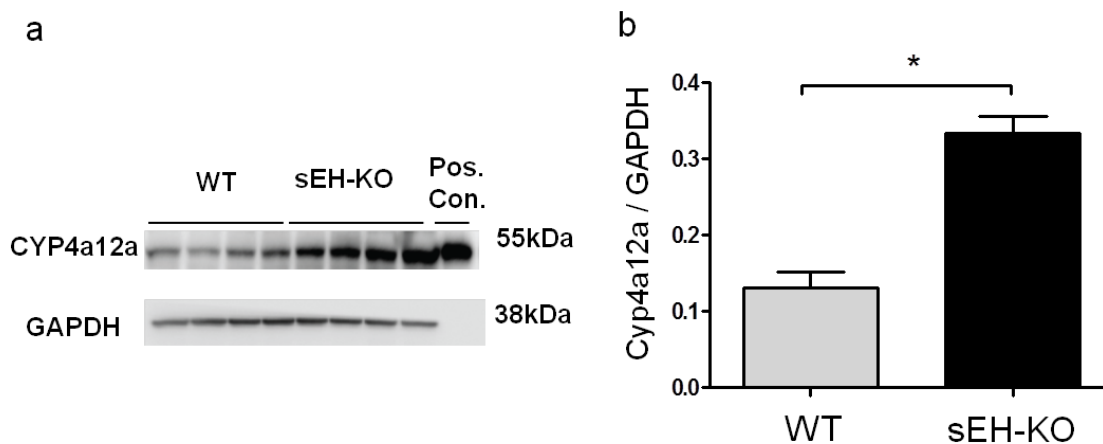


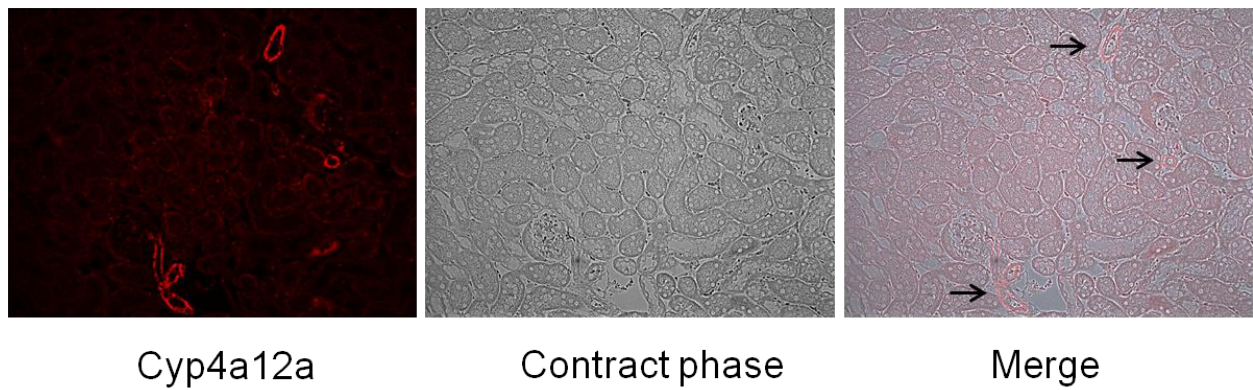
#### Figure 25: Renal protein expression of Cyp4a12a was upregulated in sEH-KO mice

Representative Western blot (a) and statistic evaluation (b) showing that Cyp4a12a protein was upregulated in sEH-KO mice. Mean  $\pm$  SEM (n=5-7 per group). \*  $p<0.05$  vs WT.

#### 4.2.4.3 Intrarenal localization of Cyp4a12a protein expression

Since 20-HETE has been shown to play a complex role in the regulation of renal vascular tone and tubular function, it was important to learn more about the site where 20-HETE is overproduced in the kidney of sEH-KO mice. To visualize the intrarenal localization of Cyp4a12a, native kidney sections were incubated with a peptide-specific Cyp4a12a antibody followed by a fluorescent labeled secondary antibody. Tubular immunofluorescence was rather faint and not different comparing WT and sEH-KO mice. In contrast, renal vessels (arcuate, interlobar, and interlobular arteries) displayed clearly enhanced immunostaining for Cyp4a12a in sEH-KO mice (Figure 26a). Immunostaining occurred in renal vascular and tubular structures and could be blocked at both sites by pre-saturating the Cyp4a12a antibody with the corresponding synthetic peptide (Figure 26b).

a



b

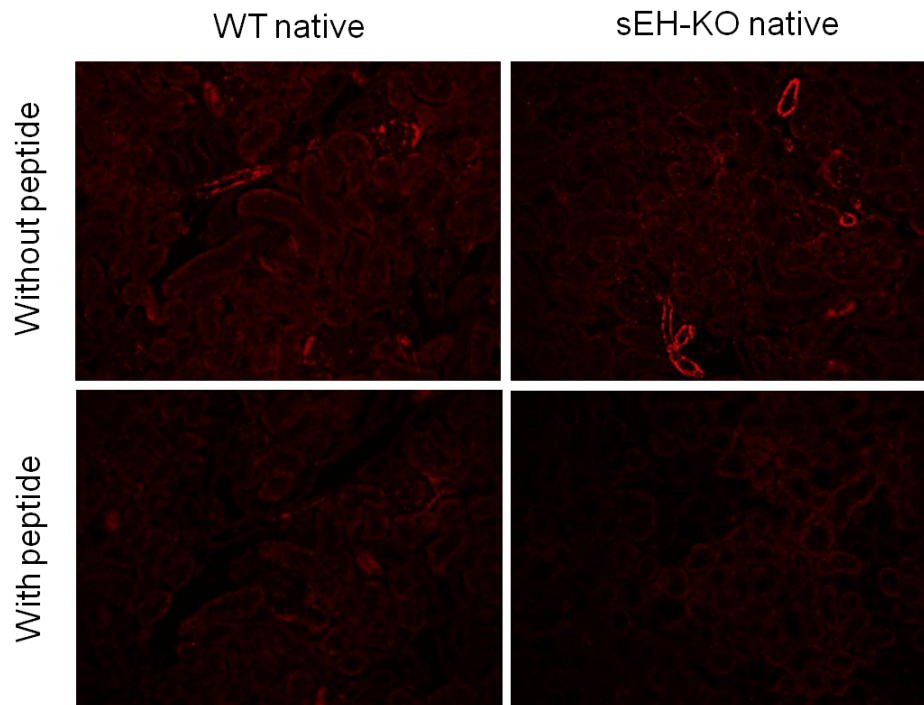


**Figure 26: Intrarenal localization of Cyp4a12a protein expression**

Images of a renal section from sEH-KO mice (a) showing how immunostaining relates to the underlying renal structures (magnification 200×; scale bar: 50 μm). Cyp4a12a immunostaining was most intense in the renal vessels (arcuate, interlobar, and interlobular arteries). Faint but specific staining occurred in tubules. No staining was detectable in glomeruli. Representative images of renal sections stained for Cyp4a12a (b) by immunofluorescence (magnification 200×; scale bar: 50 μm). sEH gene disruption resulted in upregulating the vascular expression of Cyp4a12a in mouse kidneys compared to WT mouse. The signals were blocked by pre-saturating the peptide-specific Cyp4a12a antibody with the corresponding synthetic peptide.

## 4.2.5 Potential mechanism of 20-HETE overproduction in the kidney

### 4.2.5.1 The serum and renal testosterone level in native group

Cyp4a12a expression was previously shown to determine the sex-specific differences in renal 20-HETE generation and to be inducible by androgens [70]. In order to understand the mechanism which contributes to renal overexpression of Cyp4a12a in sEH-KO mice, concentrations of plasma and renal testosterone as well as of 5- $\alpha$  dihydrotestosterone (DHT) were measured by using LC-MS/MS. Compared to WT mice, sEH-KO mice had slightly elevated testosterone levels, but there were no significant differences between these two groups in plasma or kidney (Figure 27). Unfortunately, DHT in plasma and kidney samples was not detectable.

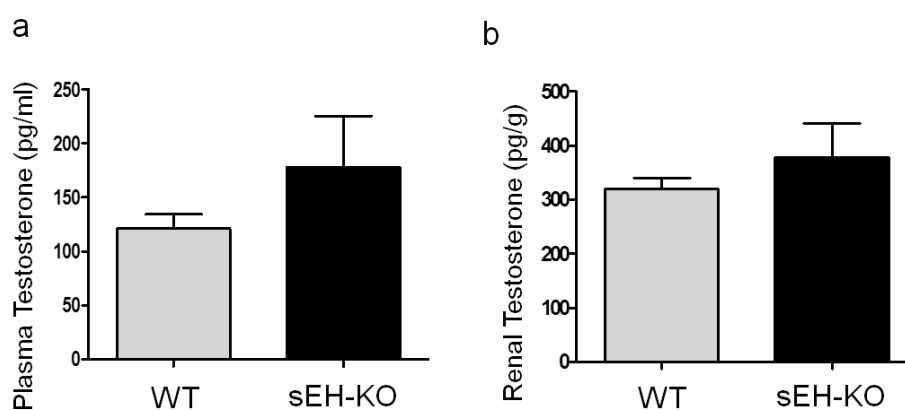


**Figure 27: Serum and renal testosterone level in native group**

Compared to WT mice, baseline concentrations of testosterone in plasma and kidney appeared moderately increased in sEH-KO mice, but there were no significant differences between these two groups. Mean  $\pm$  SEM (n=6 per group).

### 4.2.5.2 Enzymes in the androgen-related metabolism

Testosterone, the most important androgenic-anabolic steroid, can be further metabolized via two pathways. On the one hand, Srd5a iso-enzymes convert testosterone to DHT, which is a more active form than testosterone. On the other hand, aromatase (CYP19) oxidizes testosterone to estradiol, which accounts for a small part of testosterone transformation in males [76]. To assess the amounts of these enzymes which take part in the metabolism of testosterone and influence the levels of androgen-induced genes like the  $\beta$ -glucuronidase (Gusb) [77], kidney samples from native groups of WT and sEH-KO mice were analyzed by using qRT-PCR and Western blots. However, there were no statistical significant differences in mRNA levels of Srd5a1, Srd5a2, or Gusb, or in protein abundance of Cyp19a1 between WT and sEH-KO mice (Figure 28).

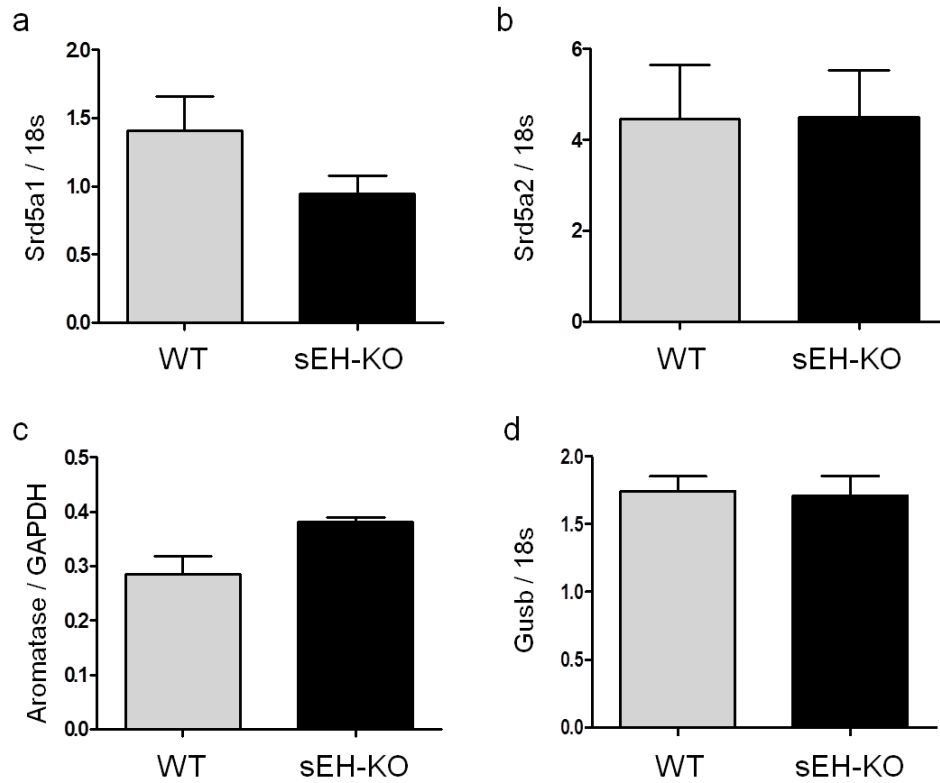


**Figure 28: Enzymes in androgen-related metabolism**

Baseline levels of enzymes associated with androgen metabolism were determined using qRT-PCR (a, b, d) or Western blot (c). No significant differences were detected in these enzymes between WT and sEH-KO mice. Mean ± SEM (n=6 per groups).

## 5. DISCUSSION

In this study, we investigated the role of epoxyeicosatrienoic acid levels (EETs) using pharmacological or genetic approaches in rat and mouse models of I/R-induced AKI. Our experimental study in rats showed that pretreating the kidney with a synthetic 14,15-EET analog significantly alleviated I/R-induced renal injury. Then we investigated the effect of global sEH gene disruption on the development of ischemic AKI in mice. Contrary to our expectation, sEH deficiency did not ameliorate I/R-induced renal damage, but rather significantly aggravated experimental AKI in mice. Oxylin profiling as well as analysis of Cyp4a12a expression revealed increased renal vascular 20-HETE formation as a factor that potentially causes the increased susceptibility of sEH-KO mice to I/R-induced renal damage.

### 5.1 Establishment of I/R-induced AKI animal models

Ischemic AKI is a major kidney disease associated with increasing prevalence, high mortality and morbidity rates. Different experimental models have been used to study the pathogenetic mechanisms of ischemic AKI and to develop renoprotective strategies [69]. Currently, two kinds of warm renal I/R models are mainly used: bilateral renal I/R and unilateral renal I/R [69]. The bilateral ischemic AKI model is related to human pathological conditions, however, the assessment of the severity of AKI is not easy, since renal recovery in this model is faster. In our study, we used unilateral nephrectomy accompanied by contralateral clamping model, which mimics the clinical situation of renal transplantation, and make it possible to assess the renal function and morphology of the ischemic kidney separately with no involvement of the nephrectomized kidney. This strategy avoids the limitation in unilateral I/R model without removal of the contralateral kidney [78, 79].

Due to well-described differences in gender or age, we performed our study both on age-matched male rats and mice. Our rat model with 45 min of warm ischemia mimics the clinical situation (renal ischemia during partial resection of the kidney or vessel anastomosis during kidney transplantation) and is consistent with the model used in a previous study [32]. In mice, ischemia was induced by clamping the left renal pedicle for 22 min. Ischemia time was established according to the balance between injury and reversibility in our preliminary tests. The serum, urine, and kidney samples were harvested according to our target time point post surgery.

To monitor the success of the animal model, renal function and kidney pathology were determined at the endpoint of the experiment. In our model, we observed a decline of renal

function that can be detected by increases in serum creatinine and blood urea nitrogen after I/R injury. Moreover, the histological examination of kidney tissues was the direct way to verify and localize the kidney injury by methods such as HE staining, PAS staining, and TUNEL assay [3]. Taken together, the changes in kidney function, tubular damage, apoptosis, and inflammation in various segments of the renal cortex and outer medulla confirmed the success of our animal AKI model.

## **5.2 The synthetic EET analog alleviates I/R-induced kidney damage**

The EET family of eicosanoids consists of four regioisomers (5,6-, 8,9-, 11,12-, and 14,15-EET); each of which can be formed as either the R,S or the S,R enantiomer [80]. The properties of the individual metabolites suggest that the renoprotective effects frequently attributed to the whole EET-family are in fact primarily related to the vasodilatory and anti-inflammatory actions of 11,12- and 14,15-EET. In contrast, the renal effects of 5,6- and 8,9-EET are more complex due to their further and in part site specific metabolism by COX [41]. Thus, the synthetic EET analog was designed to share the functional features of the naturally occurring 11, 12- and 14, 15-EETs [65].

In the present study, we pretreated rats with a single dose of the 14,15-EET analog via renal artery infusion directly before inducing ischemia and determined the development of kidney damage at 48 h after reperfusion. AKI was assessed by five parameters: serum creatinine, blood urea nitrogen, tubular damage score, tubular cell apoptosis and inflammatory cell infiltration. Our data indicated that pretreating the kidney with a synthetic 14,15-EET analog significantly alleviates I/R-induced renal injury by decreasing the reduction of kidney function and reducing the severity of apoptosis and inflammation. Our finding is in line with the notion that EETs exhibit an anti-inflammatory and anti-apoptotic effect in several pathophysiological conditions. Previous studies demonstrated that EETs prevent endothelial activation and leukocyte adhesion by inhibiting nuclear factor- $\kappa$ B and activating peroxisome proliferator-activated receptor  $\alpha$  and  $\gamma$  signaling pathways [81, 82]. Furthermore, exogenous EETs enhanced cell viability, decreased intracellular reactive oxygen species generation, inhibited mitochondrial dysfunction, and attenuated several apoptotic signaling events [83]. Moreover, EET mediated anti-inflammatory, and anti-apoptotic effects were also shown in chronic models such as streptozotocin-induced diabetic mice [84], deoxycorticosterone acetate (DOCA)-salt hypertensive mice [85] or 5/6 nephrectomy model of chronic kidney failure [86].

The development of metabolically robust EET analogs suitable for *in vivo* application is just at the beginning [63-65]. Providing other evidence for their therapeutic potential, synthetic EET analogs rescued the metabolic syndrome phenotype of heme oxygenase 2-null mice [87], prevented adiposity and vascular dysfunction in rats fed with a high-fat diet [88], and attenuated cisplatin nephrotoxicity in rats [89]. To our best knowledge, we showed for the first time that EET analogs efficiently protect against renal I/R-injury.

### **5.3 sEH deficiency aggravates I/R-induced kidney damage**

In the present study, we noticed the amelioration of renal injury in experimental AKI rat by pretreating the kidney with a synthetic EET analog. Based on these studies, it was reasonable to hypothesize that increased baseline EET levels in sEH-KO mice would also act protectively in I/R-induced AKI.

To test this hypothesis, we first confirmed the successful sEH gene knockout in mice before starting the AKI experiments. The genotype, mRNA, protein, and activity levels of sEH were examined by using genotyping PCR, real-time PCR, western blot, and HPLC. As examined in kidney and liver samples, the sEH-KO mice indeed showed no expression of sEH mRNA or protein, and were devoid of sEH activity. Deletion of *Ephx2*, the sEH encoding gene, also resulted in a pronounced shift of the epoxy/dihydroxy metabolite ratios as analyzed in detail in liver, kidney and plasma samples. Taken together, these data clearly confirmed that the sEH-KO mouse used by us displayed a successful global gene knockout resulting in the desired complete loss of sEH function.

Next, we determined the impact of sEH gene deletion on kidney damage after I/R. The sEH-KO and WT mice underwent 22 min of renal ischemia followed by 48 h after reperfusion. To our surprise, we found exactly the opposite phenomenon than expected in our initial hypothesis. Compared to WT, sEH gene deficiency induced a stronger decline in kidney function accompanied with higher tubular lesion scores, stronger tubular apoptosis, and more intensified inflammatory cell infiltration.

Our findings are in apparent contrast to previous findings by other groups. One study showed that pharmacological inhibition of sEH enzyme protected against renal I/R-injury in mice [62]. Moreover, renoprotective effects of sEH gene deletion were reported in mouse models developing chronic kidney disease [84, 85, 90]. There are also several studies indicating that pharmacological sEH inhibition and sEH gene deletion may produce essentially the same beneficial effects as clearly demonstrated in mouse models of myocardial infarction [56, 67] and

stroke [58, 59]. The protective effects of sEH inactivation were attributed to the beneficial properties of EETs, which include vasodilation, suppression of inflammation, prevention of platelet aggregation, and protection against apoptosis [51].

Actually, the present study is among the very few indicating that sEH deficiency may also have detrimental effects in certain disease entities. One study demonstrated that sEH gene deletion renders mice refractory to cardiopulmonary resuscitation after cardiac arrest. Compared to WT mice, the sEH-KO mice had delayed blood pressure recovery after cardiopulmonary resuscitation and suffered significantly higher mortality [51]. Pharmacological sEH inhibition failed to attenuate the chronic kidney damage, instead it increased albuminuria in mice with progressive renal disease in the 5/6-nephrectomy model [91]. Moreover, opposite effects of sEH gene deletion and pharmacological inhibition were observed by analyzing angiotensin II (Ang II)-induced cardiac dysfunction and myocardial fibrosis in mice [92]. As in the case of renal I/R-injury, cardiac dysfunction and fibrosis were attenuated by sEH inhibition but aggravated by sEH gene deletion [92]. Differences in the effects of sEH gene deletion and pharmacological inhibition were also reported regarding the development of hypoxia-induced pulmonary hypertension [93]. In this study, deletion of the sEH gene mimicked the pathophysiological changes induced in the lung (pulmonary vascular remodeling) by chronic (21 days) hypoxia, while the chronic inhibition of sEH had no obvious effect on pulmonary vascular remodeling or exercise capacity [93]. Such reports suggest that downregulation or chronic inhibition of the sEH can also provoke detrimental effects instead of beneficial ones.

Both sEH-deletion and sEH-inhibition may cause the development of compensatory mechanisms in response to either increased levels of epoxy-metabolites or reduced levels of the corresponding hydrolysis products. In line with this notion, sEH-inhibition shifted the renal AA metabolism towards the lipoxygenase pathway and failed to elicit renoprotective effects in the 5/6-nephrectomy mouse model [91]. A shift in AA metabolism was also identified as the likely cause of increased Ang II-induced myocardial fibrosis in sEH-KO mice compared to pharmacological inhibition of sEH activity in WT mice [92]. Moreover, the sEH enzyme contains two domains. The C-terminal domain of sEH metabolizes EETs to their less active diols, while the N-terminal domain demonstrates lipid phosphatase activity. Deletion of the sEH gene eliminates the expression of the whole bi-functional enzyme, whereas the currently developed sEH inhibitors specifically target its C-terminal epoxide hydrolase domain [19]. Accordingly, differences observed by comparing the effects of sEH deletion and sEH inhibition may indicate

an important role of the N-terminal phosphatase domain in the given disease model as discussed for hypoxia-induced pulmonary hypertension [93].

#### **5.4 sEH deletion results in an increase of AKI related biomarkers**

Since small increases in serum creatinine may reflect significant renal insult and can be influenced by other factors, it is important to identify several potential biomarkers that may herald AKI prior to a rise in serum creatinine. We focused on two of the most promising emerging biomarkers for AKI: NGAL and KIM-1. In addition, we measured the urinary calprotectin level, which was recently established in clinical studies to distinguish between prerenal and intrinsic AKI [94]. The levels of KIM-1, NGAL, and the ratio of calprotectin/creatinine were not significantly different at baseline and UniNx controls. However, the three biomarkers tended to be 1.5 to 2 times higher 48 h after reperfusion, especially in sEH-KO mice. However, for KIM-1 and NGAL, the differences between WT and sEH-KO in I/R groups did not reach any significant levels. We also examined the correlations between renal function parameters and these three AKI biomarkers. Each biomarker showed high positive correlation with the severity of AKI. Among the three new markers, the ratio of urinary calprotectin to creatinine showed the highest positive correlation to serum creatinine.

In our study, the alterations of those three biomarkers are consistent with the changes in kidney functions, which confirmed that the sEH-KO mice presented aggravated ischemia AKI. Furthermore, increased levels of these three biomarkers correlate with decreasing glomerular filtration and increasing renal parenchymal tubular damage [95]. The abundant expressions of these biomarkers in renal tissues are related to reduced filtration [95]. And the over-excretion of urinary biomarker is thought to be the consequence of damaged renal compartments and reduced reabsorption in the tubules with the collapse of the proximal tubule endocytic complex [95]. In our current study, we showed that the urinary calprotectin-creatinine ratio had the highest positive correlation to the renal function parameter. This finding demonstrated that the urine samples might be the recommended ones to establish biomarker for detecting and monitoring the severity of AKI. In addition, there were no significant differences between WT and sEH-KO mice among those three biomarkers. This might be due to the biomarker expression curve during AKI development. Some studies in AKI patients after cardiac surgery demonstrated that the peak of urine NGAL came 2 h after the ischemic insult [96], and the peak concentration in serum was reached at 6 h [97]. Given this situation, it is likely that the biomarkers rising quickly in response to AKI may have already peaked and become normal by the time we measured them at 48 h after

I/R induction. This may have resulted in our underestimating the peak degree of elevation and thereby reducing the diagnostic value of the experiment [98].

Anyway, these three biomarkers proved to be promising candidates for detecting renal injury in ischemic AKI. And they may serve as potential endogenous biomarkers, along with the established markers of renal functional impairment to increase the diagnostic sensitivity.

## **5.5 sEH-deficiency causes renal vascular-specific 20-HETE overproduction**

Searching for potential mechanisms predisposing the sEH-KO mice to increased I/R-induced renal damage, we compared the oxylipin profiles of WT and sEH-KO mice under baseline conditions. Remarkably, our data indicate that sEH deficiency was associated with a kidney-specific upregulation of 20-HETE formation. The renal 20-HETE levels were 2-fold higher in sEH-KO than WT mice. In contrast, plasma 20-HETE levels were decreased and hepatic 20-HETE levels were not significantly different between sEH-KO and WT mice. A shift in AA metabolism was also identified as the likely cause for increased Ang II-induced myocardial fibrosis in sEH-KO mice compared to pharmacological inhibition of sEH activity in WT mice [92]. Moreover, despite increased endogenous EET levels, sEH-KO mice display normal blood pressure under baseline conditions and show a reduced hypertensive response to lipopolysaccharides challenge [66]. The same study revealed largely increased AA  $\omega$ -hydroxylase activities in the kidneys of sEH-KO compared to WT mice. Accordingly, it has been suggested that blood pressure homeostasis is achieved in sEH-KO mice by compensatory upregulation of renal 20-HETE formation [66].

To elucidate the origin of increased renal 20-HETE levels in sEH-KO mice, we analyzed native kidneys from sEH-KO and WT mice for the expression of 20-HETE producing and degrading enzymes. In line with the increased renal 20-HETE content, Cyp4a12a, the major murine 20-HETE generating CYP enzyme, was two-fold higher both at mRNA and protein levels in sEH-KO compared to WT mice. Therefore, our observation revealed that renal overproduction of 20-HETE was controlled by the increased gene and protein expression of CYP4a12a in kidneys of sEH-KO mice. Considerable evidence indicated that the sex- and strain-specific differences of renal 20-HETE production in mouse were determined by the expression of Cyp4a12a [70].

It is worth noting that, 20-HETE played contradictory roles during development of hypertension in previous studies by other groups [99, 100]. This apparent contradiction has been largely

resolved by the complex vascular and tubular roles of 20-HETE in the kidney. According to the renal site-specific and dual roles of 20-HETE, we did further studies to clarify the localization of 20-HETE overproduction in the kidney of sEH-KO mice. The expression of 20-HETE producing Cyp4a12a in the kidney was detected with immunofluorescence staining. To our surprise, tubular immunofluorescence was rather faint and not significantly different between WT and sEH-KO mice. The structures displaying clearly enhanced Cyp4a12a immunostaining in sEH-KO mice represented renal vessels (arcuate artery, interlobar, and interlobular artery). These findings suggest vascular overproduction of 20-HETE as the factor potentially causing the increased susceptibility of sEH-KO mice to I/R-induced renal damage.

Supporting this notion, overproduction of 20-HETE has the potential of mediating sustained vasoconstriction [101], promoting inflammatory activation of endothelial cells [102-104], and exacerbating the damage of tubular epithelial cells following adenosine triphosphate depletion-recovery [13]. Nakamura et al. investigated the effects of cisplatin treatment on the rat kidney and found that it significantly elevated the level of CYP4A1 and enhanced the production of 20-HETE, which led to pronounced renal injury and nephrotoxic effect of cisplatin [105]. Other studies also demonstrated a detrimental role of CYP4A and 20-HETE in ischemic injury of the heart [106] and brain[107].

Taken together, our data show that sEH gene deletion caused a compensatory upregulation of renal vascular 20-HETE formation. Enhanced 20-HETE production obviously outweighed the potential benefits of reduced EET degradation, thus providing a potential explanation for the observed increased susceptibility of sEH-KO mice to renal I/R-injury.

## **5.6 The imbalance of 20-HETE and EETs contributes to the pathophysiology of AKI**

EETs and 20-HETE are synthesized from free AA by CYP epoxygenases and hydroxylases, respectively [26, 28, 29]. Once produced, 20-HETE and EETs are partially re-esterified into phospholipids [26, 28, 31]. This membrane pool is accessible to phospholipases activated during ischemia and thus provides a potential source of free 20-HETE and EETs even when de novo synthesis is limited due to hypoxia [108].

Measuring the levels of free and esterified CYP-eicosanoids in rats, we found that in the native kidneys, about 94 % of total 20-HETE, 98 % of total EETs, and 88 % of total DHETs became only detectable after alkaline hydrolysis indicating that the metabolites were predominantly

esterified into membrane phospholipids under baseline conditions. 20-HETE, but not EETs, was released during ischemia and then became almost completely re-esterified within about 2 h of reperfusion. Accordingly, ischemia induced an imbalance of these metabolites compared with physiological conditions. Also in the heart, 20-HETE is presumably more readily released than EETs as indicated by the different levels of these metabolites in the coronary venous plasma before and after ischemia [33]. Moreover, our previous study also showed that early inhibition of 20-HETE synthesis or action protects from I/R-induced AKI in our uninephrectomized rat model [32]. The inhibitor and the antagonist of 20-HETE were applied as low dose bolus injections directly into the renal artery immediately before vascular clamping in order to achieve high intrarenal drug levels during ischemia and a rapid washout upon reperfusion. Blockade of 20-HETE attenuated renal dysfunction, inflammatory cell infiltration, and markedly reduced tubular damage as measured 48 h after reperfusion. Moreover, the 20-HETE antagonist accelerated the recovery of renal blood flow and re-oxygenation in the early reperfusion phase [32]. Therefore, it has been proposed that ischemia induces an imbalance of 20-HETE and EETs, and that 20-HETE plays its detrimental role predominantly in the initiation phase of ischemic AKI by eliciting pro-inflammatory and pro-apoptotic pathways and by mediating sustained vasoconstriction. The mechanisms leading to this apparent selectivity of ischemia-induced 20-HETE release are still unclear. On the one hand, EETs and 20-HETE might be stored in different membrane compartments and their liberation may require different PLA2 enzymes that are not equally activated during ischemia. On the other hand, the differential accumulation of free EETs and 20-HETE may be primarily due to differences in their further metabolic fate. Free EETs are rapidly metabolized by sEH, an enzyme that does not require molecular oxygen and may be thus active also in the ischemic kidney. In contrast, major routes of 20-HETE metabolism are oxygen-dependent because they are initiated by cyclooxygenases [41, 109] and CYP enzymes [110]. Thus, hypoxia may limit the further metabolism of 20-HETE but not that of EETs.

Moreover, our data in mice demonstrated that renal function declined more severely in sEH-KO mice as indicated by higher serum creatinine and urea levels. Ischemic AKI caused marked tubular epithelial cell apoptosis and inflammatory cell infiltration in the kidney tissue. The sEH-KO mice featured stronger tubular lesion scores, tubular apoptosis, and inflammation compared to WT. Interestingly, sEH deficiency caused a compensatory renal vascular-specific overproduction of 20-HETE. Based on the rat data discussed above, it can be reasonably assumed that the more esterified 20-HETE is stored under normal conditions, the more 20-HETE

is released during ischemia eventually resulting in the observed aggravation of I/R induced kidney damage in sEH-KO mice.

The roles of 20-HETE in I/R have been demonstrated by several studies. The cascade of events in I/R-induced renal injury leads to the commencement of deleterious cycles of endothelial dysfunction, oxidative stress, apoptosis, and inflammation that finally culminates in delayed death of cells even when the organs are effectively reperfused [111]. I/R-induced first-phase vascular injury manifests as impaired flow-mediated vasodilation mainly due to a reduction in nitric oxide synthesis and bioavailability [112]. Free 20-HETE, generated during I/R-injury, inhibits the release and action of nitric oxide via endothelial nitric oxide synthase uncoupling, thereby promoting oxidative stress and endothelial dysfunction [99, 113]. Thus, the function of released 20-HETE in the vasculature outweighs the beneficial effects of nitric oxide and then leads to reduced tissue blood flow [113]. Emerging evidence also indicates that increased 20-HETE levels exert deleterious effects on glomerular epithelial cells as well as tubular epithelial cells by stimulating the overproduction of reactive oxygen species [114-117]. The mechanism of this effect is that 20-HETE stimulates NADPH oxidase-derived superoxide production, and then further damages the DNA, proteins and lipids, triggers apoptosis and raises mitochondrial dysfunction [118-120]. Moreover, a wealth of data from clinical as well as experimental studies point to a prominent role of inflammation in renal I/R-injury [111]. 20-HETE by itself is known as a proinflammatory agent that triggers the activation of nuclear factor- $\kappa$ B and mitogen-activated protein kinase/extracellular signal-regulated kinase signaling pathways [103]. Treatment with a 20-HETE synthesis inhibitor confers anti-oxidative and anti-inflammatory effects by disrupting 20-HETE-mediated autocrine/paracrine signaling pathways in the vascular wall [121].

## **5.7 The potential mechanism of 20-HETE overproduction**

As discussed in the previous chapter, 20-HETE plays an important role in the regulation of I/R-induced AKI process. It acts as a second messenger in signaling pathways modulating vascular tone, apoptosis, and inflammation [75]. In the present study, we showed that the severity of kidney damage in sEH-KO mice may depend on the extent of 20-HETE production. Accordingly, the question arises, which mechanism has been responsible for the upregulation of renal 20-HETE formation observed in sEH-KO mice?

Renal Cyp4a12a expression is largely male-specific and can be further increased by treating with androgens [70], which results in increased vascular 20-HETE production [122]. Different mouse

strains largely differ in blood testosterone levels and C57BL/6 is considered as being chronically testosterone-deficient [70]. Interestingly, androgen treatment of male C57BL/6 mice induced most pronounced upregulation of Cyp4a12a/20-HETE among the compared strains [70]. Androgen-induced overproduction of 20-HETE in mice and rats is associated with the development of hypertension [70]. In addition, EETs showed the ability to inhibit cyclic adenosine monophosphate-induced aromatase activity in vascular smooth muscle cells [123]. Based on these findings, we initially assumed that EET-mediated downregulation of aromatase activity and increased testosterone levels might account for the upregulation of 20-HETE formation in sEH-KO mice.

To test this hypothesis, we analyzed the plasma and renal concentrations of testosterone and DHT, as well as the expressions of several enzymes that relate to the testosterone metabolism in the kidney. Mice were individually housed one day before being sacrificed. Blood was collected between 9:00 and 12:00 a.m. by heart puncture. Kidney samples were prepared as described previously [124]. In the present study, DHT levels were not detectable. Furthermore, neither the testosterone levels nor the testosterone-related enzyme expressions showed significant differences between sEH-KO and WT mice. However, another study demonstrated that male sEH-KO mice featured decreased plasma testosterone levels, suggesting that sEH may regulate circulating levels of testosterone through cholesterol biosynthesis and metabolism [125]. Thus, the mechanistic link between sEH gene deletion and Cyp4a12a overexpression is unclear and remains to be elucidated. In particular, additional animal studies will be needed to finally prove or refute the hypothesis of increased systemic or local androgen levels triggering Cyp4a12a overexpression in the renal vasculature of sEH-KO mice. In follow-up studies, it should be considered that testosterone secretion is influenced by several factors. First of all, testosterone pulsatile release has two different types. Spontaneous release typically occurs every 3-4 h, while reflexive release of testosterone is less frequent as a result of encountering a novel female or ejaculation [126]. In male mammals, testosterone is released in a pulsatile fashion in which high “pulsatile” levels are periodically superimposed upon low “basal” levels [127]. Depending on the time points at which blood samples were taken from animals, investigators reported large variabilities in testosterone concentrations, leading to both overestimating basal and underestimating peak levels [127]. Secondly, other factors, such as housing density, stress, and unfamiliar environment, can also affect the blood concentration of androgens or influence the testosterone excretion [126, 128]. Finally, female pheromone also contributes to normal

testosterone maintenance [129]. Further studies are still ongoing to clarify the underlying mechanisms of how 20-HETE is overproduced in the kidney of sEH-KO mice.

## 5.8 Novel therapeutic options for the prevention of ischemic AKI?

In clinical practice, I/R-induced tissue injury accounts for a significant number of organ failures, including ischemic AKI. The knowledge of mechanisms mediating I/R-injury in the general setting and the translation of the experimental findings into clinical applicability needs to be expanded. Our results, both in rats and mice, revealed that an imbalance of 20-HETE and EETs in the kidney plays a pivotal role in setting the stage for the detrimental cascade of events leading to renal I/R-injury. Moreover, in kidney-transplanted patients, the released extent of released 20-HETE and a gene polymorphism leading to reduced sEH activity were linked to allograft dysfunction and decreased graft survival [49, 130]. Based on these experimental and clinical findings, we believe that targeting the CYP-eicosanoid pathway may offer novel strategies for the prevention of AKI. Pharmacological tools already developed for preclinical studies include 20-HETE antagonists [32, 131, 132], sEH inhibitors [62, 133], and EET analogs [65] (Figure 29).

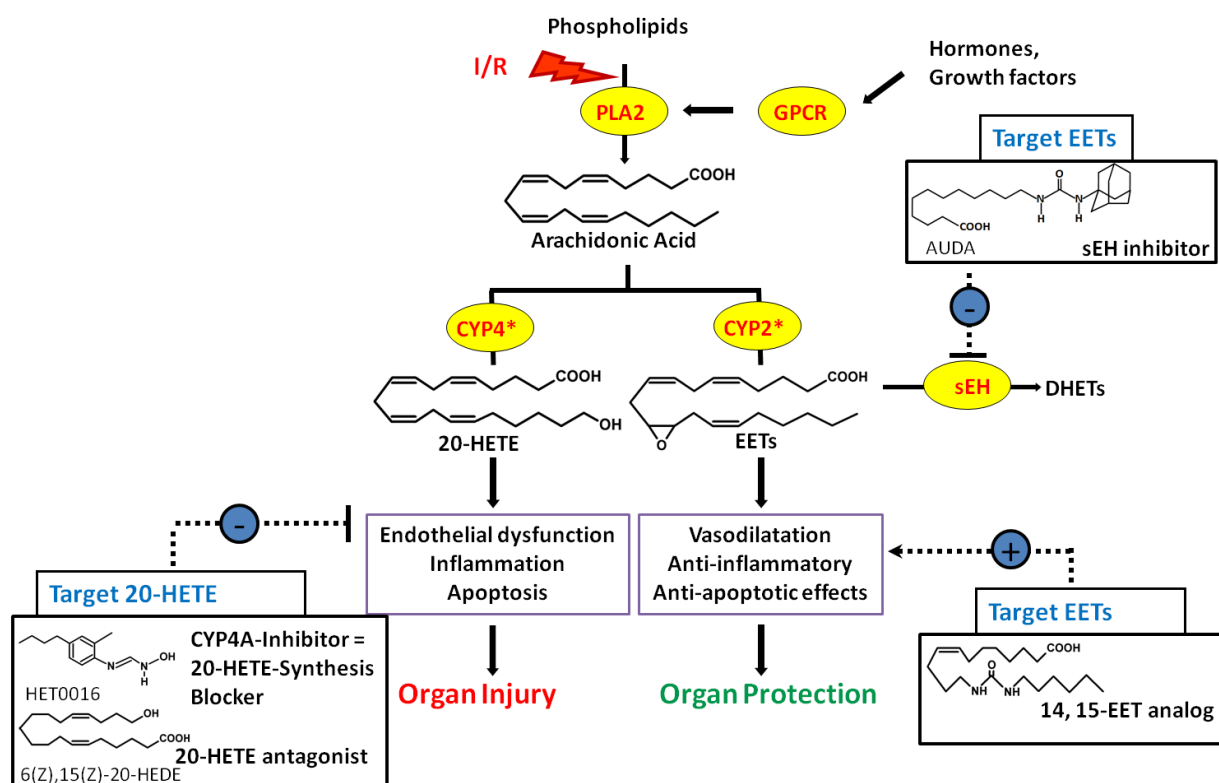


**Figure 29: Prospects--novel therapeutic options for the prevention of ischemic AKI by targeting renal CYP-dependent eicosanoids pathway**

Considering the different vascular and tubular roles of 20-HETE in renal physiology, further studies are required to strictly define the therapeutic window for 20-HETE antagonists. Whereas these compounds are highly potent in antagonizing the vasoconstrictive and pro-inflammatory actions of 20-HETE during the initiation phase of AKI, they might also have long-term adverse effects by interfering with the regulation of tubular salt transport [50]. The development of sEH inhibitors is already highly advanced [67]; however, the present as well as several other studies (compare 4.3) indicate that long-term sEH deficiency might cause shifts in the AA metabolism that obliterate the beneficial effects of stabilizing the endogenous EET levels. To our knowledge, the present study is the first showing that renal I/R injury can be substantially ameliorated by pretreating the kidney with a synthetic EET analog. Unlike sEH inhibitors, EET analogs are expected to be effective also under disease conditions that are associated with decreased EET biosynthesis. Moreover, unlike 20-HETE antagonists, EET analogs might be free of negative side effects on tubular salt transport. Provided that these potential advantages of EET analogs can be verified by future studies, synthetic compounds stimulating the mechanisms of EET action will offer novel therapeutic options for the prevention of ischemic AKI.

## 6. BIBLIOGRAPHY

1. Rewa, O. and Bagshaw S.M., Acute kidney injury-epidemiology, outcomes and economics. *Nat Rev Nephrol*, 2014. **10**(4): p. 193-207.
2. Kam Tao Li, P., Burdmann E.A., and Mehta R.L., Acute kidney injury: Global health alert. *J Nephropathol*, 2013. **2**(2): p. 90-97.
3. Bonventre, J.V. and Yang L., Cellular pathophysiology of ischemic acute kidney injury. *J Clin Invest*, 2011. **121**(11): p. 4210-4221.
4. Basile, D.P., Anderson M.D., and Sutton T.A., Pathophysiology of acute kidney injury. *Compr Physiol*, 2012. **2**(2): p. 1303-1353.
5. Devarajan, P., Update on mechanisms of ischemic acute kidney injury. *J Am Soc Nephrol*, 2006. **17**(6): p. 1503-1520.
6. Sutton, T.A., Fisher C.J., and Molitoris B.A., Microvascular endothelial injury and dysfunction during ischemic acute renal failure. *Kidney Int*, 2002. **62**(5): p. 1539-1549.
7. Kalogeris, T., Baines C.P., Krenz M., and Korthuis R.J., Cell biology of ischemia/reperfusion injury. *Int Rev Cell Mol Biol*, 2012. **298**: p. 229-317.
8. Kosieradzki, M. and Rowinski W., Ischemia/reperfusion injury in kidney transplantation: mechanisms and prevention. *Transplant Proc*, 2008. **40**(10): p. 3279-3288.
9. Gross, G.J., Falck J.R., Gross E.R., Isbell M., Moore J., and Nithipatikom K., Cytochrome P450 and arachidonic acid metabolites: role in myocardial ischemia/reperfusion injury revisited. *Cardiovasc Res*, 2005. **68**(1): p. 18-25.
10. Seubert, J.M., Zeldin D.C., Nithipatikom K., and Gross G.J., Role of epoxyeicosatrienoic acids in protecting the myocardium following ischemia/reperfusion injury. *Prostaglandins Other Lipid Mediat*, 2007. **82**(1-4): p. 50-59.
11. Nithipatikom, K., Gross E.R., Endsley M.P., Moore J.M., Isbell M.A., Falck J.R., Campbell W.B., and Gross G.J., Inhibition of cytochrome P450 $\omega$ -hydroxylase: a novel endogenous cardioprotective pathway. *Circ Res*, 2004. **95**(8): p. e65-71.
12. Imig, J.D., Simpkins A.N., Renic M., and Harder D.R., Cytochrome P450 eicosanoids and cerebral vascular function. *Expert Rev Mol Med*, 2011. **13**: p. e7.
13. Nilakantan, V., Maenpaa C., Jia G., Roman R.J., and Park F., 20-HETE-mediated cytotoxicity and apoptosis in ischemic kidney epithelial cells. *Am J Physiol Renal Physiol*, 2008. **294**(3): p. F562-570.
14. Nelson, D.R., Zeldin D.C., Hoffman S.M., Maltais L.J., Wain H.M., and Nebert D.W., Comparison of cytochrome P450 (CYP) genes from the mouse and human genomes, including nomenclature recommendations for genes, pseudogenes and alternative-splice variants. *Pharmacogenetics*, 2004. **14**(1): p. 1-18.
15. Nelson, D.R., Koymans L., Kamataki T., Stegeman J.J., Feyereisen R., Waxman D.J., Waterman M.R., Gotoh O., Coon M.J., Estabrook R.W., Gunsalus I.C., and Nebert D.W., P450 superfamily: update on new sequences, gene mapping, accession numbers and nomenclature. *Pharmacogenetics*, 1996. **6**(1): p. 1-42.
16. Seliskar, M. and Rozman D., Mammalian cytochromes P450--importance of tissue specificity. *Biochim Biophys Acta*, 2007. **1770**(3): p. 458-466.
17. Schunck., W.H. and Schmidt C., Cytochrome P450-dependent eicosanoids. In: M Bader, ed. *Cardiovascular Hormone Systems*. Germany: WILEY-VCH, 2008: p. 333-372.
18. Hammock, B.D., Gill S.S., Stamoudis V., and Gilbert L.I., Soluble mammalian epoxide hydratase: action on juvenile hormone and other terpenoid epoxides. *Comp Biochem Physiol B*, 1976. **53**(2): p. 263-265.
19. Harris, T.R. and Hammock B.D., Soluble epoxide hydrolase: gene structure, expression and deletion. *Gene*, 2013. **526**(2): p. 61-74.

20. Cronin, A., Mowbray S., Durk H., Homburg S., Fleming I., Fisslthaler B., Oesch F., and Arand M., The N-terminal domain of mammalian soluble epoxide hydrolase is a phosphatase. *Proc Natl Acad Sci U S A*, 2003. **100**(4): p. 1552-1557.
21. Newman, J.W., Morisseau C., Harris T.R., and Hammock B.D., The soluble epoxide hydrolase encoded by EPXH2 is a bifunctional enzyme with novel lipid phosphate phosphatase activity. *Proc Natl Acad Sci U S A*, 2003. **100**(4): p. 1558-1563.
22. Argiriadi, M.A., Morisseau C., Hammock B.D., and Christianson D.W., Detoxification of environmental mutagens and carcinogens: structure, mechanism, and evolution of liver epoxide hydrolase. *Proc Natl Acad Sci U S A*, 1999. **96**(19): p. 10637-10642.
23. Tran, K.L., Aronov P.A., Tanaka H., Newman J.W., Hammock B.D., and Morisseau C., Lipid sulfates and sulfonates are allosteric competitive inhibitors of the N-terminal phosphatase activity of the mammalian soluble epoxide hydrolase. *Biochemistry*, 2005. **44**(36): p. 12179-12187.
24. Morisseau, C. and Hammock B.D., Impact of soluble epoxide hydrolase and epoxyeicosanoids on human health. *Annu Rev Pharmacol Toxicol*, 2013. **53**: p. 37-58.
25. Enayetallah, A.E. and Grant D.F., Effects of human soluble epoxide hydrolase polymorphisms on isoprenoid phosphate hydrolysis. *Biochem Biophys Res Commun*, 2006. **341**(1): p. 254-260.
26. Capdevila, J.H., Falck J.R., and Harris R.C., Cytochrome P450 and arachidonic acid bioactivation. Molecular and functional properties of the arachidonate monooxygenase. *J Lipid Res*, 2000. **41**(2): p. 163-181.
27. Nebert, D.W. and Russell D.W., Clinical importance of the cytochromes P450. *Lancet*, 2002. **360**(9340): p. 1155-1162.
28. Roman, R.J., P-450 metabolites of arachidonic acid in the control of cardiovascular function. *Physiol Rev*, 2002. **82**(1): p. 131-185.
29. Konkel, A. and Schunck W.H., Role of cytochrome P450 enzymes in the bioactivation of polyunsaturated fatty acids. *Biochim Biophys Acta*, 2011. **1814**(1): p. 210-222.
30. Capdevila, J.H. and Falck J.R., Biochemical and molecular properties of the cytochrome P450 arachidonic acid monooxygenases. *Prostaglandins Other Lipid Mediat*, 2002. **68-69**: p. 325-344.
31. Carroll, M.A., Balazy M., Huang D.D., Rybalova S., Falck J.R., and McGiff J.C., Cytochrome P450-derived renal HETEs: storage and release. *Kidney Int*, 1997. **51**(6): p. 1696-1702.
32. Hoff, U., Lukitsch I., Chaykovska L., Ladwig M., Arnold C., Manthati V.L., Fuller T.F., Schneider W., Gollasch M., Muller D.N., Flemming B., Seeliger E., Luft F.C., Falck J.R., Dragun D., and Schunck W.H., Inhibition of 20-HETE synthesis and action protects the kidney from ischemia/reperfusion injury. *Kidney Int*, 2011. **79**(1): p. 57-65.
33. Nithipatikom, K., DiCamelli R.F., Kohler S., Gumina R.J., Falck J.R., Campbell W.B., and Gross G.J., Determination of cytochrome P450 metabolites of arachidonic acid in coronary venous plasma during ischemia and reperfusion in dogs. *Anal Biochem*, 2001. **292**(1): p. 115-124.
34. Inceoglu, B., Schmelzer K.R., Morisseau C., Jinks S.L., and Hammock B.D., Soluble epoxide hydrolase inhibition reveals novel biological functions of epoxyeicosatrienoic acids (EETs). *Prostaglandins Other Lipid Mediat*, 2007. **82**(1-4): p. 42-49.
35. Kroetz, D.L. and Zeldin D.C., Cytochrome P450 pathways of arachidonic acid metabolism. *Curr Opin Lipidol*, 2002. **13**(3): p. 273-283.
36. Zelasko, S., Arnold W.R., and Das A., Endocannabinoid metabolism by cytochrome P450 monooxygenases. *Prostaglandins Other Lipid Mediat*, 2014: p. 112-123.

37. Eid S, Cesar A M , Christopher M E , Ahmed H , Awad R , and A E.A., New Mechanistic Insights in the Development of Diabetic Nephropathy: Role of Cytochromes P450 and Their Metabolites. *J Endocr Disord*, 2014. **1**(1): p. 1-6.
38. Campbell, W.B. and Falck J.R., Arachidonic acid metabolites as endothelium-derived hyperpolarizing factors. *Hypertension*, 2007. **49**(3): p. 590-596.
39. Campbell, W.B. and Fleming I., Epoxyeicosatrienoic acids and endothelium-dependent responses. *Pflugers Arch*, 2010. **459**(6): p. 881-895.
40. Zou, A.P., Fleming J.T., Falck J.R., Jacobs E.R., Gebremedhin D., Harder D.R., and Roman R.J., 20-HETE is an endogenous inhibitor of the large-conductance Ca(2+)-activated K<sup>+</sup> channel in renal arterioles. *Am J Physiol*, 1996. **270**(1 Pt 2): p. R228-237.
41. McGiff, J.C. and Quilley J., 20-HETE and the kidney: resolution of old problems and new beginnings. *Am J Physiol*, 1999. **277**(3 Pt 2): p. R607-623.
42. Alonso-Galicia, M., Sun C.W., Falck J.R., Harder D.R., and Roman R.J., Contribution of 20-HETE to the vasodilator actions of nitric oxide in renal arteries. *Am J Physiol*, 1998. **275**(3 Pt 2): p. F370-378.
43. Maier, K.G. and Roman R.J., Cytochrome P450 metabolites of arachidonic acid in the control of renal function. *Curr Opin Nephrol Hypertens*, 2001. **10**(1): p. 81-87.
44. Schwartzman, M.L., da Silva J.L., Lin F., Nishimura M., and Abraham N.G., Cytochrome P450 4A expression and arachidonic acid omega-hydroxylation in the kidney of the spontaneously hypertensive rat. *Nephron*, 1996. **73**(4): p. 652-663.
45. Roman, R.J. and Alonso-Galicia M., P-450 Eicosanoids: A Novel Signaling Pathway Regulating Renal Function. *News Physiol Sci*, 1999. **14**: p. 238-242.
46. Liu, X., Wu J., Liu H., Lai G., and Zhao Y., Disturbed ratio of renal 20-HETE/EETs is involved in androgen-induced hypertension in cytochrome P450 4F2 transgenic mice. *Gene*, 2012. **505**(2): p. 352-359.
47. Fan, F., Muroya Y., and Roman R.J., Cytochrome P450 eicosanoids in hypertension and renal disease. *Curr Opin Nephrol Hypertens*, 2015. **24**(1): p. 37-46.
48. Omura, T., Tanaka Y., Miyata N., Koizumi C., Sakurai T., Fukasawa M., Hachiuma K., Minagawa T., Susumu T., Yoshida S., Nakaike S., Okuyama S., Harder D.R., and Roman R.J., Effect of a new inhibitor of the synthesis of 20-HETE on cerebral ischemia reperfusion injury. *Stroke*, 2006. **37**(5): p. 1307-1313.
49. Dolegowska, B., Blogowski W., and Domanski L., Is it possible to predict the early post-transplant allograft function using 20-HETE measurements? A preliminary report. *Transpl Int*, 2009. **22**(5): p. 546-553.
50. Regner, K.R., Zuk A., Van Why S.K., Shames B.D., Ryan R.P., Falck J.R., Manthati V.L., McMullen M.E., Ledbetter S.R., and Roman R.J., Protective effect of 20-HETE analogues in experimental renal ischemia reperfusion injury. *Kidney Int*, 2009. **75**(5): p. 511-517.
51. Hutchens, M.P., Nakano T., Dunlap J., Traystman R.J., Hurn P.D., and Alkayed N.J., Soluble epoxide hydrolase gene deletion reduces survival after cardiac arrest and cardiopulmonary resuscitation. *Resuscitation*, 2008. **76**(1): p. 89-94.
52. Wang, Z.H., Davis B.B., Jiang D.Q., Zhao T.T., and Xu D.Y., Soluble epoxide hydrolase inhibitors and cardiovascular diseases. *Curr Vasc Pharmacol*, 2013. **11**(1): p. 105-111.
53. Seubert, J.M., Sinal C.J., Graves J., DeGraff L.M., Bradbury J.A., Lee C.R., Goralski K., Carey M.A., Luria A., Newman J.W., Hammock B.D., Falck J.R., Roberts H., Rockman H.A., Murphy E., and Zeldin D.C., Role of soluble epoxide hydrolase in postischemic recovery of heart contractile function. *Circ Res*, 2006. **99**(4): p. 442-450.
54. Gross, G.J. and Nithipatikom K., Soluble epoxide hydrolase: a new target for cardioprotection. *Curr Opin Investig Drugs*, 2009. **10**(3): p. 253-258.

55. Batchu, S.N., Lee S.B., Samokhvalov V., Chaudhary K.R., El-Sikhry H., Weldon S.M., and Seubert J.M., Novel soluble epoxide hydrolase inhibitor protects mitochondrial function following stress. *Can J Physiol Pharmacol*, 2012. **90**(6): p. 811-823.
56. Motoki, A., Merkel M.J., Packwood W.H., Cao Z., Liu L., Iliff J., Alkayed N.J., and Van Winkle D.M., Soluble epoxide hydrolase inhibition and gene deletion are protective against myocardial ischemia-reperfusion injury in vivo. *Am J Physiol Heart Circ Physiol*, 2008. **295**(5): p. H2128-2134.
57. Qiu, H., Li N., Liu J.Y., Harris T.R., Hammock B.D., and Chiamvimonvat N., Soluble epoxide hydrolase inhibitors and heart failure. *Cardiovasc Ther*, 2011. **29**(2): p. 99-111.
58. Zhang, W., Koerner I.P., Noppens R., Grafe M., Tsai H.J., Morisseau C., Luria A., Hammock B.D., Falck J.R., and Alkayed N.J., Soluble epoxide hydrolase: a novel therapeutic target in stroke. *J Cereb Blood Flow Metab*, 2007. **27**(12): p. 1931-1940.
59. Zhang, W., Otsuka T., Sugo N., Ardeshiri A., Alhadid Y.K., Iliff J.J., DeBarber A.E., Koop D.R., and Alkayed N.J., Soluble epoxide hydrolase gene deletion is protective against experimental cerebral ischemia. *Stroke*, 2008. **39**(7): p. 2073-2078.
60. Shaik, J.S., Ahmad M., Li W., Rose M.E., Foley L.M., Hitchens T.K., Graham S.H., Hwang S.H., Hammock B.D., and Poloyac S.M., Soluble epoxide hydrolase inhibitor trans-4-[4-(3-adamantan-1-yl-ureido)-cyclohexyloxy]-benzoic acid is neuroprotective in rat model of ischemic stroke. *Am J Physiol Heart Circ Physiol*, 2013. **305**(11): p. H1605-1613.
61. Jia, Y., Grafe M.R., Gruber A., Alkayed N.J., and Wang R.K., In vivo optical imaging of revascularization after brain trauma in mice. *Microvasc Res*, 2011. **81**(1): p. 73-80.
62. Lee, J.P., Yang S.H., Lee H.Y., Kim B., Cho J.Y., Paik J.H., Oh Y.J., Kim D.K., Lim C.S., and Kim Y.S., Soluble epoxide hydrolase activity determines the severity of ischemia-reperfusion injury in kidney. *PLoS One*, 2012. **7**(5): p. e37075.
63. Imig, J.D., Elmarakby A., Nithipatikom K., Wei S., Capdevila J.H., Tuniki V.R., Sangras B., Anjaiah S., Manthathi V.L., Sudarshan Reddy D., and Falck J.R., Development of epoxyeicosatrienoic acid analogs with in vivo anti-hypertensive actions. *Front Physiol*, 2010. **1**: p. 157.
64. Sudhahar, V., Shaw S., and Imig J.D., Epoxyeicosatrienoic acid analogs and vascular function. *Curr Med Chem*, 2010. **17**(12): p. 1181-1190.
65. Falck, J.R., Kodela R., Manne R., Atcha K.R., Puli N., Dubasi N., Manthathi V.L., Capdevila J.H., Yi X.Y., Goldman D.H., Morisseau C., Hammock B.D., and Campbell W.B., 14,15-Epoxyeicosa-5,8,11-trienoic acid (14,15-EET) surrogates containing epoxide bioisosteres: influence upon vascular relaxation and soluble epoxide hydrolase inhibition. *J Med Chem*, 2009. **52**(16): p. 5069-5075.
66. Luria, A., Weldon S.M., Kabcenell A.K., Ingraham R.H., Matera D., Jiang H., Gill R., Morisseau C., Newman J.W., and Hammock B.D., Compensatory mechanism for homeostatic blood pressure regulation in Ephx2 gene-disrupted mice. *J Biol Chem*, 2007. **282**(5): p. 2891-2898.
67. Monti, J., Fischer J., Paskas S., Heinig M., Schulz H., Gosele C., Heuser A., Fischer R., Schmidt C., Schirdewan A., Gross V., Hummel O., Maatz H., Patone G., Saar K., Vingron M., Weldon S.M., Lindpaintner K., Hammock B.D., Rohde K., Dietz R., Cook S.A., Schunck W.H., Luft F.C., and Hubner N., Soluble epoxide hydrolase is a susceptibility factor for heart failure in a rat model of human disease. *Nat Genet*, 2008. **40**(5): p. 529-537.
68. Dragun, D., Hoff U., Park J.K., Qun Y., Schneider W., Luft F.C., and Haller H., Prolonged cold preservation augments vascular injury independent of renal transplant immunogenicity and function. *Kidney Int*, 2001. **60**(3): p. 1173-1181.

69. Wei, Q. and Dong Z., Mouse model of ischemic acute kidney injury: technical notes and tricks. *Am J Physiol Renal Physiol*, 2012. **303**(11): p. F1487-1494.
70. Muller, D.N., Schmidt C., Barbosa-Sicard E., Wellner M., Gross V., Hercule H., Markovic M., Honeck H., Luft F.C., and Schunck W.H., Mouse Cyp4a isoforms: enzymatic properties, gender- and strain-specific expression, and role in renal 20-hydroxyeicosatetraenoic acid formation. *Biochem J*, 2007. **403**(1): p. 109-118.
71. Fischer, R., Konkel A., Mehling H., Blossy K., Gapelyuk A., Wessel N., von Schacky C., Dechend R., Muller D.N., Rothe M., Luft F.C., Weylandt K., and Schunck W.H., Dietary omega-3 fatty acids modulate the eicosanoid profile in man primarily via the CYP-epoxygenase pathway. *J Lipid Res*, 2014. **55**(6): p. 1150-1164.
72. Borg, W., Shackleton C.H., Pahuja S.L., and Hochberg R.B., Long-lived testosterone esters in the rat. *Proc Natl Acad Sci U S A*, 1995. **92**(5): p. 1545-1549.
73. Newman, J.W., Morisseau C., and Hammock B.D., Epoxide hydrolases: their roles and interactions with lipid metabolism. *Prog Lipid Res*, 2005. **44**(1): p. 1-51.
74. Jump, D.B., The biochemistry of n-3 polyunsaturated fatty acids. *J Biol Chem*, 2002. **277**(11): p. 8755-8758.
75. Elshenawy, O.H., Anwar-Mohamed A., and El-Kadi A.O., 20-Hydroxyeicosatetraenoic acid is a potential therapeutic target in cardiovascular diseases. *Curr Drug Metab*, 2013. **14**(6): p. 706-719.
76. S.J. Winters and B.J. Clark, Testosterone Synthesis, Transport, and Metabolism. In: C.J. Bagatell, W.J. Bremner, eds. *Androgens in Health and Disease*. Humana Press, 2003: p. 3-22.
77. Takiue, Y., Hosoyamada M., Kimura M., and Saito H., Enhancement of androgen action in the kidneys of transgenic mice harboring the mutant human UMOD gene. *J Pharmacol Sci*, 2011. **115**(3): p. 383-389.
78. Ramakumar, S., Phull H., Purves T., Funk J., Copeland D., Ulreich J.B., Lai L.W., and Lien Y.H., Novel delivery of oligonucleotides using a topical hydrogel tissue sealant in a murine partial nephrectomy model. *J Urol*, 2005. **174**(3): p. 1133-1136.
79. Phull, H., Lien Y.H., Salkini M.W., Escobar C., Lai L.W., and Ramakumar S., Delivery of intercellular adhesion molecule-1 antisense oligonucleotides using a topical hydrogel tissue sealant in a murine partial nephrectomy/ischemia model. *Urology*, 2008. **72**(3): p. 690-695.
80. Zeldin, D.C., Epoxygenase pathways of arachidonic acid metabolism. *J Biol Chem*, 2001. **276**(39): p. 36059-36062.
81. Deng, Y., Theken K.N., and Lee C.R., Cytochrome P450 epoxygenases, soluble epoxide hydrolase, and the regulation of cardiovascular inflammation. *J Mol Cell Cardiol*, 2010. **48**(2): p. 331-341.
82. Samokhvalov, V., Vriend J., Jamieson K.L., Akhnokh M.K., Manne R., Falck J.R., and Seubert J.M., PPARgamma signaling is required for mediating EETs protective effects in neonatal cardiomyocytes exposed to LPS. *Front Pharmacol*, 2014. **5**: p. 242.
83. Chen, W., Zheng G., Yang S., Ping W., Fu X., Zhang N., Wang D.W., and Wang J., CYP2J2 and EETs Protect against Oxidative Stress and Apoptosis in Vivo and in Vitro Following Lung Ischemia/Reperfusion. *Cell Physiol Biochem*, 2014. **33**(6): p. 1663-1680.
84. Elmarakby, A.A., Faulkner J., Al-Shabrawey M., Wang M.H., Maddipati K.R., and Imig J.D., Deletion of soluble epoxide hydrolase gene improves renal endothelial function and reduces renal inflammation and injury in streptozotocin-induced type 1 diabetes. *Am J Physiol Regul Integr Comp Physiol*, 2011. **301**(5): p. R1307-1317.
85. Manhiani, M., Quigley J.E., Knight S.F., Tasoobshirazi S., Moore T., Brands M.W., Hammock B.D., and Imig J.D., Soluble epoxide hydrolase gene deletion attenuates renal

- injury and inflammation with DOCA-salt hypertension. *Am J Physiol Renal Physiol*, 2009. **297**(3): p. F740-748.
86. Zhao, G., Tu L., Li X., Yang S., Chen C., Xu X., Wang P., and Wang D.W., Delivery of AAV2-CYP2J2 protects remnant kidney in the 5/6-nephrectomized rat via inhibition of apoptosis and fibrosis. *Hum Gene Ther*, 2012. **23**(7): p. 688-699.
  87. Sodhi, K., Inoue K., Gotlinger K.H., Canestraro M., Vanella L., Kim D.H., Manthathi V.L., Koduru S.R., Falck J.R., Schwartzman M.L., and Abraham N.G., Epoxyeicosatrienoic acid agonist rescues the metabolic syndrome phenotype of HO-2-null mice. *J Pharmacol Exp Ther*, 2009. **331**(3): p. 906-916.
  88. Sodhi, K., Puri N., Inoue K., Falck J.R., Schwartzman M.L., and Abraham N.G., EET agonist prevents adiposity and vascular dysfunction in rats fed a high fat diet via a decrease in Bach 1 and an increase in HO-1 levels. *Prostaglandins Other Lipid Mediat*, 2012. **98**(3-4): p. 133-142.
  89. Khan, M.A., Liu J., Kumar G., Skapek S.X., Falck J.R., and Imig J.D., Novel orally active epoxyeicosatrienoic acid (EET) analogs attenuate cisplatin nephrotoxicity. *FASEB J*, 2013. **27**(8): p. 2946-2956.
  90. Kim, J., Imig J.D., Yang J., Hammock B.D., and Padanilam B.J., Inhibition of soluble epoxide hydrolase prevents renal interstitial fibrosis and inflammation. *Am J Physiol Renal Physiol*, 2014. **307**(8): p. F971-980.
  91. Jung, O., Jansen F., Mieth A., Barbosa-Sicard E., Pliquett R.U., Babelova A., Morisseau C., Hwang S.H., Tsai C., Hammock B.D., Schaefer L., Geisslinger G., Amann K., and Brandes R.P., Inhibition of the soluble epoxide hydrolase promotes albuminuria in mice with progressive renal disease. *PLoS One*, 2010. **5**(8): p. e11979.
  92. Li, L., Li N., Pang W., Zhang X., Hammock B.D., Ai D., and Zhu Y., Opposite effects of gene deficiency and pharmacological inhibition of soluble epoxide hydrolase on cardiac fibrosis. *PLoS One*, 2014. **9**(4): p. e94092.
  93. Keseru, B., Barbosa-Sicard E., Schermuly R.T., Tanaka H., Hammock B.D., Weissmann N., Fisslthaler B., and Fleming I., Hypoxia-induced pulmonary hypertension: comparison of soluble epoxide hydrolase deletion vs. inhibition. *Cardiovasc Res*, 2010. **85**(1): p. 232-240.
  94. Heller, F., Frischmann S., Grunbaum M., Zidek W., and Westhoff T.H., Urinary calprotectin and the distinction between prerenal and intrinsic acute kidney injury. *Clin J Am Soc Nephrol*, 2011. **6**(10): p. 2347-2355.
  95. Blazquez-Medela, A.M., Garcia-Sanchez O., Blanco-Goza V., Quiros Y., Montero M.J., Martinez-Salgado C., Lopez-Novoa J.M., and Lopez-Hernandez F.J., Hypertension and hyperglycemia synergize to cause incipient renal tubular alterations resulting in increased NGAL urinary excretion in rats. *PLoS One*, 2014. **9**(8): p. e105988.
  96. Mishra, J., Dent C., Tarabishi R., Mitsnefes M.M., Ma Q., Kelly C., Ruff S.M., Zahedi K., Shao M., Bean J., Mori K., Barasch J., and Devarajan P., Neutrophil gelatinase-associated lipocalin (NGAL) as a biomarker for acute renal injury after cardiac surgery. *Lancet*, 2005. **365**(9466): p. 1231-1238.
  97. Parikh, C.R., Coca S.G., Thiessen-Philbrook H., Shlipak M.G., Koyner J.L., Wang Z., Edelstein C.L., Devarajan P., Patel U.D., Zappitelli M., Krawczeski C.D., Passik C.S., Swaminathan M., and Garg A.X., Postoperative biomarkers predict acute kidney injury and poor outcomes after adult cardiac surgery. *J Am Soc Nephrol*, 2011. **22**(9): p. 1748-1757.
  98. Sirota, J.C., Walcher A., Faubel S., Jani A., McFann K., Devarajan P., Davis C.L., and Edelstein C.L., Urine IL-18, NGAL, IL-8 and serum IL-8 are biomarkers of acute kidney injury following liver transplantation. *BMC Nephrol*, 2013. **14**: p. 17.

99. Singh, H., Cheng J., Deng H., Kemp R., Ishizuka T., Nasjletti A., and Schwartzman M.L., Vascular cytochrome P450 4A expression and 20-hydroxyeicosatetraenoic acid synthesis contribute to endothelial dysfunction in androgen-induced hypertension. *Hypertension*, 2007. **50**(1): p. 123-129.
100. Hoagland, K.M., Flasch A.K., and Roman R.J., Inhibitors of 20-HETE formation promote salt-sensitive hypertension in rats. *Hypertension*, 2003. **42**(4): p. 669-673.
101. Imig, J.D., Epoxyeicosatrienoic acids, 20-hydroxyeicosatetraenoic acid, and renal microvascular function. *Prostaglandins Other Lipid Mediat*, 2013. **104-105**: p. 2-7.
102. Cheng, J., Wu C.C., Gotlinger K.H., Zhang F., Falck J.R., Narsimhaswamy D., and Schwartzman M.L., 20-hydroxy-5,8,11,14-eicosatetraenoic acid mediates endothelial dysfunction via IkappaB kinase-dependent endothelial nitric-oxide synthase uncoupling. *J Pharmacol Exp Ther*, 2010. **332**(1): p. 57-65.
103. Ishizuka, T., Cheng J., Singh H., Vitto M.D., Manthati V.L., Falck J.R., and Laniado-Schwartzman M., 20-Hydroxyeicosatetraenoic acid stimulates nuclear factor-kappaB activation and the production of inflammatory cytokines in human endothelial cells. *J Pharmacol Exp Ther*, 2008. **324**(1): p. 103-110.
104. Inoue, K., Sodhi K., Puri N., Gotlinger K.H., Cao J., Rezzani R., Falck J.R., Abraham N.G., and Laniado-Schwartzman M., Endothelial-specific CYP4A2 overexpression leads to renal injury and hypertension via increased production of 20-HETE. *Am J Physiol Renal Physiol*, 2009. **297**(4): p. F875-884.
105. Nakamura, M., Imaoka S., Tanaka E., Misawa S., and Funae Y., cis-Diamminedichloroplatinum induces peroxisomes as well as CYP4A1 in rat kidney. *Res Commun Mol Pathol Pharmacol*, 1998. **99**(1): p. 23-32.
106. Gross, E.R., Nithipatikom K., Hsu A.K., Peart J.N., Falck J.R., Campbell W.B., and Gross G.J., Cytochrome P450 omega-hydroxylase inhibition reduces infarct size during reperfusion via the sarcolemmal KATP channel. *J Mol Cell Cardiol*, 2004. **37**(6): p. 1245-1249.
107. Miyata, N., Seki T., Tanaka Y., Omura T., Taniguchi K., Doi M., Bandou K., Kametani S., Sato M., Okuyama S., Cambj-Sapunar L., Harder D.R., and Roman R.J., Beneficial effects of a new 20-hydroxyeicosatetraenoic acid synthesis inhibitor, TS-011 [N-(3-chloro-4-morpholin-4-yl) phenyl-N'-hydroxyimido formamide], on hemorrhagic and ischemic stroke. *J Pharmacol Exp Ther*, 2005. **314**(1): p. 77-85.
108. Nakamura, H., Nemenoff R.A., Gronich J.H., and Bonventre J.V., Subcellular characteristics of phospholipase A2 activity in the rat kidney. Enhanced cytosolic, mitochondrial, and microsomal phospholipase A2 enzymatic activity after renal ischemia and reperfusion. *J Clin Invest*, 1991. **87**(5): p. 1810-1818.
109. Cheng, M.K., McGiff J.C., and Carroll M.A., Renal arterial 20-hydroxyeicosatetraenoic acid levels: regulation by cyclooxygenase. *Am J Physiol Renal Physiol*, 2003. **284**(3): p. F474-479.
110. Muller, D.N., Theuer J., Shagdarsuren E., Kaergel E., Honeck H., Park J.K., Markovic M., Barbosa-Sicard E., Dechend R., Wellner M., Kirsch T., Fiebeler A., Rothe M., Haller H., Luft F.C., and Schunck W.H., A peroxisome proliferator-activated receptor-alpha activator induces renal CYP2C23 activity and protects from angiotensin II-induced renal injury. *Am J Pathol*, 2004. **164**(2): p. 521-532.
111. Ahmad, M., Dar N.J., Bhat Z.S., Hussain A., Shah A., Liu H., and Graham S.H., Inflammation in ischemic stroke: mechanisms, consequences and possible drug targets. *CNS Neurol Disord Drug Targets*, 2014. **13**(8): p. 1378-1396.
112. Pushpakumar, S., Kundu S., and Sen U., Endothelial dysfunction: the link between homocysteine and hydrogen sulfide. *Curr Med Chem*, 2014. **21**(32): p. 3662-3672.

113. Cheng, J., Ou J.S., Singh H., Falck J.R., Narsimhaswamy D., Pritchard K.A., Jr., and Schwartzman M.L., 20-hydroxyecosatetraenoic acid causes endothelial dysfunction via eNOS uncoupling. *Am J Physiol Heart Circ Physiol*, 2008. **294**(2): p. H1018-1026.
114. Gebremedhin, D., Gopalakrishnan S., and Harder D.R., Endogenous events modulating myogenic regulation of cerebrovascular function. *Curr Vasc Pharmacol*, 2014. **12**(6): p. 810-817.
115. Eid, A.A., Gorin Y., Fagg B.M., Maalouf R., Barnes J.L., Block K., and Abboud H.E., Mechanisms of podocyte injury in diabetes: role of cytochrome P450 and NADPH oxidases. *Diabetes*, 2009. **58**(5): p. 1201-1211.
116. Eid, S., Abou-Kheir W., Sabra R., Daoud G., Jaffa A., Ziyadeh F.N., Roman L., and Eid A.A., Involvement of renal cytochromes P450 and arachidonic acid metabolites in diabetic nephropathy. *J Biol Regul Homeost Agents*, 2013. **27**(3): p. 693-703.
117. Eid, S., Maalouf R., Jaffa A.A., Nassif J., Hamdy A., Rashid A., Ziyadeh F.N., and Eid A.A., 20-HETE and EETs in diabetic nephropathy: a novel mechanistic pathway. *PLoS One*, 2013. **8**(8): p. e70029.
118. Regner, K.R. and Roman R.J., Role of medullary blood flow in the pathogenesis of renal ischemia-reperfusion injury. *Curr Opin Nephrol Hypertens*, 2012. **21**(1): p. 33-38.
119. Lameire, N. and Vanholder R., Pathophysiologic features and prevention of human and experimental acute tubular necrosis. *J Am Soc Nephrol*, 2001. **12 Suppl 17**: p. S20-32.
120. Gottlieb, R.A., Cytochrome P450: major player in reperfusion injury. *Arch Biochem Biophys*, 2003. **420**(2): p. 262-267.
121. Toth, P., Csiszar A., Sosnowska D., Tucsek Z., Cseplo P., Springo Z., Tarantini S., Sonntag W.E., Ungvari Z., and Koller A., Treatment with the cytochrome P450 omega-hydroxylase inhibitor HET0016 attenuates cerebrovascular inflammation, oxidative stress and improves vasomotor function in spontaneously hypertensive rats. *Br J Pharmacol*, 2013. **168**(8): p. 1878-1888.
122. Wu, C.C., Mei S., Cheng J., Ding Y., Weidenhammer A., Garcia V., Zhang F., Gotlinger K., Manthati V.L., Falck J.R., Capdevila J.H., and Schwartzman M.L., Androgen-sensitive hypertension associates with upregulated vascular CYP4A12-20-HETE synthase. *J Am Soc Nephrol*, 2013. **24**(8): p. 1288-1296.
123. Snyder, G.D., Krishna U.M., Falck J.R., and Spector A.A., Evidence for a membrane site of action for 14,15-EET on expression of aromatase in vascular smooth muscle. *Am J Physiol Heart Circ Physiol*, 2002. **283**(5): p. H1936-1942.
124. Titus, M.A., Schell M.J., Lih F.B., Tomer K.B., and Mohler J.L., Testosterone and dihydrotestosterone tissue levels in recurrent prostate cancer. *Clin Cancer Res*, 2005. **11**(13): p. 4653-4657.
125. Luria, A., Morisseau C., Tsai H.J., Yang J., Inceoglu B., De Taeye B., Watkins S.M., Wiest M.M., German J.B., and Hammock B.D., Alteration in plasma testosterone levels in male mice lacking soluble epoxide hydrolase. *Am J Physiol Endocrinol Metab*, 2009. **297**(2): p. E375-383.
126. Mucignat-Caretta, C., Cavaggioni A., Redaelli M., Da Dalt L., Zagotto G., and Gabai G., Age and isolation influence steroids release and chemical signaling in male mice. *Steroids*, 2014. **83**: p. 10-16.
127. Nyby, J.G., Reflexive testosterone release: a model system for studying the nongenomic effects of testosterone upon male behavior. *Front Neuroendocrinol*, 2008. **29**(2): p. 199-210.
128. Jean-Faucher, C., Berger M., De Turckheim M., Veysièrè G., and Jean C., Effects of dense housing on the growth of reproductive organs, plasma testosterone levels and fertility of male mice. *J Endocrinol*, 1981. **90**(3): p. 397-402.

129. Purvis, K. and Haynes N.B., Effect of the odour of female rat urine on plasma testosterone concentrations in male rats. *J Reprod Fertil*, 1978. **53**(1): p. 63-65.
130. Lee, S.H., Lee J., Cha R., Park M.H., Ha J.W., Kim S., and Kim Y.S., Genetic variations in soluble epoxide hydrolase and graft function in kidney transplantation. *Transplant Proc*, 2008. **40**(5): p. 1353-1356.
131. Sato, M., Ishii T., Kobayashi-Matsunaga Y., Amada H., Taniguchi K., Miyata N., and Kameo K., Discovery of a N'-hydroxyphenylformamidine derivative HET0016 as a potent and selective 20-HETE synthase inhibitor. *Bioorg Med Chem Lett*, 2001. **11**(23): p. 2993-2995.
132. Alonso-Galicia, M., Falck J.R., Reddy K.M., and Roman R.J., 20-HETE agonists and antagonists in the renal circulation. *Am J Physiol*, 1999. **277**(5 Pt 2): p. F790-796.
133. Takai, K., Nakajima T., Takanashi Y., Sone T., Nariai T., Chiyo N., Nakatani S., Ishikawa C., Yamaguchi N., Fujita K., and Yamada K., Structure-based optimization of cyclopropyl urea derivatives as potent soluble epoxide hydrolase inhibitors for potential decrease of renal injury without hypotensive action. *Bioorg Med Chem*, 2014. **22**(5): p. 1548-1557.

## **AFFIDAVIT**

“I, Ye Zhu certify under penalty of perjury by my own signature that I have submitted the thesis on the topic ‘Role of Cytochrome P450 (CYP) dependent eicosanoids in experimental Acute Kidney Injury (AKI)’. I wrote this thesis independently and without assistance from third parties, I used no other aids than the listed sources and resources.

All points based literally or in spirit on publications or presentations of other authors are, as such, in proper citations (see "uniform requirements for manuscripts (URM)" the ICMJE [www.icmje.org](http://www.icmje.org)) indicated. The sections on methodology (in particular practical work, laboratory requirements, statistical processing) and results (in particular images, graphics and tables) correspond to the URM (s.o) and are answered by me. My interest in any publications to this dissertation corresponds to those that are specified in the following joint declaration with the responsible person and supervisor. All publications resulting from this thesis and which I am author correspond to the URM (see above) and I am solely responsible.

The importance of this affidavit and the criminal consequences of a false affidavit (section 156,161 of the Criminal Code) are known to me and I understand the rights and responsibilities stated therein.

Date

Signature

## **CURRICULUM VITAE**

Mein Lebenslauf wird aus datenschutzrechtlichen Gründen in der elektronischen Version meiner Arbeit nicht veröffentlicht.

## PUBLICATION

### Publication

Kusch A, Hoff U, Bubalo G, Zhu Y, Fechner M, Schmidt UR, Marko L, Müller DN, Schmidt-Ott KM, Gürgen D, Blum M, Schunck WH, Dragun D. Novel signalling mechanisms and targets in renal ischemia and reperfusion injury. *Acta Physiol (Oxf)*. 2013, 208(1): 25-40. **IF=4.38**

L Chen, L Markó, M Kaßmann, Y Zhu, KY Wu, M Gollasch. Role of TRPV1 channels in ischemia/reperfusion-induced acute kidney injury. *Plos One*. 2014 Oct 17; 9(10): e109842. **IF=3.534**

Zhang H, Zhu Y, Jia N, Zhang HT, Zheng J, Zhu WP, Zhou WY, Lin YJ, Wang XH. Expression and significance of neutrophil gelatinase-associated lipocalin in renal interstitial fibrosis in rats. *ZhongHua YiXue Za Zhi*. 2012, 92(36): 2565-2569. (Chinese)

Zhang H, Xu L, Zhang HT, Zheng J, Jia N, Zhu Y, Li LL, Lin YJ, Li ZH. Expression and significance of NGAL in MRL/lpr lupus-prone mice. *Chinese Journal of Rheumatology*. 2014,10(9):692-696. (Chinese)

### Abstracts and Posters

M Kaßmann, Y Zhu, Zh M Zhu, M Tepel, M Gollasch. Posterpresentation: TRPV1 and acute kidney injury. Symposium of the mechanism of AKI, 2012, Copenhagen, Damark.

Y Zhu, M Fechner, U Hoff, G Bubalo, T Hoppenheit, C Westphal, M Blum, W Schneider, M Rothe, WH Schunck, D Dragun. Posterpresentation: 20-Hydroxyeicosatetraenoic acid (20-HETE) overproduction exerts ischemic acute kidney injury in mice deficient for soluble epoxy hydrolase (sEH). Jahrestagung der Deutschen Gesellschaft für Nephrologie (DGfN), 2013, Berlin, Germany.

G Bubalo, M Blum, M Fechner, U Hoff, Y Zhu, A Pohlmann, J Hentschel, K Arakelyan, E Seeliger, B Flemming, W Schneider, M Rothe, JR Falck, T Niendorf, WH Schunck, D Dragun. Posterpresentation: Epoxyeicosatrienoic acids increase intrarenal reoxygenation and prosurvival signaling and protect against renal ischemia/reperfusion injury. Jahrestagung der Deutschen Gesellschaft für Nephrologie (DGfN), 2013, Berlin, Germany. **(Received poster Award)**

Y Zhu, M Fechner, U Hoff, G Bubalo, T Hoppenheit, C Westphal, M Blum, W Schneider, M Rothe, WH Schunck, D Dragun. Posterpresentation:20-Hydroxyeicosatetraenoic acid (20-HETE) overproduction exerts ischemic acute kidney injury in mice deficient for soluble epoxy hydrolase

(sEH). Jahrestagung der Deutschen Transplantationsgesellschaft (DTG), 2013, Frankfurt, Germany.

G Bubalo, M Blum, M Fechner, U Hoff, Y Zhu, A Pohlmann, J Hentschel, K Arakelyan, E Seeliger, B Flemming, W Schneider, M Rothe, JR Falck, T Niendorf, WH Schunck, D Dragun. Posterpresentation: Epoxyeicosatrienoic acids increase intrarenal reoxygenation and prosurvival signaling and protect against renal ischemia/reperfusion injury. American Society of Nephrology (ASN), 2013, Atlanta, USA.

A Pohlmann, J Hentschel, U Hoff, G Bubalo, M Fechner, M Blum, Y Zhu, K Arakelyan, E Seeliger, D Gurgun, W Schneider, M Rothe, VL Manthati, JR Falck, WH Schunck, D Dragun, T Niendorf. Posterpresentation: Parametric Mapping of Renal T2\* Demonstrates Beneficial Effect of Epoxyeicosatrienoic Acid for Preventing Acute Kidney Injury. International Society for Magnetic Resonance in Medicine (ISMRM), 2014, Salt Lake City, Utah, USA.

L Chen, L Markó, M Kaßmann, Y Zhu, KY Wu, M Gollasch. Posterpresentation: The role of TRPV1 in acute kidney injury. Jahrestagung der Deutschen Gesellschaft für Nephrologie (DGfN), 2013, Berlin, Germany. **(Received poster Award)**

## ACKNOWLEDGEMENT

The writing of this medical dissertation has been a precious journey in my academic life. I could not have travelled this far without the passionate and continued support of my advisors, colleagues, and family during these years of study in Berlin.

First and foremost, I would like to express my heartfelt gratitude to Professor Dr. Duska Dragun, my main advisor and supervisor, for the golden opportunity to perform my doctoral thesis at her department in Charité Universitätsmedizin Berlin. Her great research experience, interesting ideas and concepts have a remarkable influence on my work. Meanwhile, I want to express my sincere gratitude to Dr. Wolf-Hagen Schunck for offering the opportunity and providing support to carry out this study in the Max-Delbrueck Center for Molecular Medicine (MDC), and for his excellent guidance, encouragement, and care throughout the entire period of my study.

Second, I am thankful to all members and colleagues from the research groups of Prof. Dr. Duska Dragun and Dr. Wolf-Hagen Schunck, who shared their wonderful experiences with me. I am deeply indebted to Dr. U Hoff, Dr. M Fechner, Dr. D Gürgen, and Dr. C Westphal for their cordial help in designing the experiments, animal model building and my thesis revision. And I'm also grateful to Dr. RA Catar, Dr. A Philippe, Dr. A Kusch, and Dr. A Konkel, who helped me a lot in either experiment or novel technique guidance. In addition, I thank Dr. Michael Rothe and Gregor Mueller, for their help in LC-MS/MS measurement and their wonderful suggestions on the protocol improvement. I highly appreciate the help and technical assistance from Christel Andrée, Ramona Zummach, and Saskia Reichert over the years of my study.

Furthermore, I would like to thank Dr. T Schaub, Nan Zhu, Tim Wasser, Maximilian Blum, and Gordana Bubalo for their continuous encouragement and help in both research work and daily life. And I am grateful for financial support from the China Scholarship Council.

Finally, special thanks go to all my family members. Without their endless love and support, I can never achieve all these.